

2021 • 2022

Faculteit Industriële Ingenieurswetenschappen  
master in de industriële wetenschappen: chemie

## Masterthesis

Microinjection moulding and material testing of polyolefins on a  
smeel scale

PROMOTOR :  
Prof. dr. Anton GINZBURG

COPROMOTOR :  
ing. Jules HENROTTE

Luca Cannas

Scriptie ingediend tot het behalen van de graad van master in de industriële wetenschappen: chemie

Gezamenlijke opleiding UHasselt en KU Leuven



2021 • 2022

Faculteit Industriële Ingenieurswetenschappen  
master in de industriële wetenschappen: chemie

## Masterthesis

Microinjection moulding and material testing of polyolefins on a  
smeel scale

PROMOTOR :

Prof. dr. Anton GINZBURG

COPROMOTOR :

ing. Jules HENROTTE

**Luca Cannas**

Scriptie ingediend tot het behalen van de graad van master in de industriële wetenschappen: chemie



**KU LEUVEN**



## Acknowledgments

With the completion of this master's thesis, I complete my study in industrial engineering sciences in chemistry, with a specialization in sustainable processes and plastics. My years as a student at Hasselt University have allowed me to grow as a person and have given me a great deal of insight into industrial chemistry and everything that the chemical sector entails. During these years I have been able to develop myself into a person who can think problem-solving and make correct use of the acquired knowledge, but who has also acquired the necessary tools to independently learn and apply new knowledge. Through this program, I was able to experience what it is like to collaborate with engineers in a group. Thanks to the group assignments and other activities, I regularly had the opportunity to have a healthy, but necessary dose of self-reflection. Thanks to the group assignments I have acquired the necessary 'tools' to be able to analyse and improve my pitfalls and points for improvement as an engineer and as a person.

I would like to thank the people who guided me through this unforgettable experience. First of all, I would like to thank my internal and external promoters, Prof. Dr. Anton Ginzburg and PhD. Ing Jules Henrotte. During this thesis, their advice and guidance ensured that I kept on the right track. Both were always ready to answer my questions and I have learned a lot from them. In addition, I would like to thank Prof. Dr. Ir. Ginzburg for allowing me to be part of the SMaRT (Soft Matter, Rheology and Technology) research group under his leadership. In addition to my promoters, I would like to thank Prof. Dr. Ir. Leen Braeken. Without her efforts, it would not have been possible to participate in this master's thesis. I would also like to thank the other employees and students who are part of the SMaRT research group. These people created a pleasant atmosphere in the laboratory and have also advised me throughout this research. Finally, I would like to thank my parents for all the support they have shown throughout my entire school career. They always motivated me to study, but also to grow as a person. Without my parents, I would not be the same person, let alone be the same aspiring engineer, that I am today. More importantly, without my parents, I would never have dreamed of achieving a result like this.



# Table of contents

Table of tables	17
Table of figures	19
List of symbols	21
Abstract in English	25
Abstract in Dutch	27
<b>1. Introduction</b>	<b>19</b>
1.1. Context	19
1.2. Problem definition	19
1.3. Research objectives	20
1.4. Plan of approach	21
<b>2. Theoretical background information</b>	<b>23</b>
2.1. Polymers	23
2.1.1. Polymers used in microinjection moulding	23
2.1.2. Polypropylene (PP)	29
2.2. Injection moulding	31
2.3. Microinjection moulding	37
2.3.1. Contaminations	39
2.3.2. Plasticization	41
2.3.3. Injection	43
2.3.4. Holding and cooling	47
2.3.5. Demoulding	49
2.3.6. Purging	53
2.3.7. Mould insert production techniques	57
2.3.8. Ultrasound microinjection moulding techniques	59
2.4. Analysis techniques	61
2.4.1. Rheometry	61
2.4.2. Differential scanning calorimetry (DSC)	63
2.4.3. Mechanical testing	65
<b>3. Materials and methodology</b>	<b>69</b>
3.1. Microinjection moulding machine	69
3.2. Rotational rheometer (MCR302L, Anton Paar)	71
3.3. Differential scanning Calorimetric analysis machine (2920 TA, TA Instruments)	73
3.4. Tensile testing machine (Quasar 50kN, Galdabini)	73
3.5. Flexibility testing machine	73
3.6. Polymeric materials	75
3.7. Viscosity curve of the microinjection moulding machine	77
<b>4. Results</b>	<b>79</b>
4.1. Viscosity curve of the Fanuc ROBOSHOT	79
4.1.1. Influence of the screw RPM	79
4.1.2. Influence of the temperature	81
4.2. Minimal required amount of material to perform one single shot with the Fanuc ROBOSHOT	83
4.3. System purging experiments	85
4.3.1. RPM influence in combination with maximum injection pressure	85
4.3.1.1. More viscous (PHC31) change to less viscous (515A)	85
4.3.1.2. Less viscous (515A) change to more viscous (PHC31)	87
4.3.2. RPM influence in combination with low injection pressure	87
4.3.2.1. More viscous (PHC31) change to less viscous (515A)	87
4.3.2.2. Less viscous (515A) change to more viscous (PHC31)	89
4.3.3. P influence in combination with low screw RPM	91

4.3.3.1. More viscous (PHC31) change to less viscous (515A)	91
4.3.3.2. Less viscous (515A) change to more viscous (PHC31)	93
4.4. Determination of the accuracy and reproducibility of the conventional PP25 and smaller PP08 probes (MCR302e)	95
4.4.1. 515A	95
4.4.2. PHC31	97
4.4.3. Time/frequency-temperature superposition of PHC31	99
4.5. Tensile analyses	103
4.6. Flexibility analyses	105
5. Conclusions	107
References	109
Appendices	115

## Table of tables

Table 1: Advantages and disadvantages of polypropylene.	30
Table 2: Mechanical and thermal properties of commercially sold polypropylene types (Novolen – Targor GmbH).	30
Table 3: Comparison between hydraulic and electrical injection moulding systems.	31
Table 4: The advantages and disadvantages of a variotherm process in comparison to a fixed temperature.	35
Table 5: Systems for variotherm micro mould applications.	35
Table 6: Comparison of heater system power-densities.	41
Table 7: Theoretical laws to describe the shear thinning behaviour of a polymer melt inside the mould.	43
Table 8: Rule of thumb for the estimation of the cooling time for conventional plastics.	47
Table 9: Field of appliance and limiting factors of demoulding techniques.	50
Table 10: In-mould shrinkage influence factors.	51
Table 11: Shrinkage values of semi-crystalline polymers.	51
Table 12: Recommended purging agents.	55
Table 13: Recommended plastic changing profiles.	56
Table 14: The different processes for mould fabrication.	57
Table 15: Aspect ratio limits of deep x-ray lithography.	58
Table 16: Comparison of variotherm and ultrasound assisted microinjection moulding techniques.	59
Table 17: General overview of the mechanical and environmental specifications of the Fanuc Roboshot S-2000i30B.	69
Table 18: PP25 (79044) and PP08 (5681) specifications.	71
Table 19: PHC31-81 datasheet.	75
Table 20: 515A specification sheet.	75
Table 21: Temperature profile of the injection system (°C)	77
Table 23: PP25 and PP08 comparison 515A.	96
Table 24: PP25 and PP08 comparison PHC31.	97
Table 25: TTS PP25 deviation results.	100
Table 26: PP08 master curve deviation results and compared difference to the PP25 probe master curve.	102
Table 27: Tensile strength analyses results.	103
Table 28: Flexibility analyses results.	105
Table 29: Overview of different materials for micro moulding.	115
Table 30: Commercially available micro injection moulding machines and their characteristics.	115



## Table of figures

Figure 1: Tensile bar dimensions (sample weight = 200 mg).	20
Figure 2: Exemplary viscosity curve of an injection moulding machine (typical polymeric melt behaviour (shear thinning)).	21
Figure 3: Viscosity and shear stress in function of the shear rate for (Non-)Newtonian fluids.	24
Figure 4: Typical three step thixotropic test.	25
Figure 5: Typical viscosity curve of polymer melts.	26
Figure 6: Molecular structure of isotactic polypropylene (iPP).	29
Figure 7: Molecular structure of syndiotactic polypropylene (sPP).	29
Figure 8: Molecular structure of atactic polypropylene (aPP).	29
Figure 9: Schematic overview of an electrical injection moulding machine.	33
Figure 10: General injection moulding process steps.	34
Figure 11: Variotherm and conventional injection moulding temperature profiles.	35
Figure 12: SIR parameters.	45
Figure 13: Micro column morphology. 1. Skin layer 2. Shear zone 3. Core layer.	49
Figure 14: Compact rotational disk rheometer schematic presentation.	63
Figure 15: Capillary rheometry schematic presentation.	63
Figure 16: Typical DSC curve (exemplary).	64
Figure 17: Typical stress-strain curve for perfect elastic solids.	66
Figure 18: Typical stress-strain characteristics: 1. Yield stress > failure stress 2. Yield stress < failure stress 3. Yield stress = failure stress 4. Brittle materials.	66
Figure 19: Three-point loading of a polymer sample (flexibility test).	67
Figure 20: Fanuc ROBOSHOT S-2000i30B.	69
Figure 21: Thermo-5 (HB-180Z2) cooling unit (HB-THERM).	69
Figure 22: MCR302e Rotational Compact Disk rheometer (Anton Paar).	71
Figure 23: PP25 (79044) parallel plate probe (left) and PP08 (5681) (right).	71
Figure 24: DSC Autosampler (TA Instruments).	73
Figure 25: Quasar 50 kN tensile testing machine.	73
Figure 26: ZwickRoell 1486 flexibility testing machine (ZwickRoell GmbH. & Co. KG).	74
Figure 27: Pelletization procedure.	76
Figure 28: Temperature profile of the injection system.	77
Figure 29: RPM influence 515A (left) and PHC31 (right) ( $T_{mid}$ temperature profile).	80
Figure 30: Temperature influence 515A (left) and PHC31 (right) (450 RPM).	81
Figure 31: DSC curves powdered grades (PPOH1 = grade 1, PPOH2 = grade 2).	84
Figure 32: Complex viscosity of 515A (left) and PHC31 (right) in the function of the angular frequency (230 °C).	85
Figure 33: PHC31 to 515A (high pressure) in the function of the screw RPM.	86
Figure 34: 515A to PHC31 (high pressure) in the function of the screw RPM.	87
Figure 35: PHC31 to 515A (low pressure) in the function of the screw RPM.	88
Figure 36: 515A to PHC31 (low pressure) in the function of the screw RPM.	89
Figure 37: PHC31 to 515A (low RPM) in the function of the pressure.	91
Figure 38: 515A to PHC31 (low RPM) in the function of the pressure.	93
Figure 39: Comparison of PP25 (left) and PP08 (right) probes (515A).	96
Figure 40: Comparison of PP25 (left) and PP08 (right) probes (PHC31).	98
Figure 41: PP25 master curve ( $T_{ref} = 190^{\circ}\text{C}$ ).	101
Figure 42: Horizontal shift factor in function of the temperature (PHC31) using PP25.	101
Figure 43: PP08 master curve ( $T_{ref} = 190^{\circ}\text{C}$ ).	102

Figure 44: Tensile strength tests in function of the percentage elongation.

104

Figure 45: Dimensions of the Fanuc Roboshot S-2000i30B.

117

## List of symbols

$a$  = width of transition between Newtonian law asymptote and power law asymptote

$a_t$  = horizontal shift factor

$A$  = empirical constant

$A'$  = empirical constant

$A_h$  = piston area in hydraulic oil ( $m^2$ )

$A_m$  = screw area in the melt ( $m^2$ )

$\alpha_f$  = expansion coefficient of free volume

$b$  = thickness sample (mm)

$b_t$  = vertical shift factor

$B = B' / \alpha_f$

$B'$  = empirical constant

$Br$  = Brinkman number

$C$  = constant of plate and cone rheometer, dependent upon characteristics of the instrument

$d_{\text{screw}}$  = screw diameter (mm)

$D$  = diameter of the rod (mm)

$E$  = activation energy (J/mol)

$E_E$  = elasticity modulus (GPa)

$E_f$  = flexibility modulus ( $N/mm^2$ )

$f_t$  = fractional free volume at temperature  $T$

$f_g$  = fractional free volume at the glass temperature

$f$  = fractional free volume

$f$  = frequency (1/s)

$F$  = applied force (N)

$G'$  = storage modulus

$G''$  = loss modulus

$G^*$  = complex modulus

$G_N^0$  = plateau modulus

$h$  = width of the sample (mm)

$h_p$  = height between rotating plates (rotational rheometry) (mm)

$\Delta H_c$  = melt cooling heat flow (J/s)

$\Delta H_h$  = melt heat flow (J/s)

$\Delta H_{r^\circ}$  = reference melt heat value (W/g)

i = imaginary part

I = sound intensity (W or dB)

$\lambda$  = heat capacity (J/(kg K))

$\sigma$  = polymer thermal conductivity (W/(m K))

$\delta$  = thermal diffusivity (mm<sup>2</sup>/s)

l = support span-length between the two outer-support rods (mm)

l<sub>o</sub> = original sample length (mm)

l<sub>s</sub> = stretched sample length (mm)

L = capillary length (= length of flow channel) (m, mm)

M<sub>e</sub> = entanglement molar mass = molar mass of filaments between the crosslinks of rubbery material (g/mol)

n = power law index: 1 for Newtonian fluid, 0 for rigid plastic element

$\eta$  = viscosity (Pa s)

$\eta_t$  = viscosity at temperature T (Pa s)

$\eta_{t0}$  = viscosity at temperature T<sub>0</sub> (Pa s)

$\rho$  = density (kg/m<sup>3</sup>)

P = power needed (Watt)

P<sub>c</sub> = thermal power transported through conduction (Watt)

P<sub>d</sub> = thermal power dissipated by flow of polymer resin (Watt)

P<sub>h</sub> = pressure in the hydraulic oil (bar)

P<sub>m</sub> = pressure in the melt (bar)

$\Delta P_r$  = pressure difference in a flow section (bar or MPa)

Q = volume flow rate (mm<sup>3</sup>/s)

r = cone radius (m)

R = gas constant (J/(K mol)) = 2.303 J/(K mol)

R<sub>c</sub> = radius of flow channel (mm)

R<sub>r</sub> = radius of ram (mm)

R<sub>m</sub> = tensile strength (N/mm<sup>2</sup>)

R<sub>p</sub> = yield strength (N/mm<sup>2</sup>)

s = deflection of the sample measured at the centre of the span length (l/2)

$S$  = maximum cavity thickness (mm)

$S_w$  = wall thickness (mm)

$t$  = time (s)

$t_c$  = cooling time (s)

$T$  = torque (N m)

$\overline{T}_E$  = ejection temperature ( $^{\circ}\text{C}$  or K)

$T_f$  = final mould temperature ( $^{\circ}\text{C}$  or K)

$T_g$  = glass transition temperature ( $^{\circ}\text{C}$ )

$T_i$  = initial mould temperature ( $^{\circ}\text{C}$  or K)

$T_M$  = melt temperature ( $^{\circ}\text{C}$  or K)

$\overline{T}_M$  = average temperature of polymer melt ( $^{\circ}\text{C}$  or K)

$\Delta\overline{T}_M$  = average temperature increase of polymer melt ( $^{\circ}\text{C}$  or K)

$T_0$  = reference temperature ( $^{\circ}\text{C}$  or K)

$T_o = T_g - f_g / \alpha_f$  = Vogel temperature ( $^{\circ}\text{C}$  or K)

$T_p$  = mould wall temperature ( $^{\circ}\text{C}$  or K)

$\overline{T}_W$  = mean mould temperature

$\overline{v}$  = flow velocity of polymer melt (m/s)

$v_{\text{abs}}$  = absolute injection speed ( $\text{cm}^3/\text{s}$ )

$v_{\text{rel}}$  = relative injection speed (mm/s)

$v_r$  = velocity of the ram (mm/s)

$V$  = space needed for molecule ( $\text{m}^3$ )

$V_f$  = available space for molecule ( $\text{m}^3$ )

$V_o$  = occupied volume of molecule ( $\text{m}^3$ )

$V_p$  = moulded part volume ( $\text{m}^3$ )

$X$  = distance (mm)

$\dot{\gamma}$  = shear rate ( $\text{s}^{-1}$ )

$\dot{\gamma}_p$  = shear rate of pseudo-plastic behaving polymer ( $\text{s}^{-1}$ )

$\dot{\gamma}_w$  = shear rate along the wall ( $\text{s}^{-1}$ )

$\gamma_0$  = shear amplitude

$\tau$  = shear stress (MPa)

$\tau_w$  = shear stress at the capillary wall (Pa)

$\tau_0$  = stress amplitude (Pa)

$\theta$  = phase angle

$\Omega$  = angular velocity of rotating plate (m/s)

$\alpha_f$  = flexural stress (N/mm<sup>2</sup>)

$\varepsilon$  = strain (MPa)

$\varepsilon_f$  = flexural strain (N/mm<sup>2</sup>)

$\omega$  = angular frequency (rad/s) =  $2\pi f$

$\omega_{reduced}$  = reduced angular frequency (rad/s) =  $a_t * \omega$

$\Xi$  = ultrasonic energy absorption coefficient (dB/ (cm MHz))

## Abstract in English

SMaRT research group (KU Leuven) mainly focusses on polymers and colloidal dispersions to develop new materials and study their processing behaviour. Today, the development and study of new materials is an exceptionally long and costly process. In addition, studying the processing behaviour requires copious amounts of material. Since newly developed materials do not have an existing synthesis process, it is one of the crucial factors to accelerate the material development cycle. The scope of this master's thesis is to reduce the required amount of material to perform a material processing step, to analyse material characteristics, and to perform system purging.

Material processing and system purging experiments are performed with the Fanuc ROBOSHOT S2000i-30B injection moulding machine. To decrease the amount of material, small tensile bars are fabricated of 0.2 g. The processing behaviour and material deterioration is characterized at rheological, mechanical, and molecular level. To decrease the required amount of material to perform analyses, the suitability of conventional techniques is examined for very small samples.

From experiments with the Fanuc resulted that it is possible to perform a single shot with only 3.0 grams of polymeric (powdered) feed. Smaller mould dimensions are advised to decrease the wastage per shot. From the purging experiments, it can be concluded that a high injection pressure and temperature are crucial to decrease the amount of purging waste. A full system purge was obtained with 14 g.



## Abstract in Dutch

De onderzoeksgroep SMaRT (KU Leuven) concentreert zich op polymeren en colloïdale dispersies om nieuwe materialen te ontwikkelen en hun verwerkingsgedrag te bestuderen. De ontwikkeling en studie van nieuwe materialen is een uitzonderlijk lang en duur proces. Voor de studie van het verwerkingsgedrag zijn grote hoeveelheden materiaal nodig. Omdat nieuwe materialen geen bestaand syntheseproces hebben is het een van de cruciale factoren om de materiaalontwikkeling te versnellen. Het doel van deze masterproef is het reduceren van de hoeveelheid materiaal voor het uitvoeren van een verwerkingsstap, het analyseren van materiaaleigenschappen, en het uitvoeren van een systeemzuivering.

De experimenten worden uitgevoerd met de Fanuc ROBOSHOT S2000i-30B (micro)s spuitgietmachine. Om de hoeveelheid materiaal te verminderen, worden kleine trekstaven van 0,2 g gefabriceerd. Het verwerkingsgedrag en de degradatie worden bestudeerd op reologisch, mechanisch en moleculair niveau. Om de hoeveelheid materiaal nodig per analyse te verminderen wordt de geschiktheid van conventionele technieken onderzocht voor kleine stalen.

Uit experimenten met de Fanuc is gebleken dat het mogelijk is om een enkel schot uit te voeren met slechts 3,0 gram polymeer (poedervormig). Kleinere matrijsafmetingen worden geadviseerd om het verlies per schot te verminderen. Uit de purgeerexperimenten is geconcludeerd dat een hoge injectiedruk en temperatuur cruciaal zijn om de hoeveelheid purgeerafval te verminderen. Een volledige systeemzuivering wordt verkregen met 14 g.



# 1. Introduction

First, the research group is presented under which this study is performed. Next, there is an extensive discussion of the problem statement. At last, the objectives and plan of approach are presented.

## 1.1. Context

Soft Matter, Rheology, and Technology, or SMaRT, is a research group founded in 1969 at the University of Leuven. SMaRT is composed of two faculties, one of which is located at the Science Park in Diepenbeek, while the head faculty is situated in Arenberg, Leuven [1]. This research is performed at the faculty located in Diepenbeek. SMaRT's research involves both soft matter physics and chemistry as well as transport phenomena, also known as classical chemical engineering. The three main research fields of SMaRT are rheology, rational processing of colloids and polymers, and chemical product design. Polymers and colloidal dispersions are the main types of materials studied. The rheological properties are investigated alongside the characterization of these materials. This is especially important because the results of a change in flow behaviour can be catastrophic for processes [2].

The increasing demand for more efficient research and development of new polymeric materials requires the industry to analyse and adapt conventional processing and testing methods, due to the conventional methods not being adapted to very small parts. Today, the material development cycle is an exceptionally long and costly process requiring many iterations per experimental step. During a typical material development cycle, the polymer is first synthesised and then further analysed at molecular and rheological level. This allows connecting the nature of catalysts to the molecular characteristics of the polymer chains, which in turn can be connected to macroscopic parameters like melt flow. Once those relationships are established, the processing behaviour of the material should be evaluated. After the processing step, the material is tested again on molecular, thermal, rheological, and mechanical properties [3]. In quick time-to-market scenarios, going through these cycles requires using fast techniques and many of those are readily available. The most challenging of all the required steps is the polymer processing step. This is because testing the processing behaviour of new specialty materials generally requires large sample amounts and it is typically not performed on a small scale, leading to more research duration and costs, and an obvious difficulty to explore a given processing behaviour at early stages of the research [4] [5].

To accelerate the material development stage, the required amount of material used in the processing step should be decreased. A known polymer processing technique at a small scale is microinjection moulding ( $\mu$ IM). For this study, the suitability of microinjection moulding for small-scale polymer research is analysed. With this process, the polymer is melted and injected into the mould cavity under high pressure and shear rates. The material is then cooled and ejected from the mould to reach a desired shape. Some known microinjection products are mobile phone components and specialty products for the pharmaceutical sector [6]. A schematic presentation of the different parts of an injection moulding machine are presented in Figure 9.

## 1.2. Problem definition

One of the limitations of the standard polymer development cycle is the large amount of material required to evaluate polymer processing behaviour. This is due to the newly developed materials not having existing fabrication methods, leading to extremely long and often costly material production to perform experiments. To overcome this problem, the required amount of product needs to be decreased. In contrast to conventional injection moulding, very small products are manufactured with microinjection moulding, resulting in the decrease of the amount of material required to make a product. This feature makes microinjection moulding a remarkably interesting candidate to study the processing

behaviour of new, specialty materials. To achieve sustainable, small-scale processing, a complete redesign is required for each process step [6] [7].

### 1.3. Research objectives

The main objective of this research is to decrease the amount of polymer used to create a component with microinjection moulding and additionally required to perform the purge of the system. At the start of this research, around 2.0 grams of the polymer melt is needed in total to fabricate a tensile bar of 0.2 g. This translates into a material efficiency of only 10%. The goal is to decrease the total amount of polymer melt to 0.5 grams, resulting in a material efficiency of 40%. The experiments will be performed with polypropylene (PP). The aim is to decrease the amount of polymer per part with no material deterioration. To obtain repeatable experiments with zero to no material deterioration, a thorough study of the microinjection moulding process is required. Material deterioration is defined as the presence of rheological, chemical, and morphological changes in the processed polymer in comparison to unprocessed virgin material. The material deterioration will be examined via several testing techniques (DSC (crystallinity changes), rheological, mechanical), discussed in detail later in chapter 2 [6]. A visual presentation of the manufactured tensile bars and the dimensions is shown in Figure 1. The tensile bars have a width of 0.6 cm and a length of 3.4 cm. The width and length of the middle section is 0.2 and 1.6 cm.

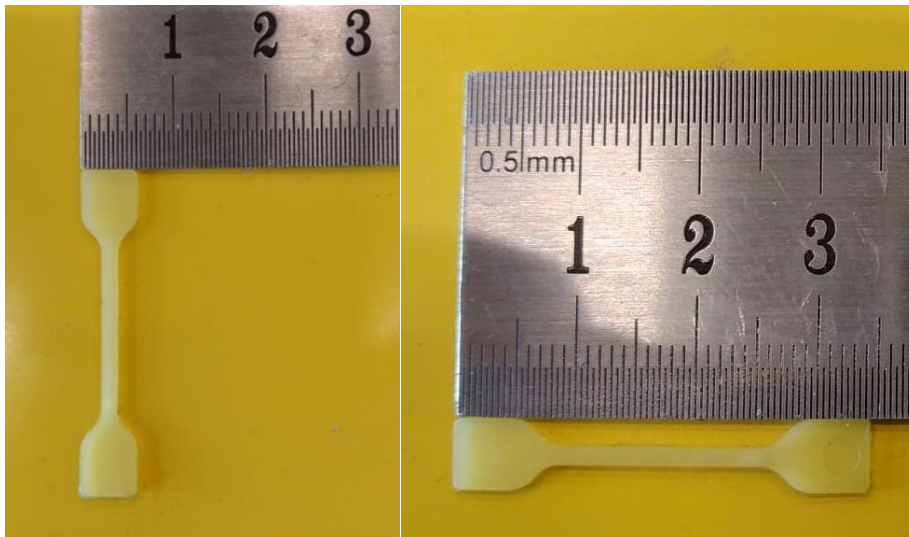


Figure 1: Tensile bar dimensions (sample weight = 200 mg).

The second objective is the decrease of the required amount of material to perform rheological tests. The development of suitable rheological testing approaches is of foremost importance to examine rheological behaviour and material deterioration. The standard rheological experiments are suitable for measuring normal-sized parts, but it is still uncertain if these tests are suitable to measure microparts and low amounts of material. To decrease the amount of material used in rheological testing protocol miniaturization is required.

The third objective envelops the examination of the existing mechanical testing methods, regarding suitability for measuring the manufactured microparts. The goal is to analyse and possibly adapt the conventional tensile and flexibility measurement methods to be suitable for microparts. The mechanical tests will be performed on the moulded small tensile bar and a conventional sized tensile bar to achieve a good comparison.

#### 1.4. Plan of approach

To improve the microinjection moulding process, it is crucial to study, comprehend, and define the capabilities, limitations, and influence parameters of  $\mu$ IM. The microinjection moulding machine that will be used, is a Fanuc ROBOSHOT-S2000i30B with a screw diameter of 14 millimetres. The experiments will be performed with polypropylene (PP). For the first objective of this research, a process window will be examined for the machine. A process window will be determined by studying the flow behaviour of the polymer melt in function of the injection speed. Here, it is the goal to examine the Newtonian region of the melt in the machine. The injection speed range of the machine is limited to only the Newtonian region, as in this region small variations in process conditions do not result in significant rheological changes in the melt, such as flow behaviour and viscosity. Generally, the range in which the Newtonian region is located for injection moulding processes is in the second Newtonian zone of the material. This is of utmost importance to reduce process variations, resulting in repeatable experiments and desired part dimensions and properties [8]. A graphical visualisation of a general viscosity curve in function of the injection speed is presented in Figure 2. The Newtonian region of the Fanuc ROBOSHOT can be derived from the higher injection speeds; moreover, from a set injection speed of 400 mm/s, the viscosity remains constant. Here, it is important to mention that the different process conditions, such as temperature and pressure influence the viscosity and thus the rheological behaviour of the polymer. As a result, the viscosity curve of the machine will be analysed before and after achieving the desired process configuration to accurately determine the process window of the system.

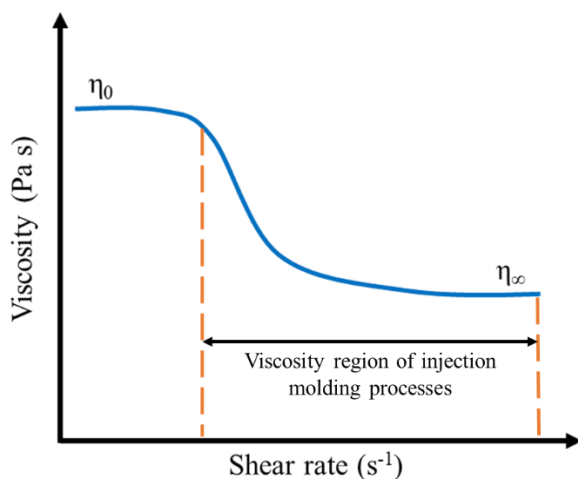


Figure 2: Exemplary viscosity curve of an injection moulding machine (typical polymeric melt behaviour (shear thinning)).

Next, the microinjection moulding process will be observed regarding the influence of the different process conditions on the material properties, part properties, and part dimensions. Here, the degree of influence of the mould temperature, the barrel and melt temperature, the injection speed, the injection and holding pressure, and the cooling time will be studied [9]. After gaining a better understanding regarding the influence of the different parameters, the following experiments will be conducted only within the Newtonian zone. For these experiments, the different parameters will be subsequently tuned to determine the optimal parameter configuration. Via this optimal parameter configuration an attempt will be made to reduce the material deterioration.

The  $\mu$ IM process will naturally lead to small-scale samples that cannot be characterized using conventional procedures. Therefore, it will be required to develop special material testing methods. However, for small scale components the mechanical and rheological testing is often limited to a small number of properties, such as tensile tests and yield kinetics for mechanical testing. Additionally, the

smaller the sample, the lesser torque it generates in conventional rheological testing methods, resulting in less accurate measurements. Generally, these measurements are lower than the actual value of the analysed sample, due to the lower generated torque from the sample. As a result, not every analysis method is applicable for such small components. This results in longer and more costly testing procedures, as no standard analysis technique is developed for small components. Today, several miniaturized testing techniques are commercially available, such as compression experiments and nano tensile testing devices for the characterization of mechanical properties. For the characterization of rheological micro scale properties is generally made use of the micro rheology testing technique. However, as indicated above, this technique is solely applicable for low-viscosity systems [4].

For this study, the rheological properties of the moulded part and virgin material will be examined via the Rotational Compact Disk rheometer from Anton Paar (MCR 302e). For these experiments, the material will be heated until molten. Next, a shear will be applied to the material by an oscillating rotational disk to analyse the rheological behaviour in function of the applied shear rate to mimic real processing behaviour of the polymer [10]. Here, the material will be examined in a range from low-to-high shear rates and vice-versa to gain a complete insight into the rheological processing behaviour of the polymer. It is important to note that oscillatory rheological measurement techniques are solely suitable for rather low shear rates. Conventional oscillatory techniques are not able to generate shear rates equal to the ones in injection moulding techniques. As a result, oscillatory techniques are primarily used to analyse the polymer structure. On the other hand, the high shear rates in injection moulding processes can be generated with capillary rheometry. It is important to note that the injection is not performed at a constant rate. The injection phase starts at high shear rates in the beginning of the mould filling. However, during the mould filling stage the injection rate and thus the shear rate is decreased in function of the injected amount of material. This is performed in order to protect the mould cavity, as well the part from deformations and overfilling.

The thermal properties of the moulded part and virgin material will be examined via differential scanning calorimetry analysis (DSC). For DSC analysis, the sample needs to be weighed very precisely before the measurement. Via the characterization of the phase transitions and melt and crystallization behaviour, it will be possible to compare the part and virgin material to each other. As a result, it will be possible to determine changes thermal properties due to microinjection moulding [11].

The difference in physical properties of the small, moulded part and conventional part size will be examined via tensile strength and flexibility testing. This is performed to analyse possible material deterioration from the microinjection moulding process regarding mechanical properties.

## 2. Theoretical background information

This chapter consists of three main topics. The first chapter discusses general information about polymers, polymer resins used for (micro)injection moulding, and the specific type of polymers used for this research. The second chapter includes information regarding conventional injection moulding, microinjection moulding, and several mould (insertion) fabrication techniques. The third chapter provides more information regarding the different used analysis techniques in this research.

### 2.1. Polymers

#### 2.1.1. Polymers used in microinjection moulding

With injection moulding, the material is exposed to extremely high shear rates during the injection phase. It is important to note that the applied shear rate is proportional to the injection speed of the melt. With injection moulding processes, it is crucial to run the process with the behaviour of the material being located in the second Newtonian region ( $\eta_{\infty}$ ). When the injection speed and thus the shear rate is set in the Newtonian region, the viscosity is independent of the applied shear rate. This can be derived as a plateau, as seen in Figure 2 for very low and high shear rates. However, when the injection speed is set to a value between both plateaus, a change in viscosity is exhibited by the melt. If the process is operated at such injection speed, ridiculously small changes in process conditions can lead to significant changes in rheological and flow behaviour, but also an inconsistent viscosity, resulting in non-uniform mould filling. This is known as shot-to-shot inconsistencies, which are highly undesired. As a result, it is crucial to analyse the Newtonian zone (and thus the injection rate – shear rate) of the injection moulding process. The effect of the shear rate has proven to be more significant on the viscosity in comparison to the temperature. The development of the viscosity curve of a moulding machine is furtherly described in 3.7 (materials and methods) [8]. Proper characterization of the flow behaviour is likely to require sophisticated and versatile instrumentation. To fully characterize a material, instrumentation is required which has the capability of extracting these parameters over a range of temperatures and shear/extension rates. Such instrumentation is described later in Chapter 3.

In general, plastics are classified into three categories: thermoplastics, elastomers, and thermosets. These three categories are based on the physical properties and the macromolecular structures of plastics. Thermosets are identified by their hard elasticity. Contrary to thermosets, elastomers display a soft elasticity. However, both thermosets and elastomers are not processed in this research and will not be furtherly discussed. Thermoplastics can be divided into two subcategories: semi-crystalline or amorphous. A semi-crystalline resin consists of ordered macromolecules, embedded with crystalline phases. Amorphous resins can be recognized by statistically distorted macromolecules. Thermoplastics are known to soften when heated and harden when cooled. To perform microinjection moulding experiments is made use of semi-crystalline, thermoplastic polyolefins, mainly isotactic homopolypropylene [12]. Overall materials can be divided into two categories: Newtonian and Non-Newtonian fluids, based on the viscous behaviour and applied shear rate. Newtonian fluids show an independency of the viscosity to the shear rate. The viscosity is not influenced by the shear rate. In contrast, non-Newtonian fluids show a change in viscosity when a shear rate is applied [8] [13].

Non-Newtonian fluids can exhibit two types of behaviour under applied shear: shear-thinning (pseudoplastic) or shear-thickening (dilatant). Important note, most liquids and melts exhibit shear-thinning behaviour. Shear thickening generally occurs at significantly high shear rates in combination with a high particle volume fraction material. Shear-thinning behaviour translates to the melt displaying a constant viscosity at incredibly low shear rates (zero shear viscosity ( $\eta_0$ )) and very high shear rates (infinite shear viscosity ( $\eta_{\infty}$ )). Nevertheless, when the shear rate is set between both Newtonian regions, the melt exhibits non-Newtonian rheological behaviour and a large drop in viscosity is exhibited. The

region in which the viscosity drop occurs is referred to as the shear-thinning region of the melt [14]. The beginning of this region is known as the critical shear rate. Shear thinning behaviour is influenced by the rearrangement of micro-structures in the plane of applied shear. At very low shear rates, the arrangement of the melt is randomly, leading to molecular and particle interactions, as well Brownian motion effects. These interactions and effects result in a high zero-shear viscosity of the melt. These effects can be negated with increased shear rates, leading to the rearrangement of layers. The melt is able to stretch and to be oriented into the flow direction. Through these aggregated structures and destroyed droplets, the amount of free space is increased and the amount of interactions is decreased, translating into a large viscosity drop. The infinite shear viscosity is related to the maximum achievable amount of melt orientation, also known as the minimum achievable viscosity of the melt. It is important to note that the infinite shear viscosity is majorly influenced by the hydrodynamic forces and the viscosity characteristics of the solvent or melt [13][15].

A visualisation of the viscosity in function of the shear rate, as well the shear stress in function of the shear rate is presented in Figure 3 for (Non-)Newtonian fluids. All plastics are considered non-Newtonian, but the rheological behaviour of polymeric melts is a combination of both Newtonian and Non-Newtonian [8].

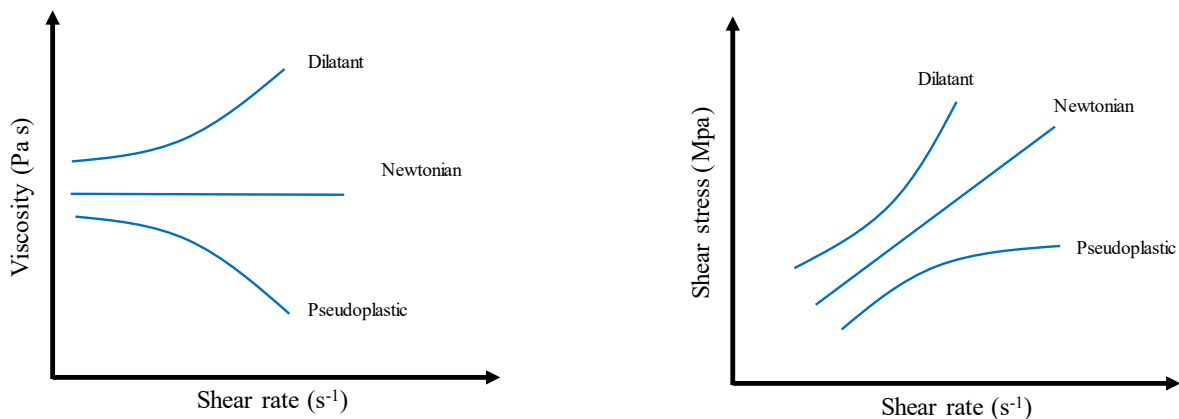


Figure 3: Viscosity and shear stress in function of the shear rate for (Non-)Newtonian fluids.

Most shear-thinning fluids and melts exhibit the affinity to revert to their original viscosity ( $\eta_0$ ) when no shear rate is longer applied. This behaviour is described as the thixotropic behaviour of shear-thinning fluids and melts and is considered to be time-dependent. The time-dependency is a result from the rearrangement of structures taking place step by step when the applied shear is changed. Important note, thixotropic materials are always shear-thinning materials. The thixotropy of a fluid or melt is generally measured via a three-step shear or oscillatory testing. With three step shear tests, the measurement is initialized by setting a low shear rate to mimic the resting behaviour of the sample. Next, a high shear rate is employed for a certain amount of time. This is performed to mimic the breakdown behaviour of the structure of the sample. Lastly, the shear rate is decreased to the low shear rate of the beginning of the test. Via this step it is possible to analyse the thixotropic behaviour of materials in function of the time. Generally, the material is analysed based on the required time to regain 90% of the original zero-shear viscosity. Here, a small recovery time translates to a less thixotropic material. With oscillatory tests it is able to measure both sides of the applied shear rate range. This makes it possible to analyse changes in the elastic structure of the material in function of the time. The elastic behaviour of the material is generally presented as  $G'$ , also known as the storage modulus [13] [14]. A graphical presentation of a general three step thixotropy test is presented in Figure 4.

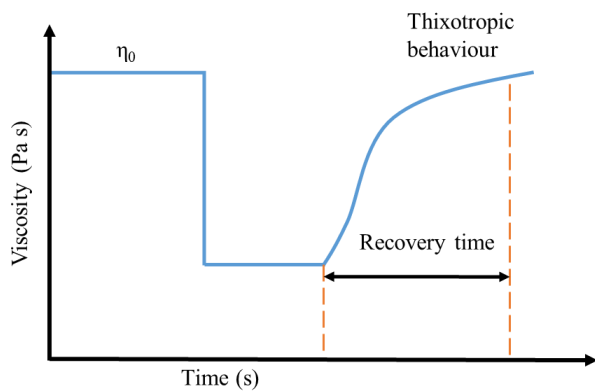


Figure 4: Typical three step thixotropic test.

Polymeric melts are generally characterized by viscoelastic behaviour. As the name implies, these materials exhibit both characteristics of viscous materials (fluids) and elastic materials (solids). The viscoelastic behaviour is generally measured via several rheological techniques, such as: oscillatory, stress-relaxation (thixotropy), and creep testing. Oscillatory testing techniques are majorly used to analyse the viscoelastic behaviour of materials. The utilized machines for these oscillatory tests are rotational rheometers, discussed later in 2.4.1. The elastic behaviour of melts is described as the energy stored in the structure of the molecules from applying a certain deformation. When no force or shear is applied to the melt, the amount of energy stored in the structure is minimal, also known as the equilibrium energy state. When a force or deformation is applied to the melt, the structures will shift from the equilibrium, resulting in an elastic force within the structures to revert back to the equilibrium state. The shear elastic deformation is generally described with a constant  $G'$ , also known as the elastic or storage modulus.  $G'$  is related to the resistance to deformation of the melt. It is important to note, ideal purely elastic melts show an independency to the time as an instantaneous strain would be derived from the moment stress is applied to the sample. Vice-versa, the strain instantly disappears the moment the stress is removed from the sample. The loss modulus ( $G''$ ), also known as the viscous modulus describes the rate of deformation when a certain stress is applied to the material. Viscoelastic materials show a combination of both storage and loss moduli, which both influence the rheological behaviour. At certain strain rates the melt will exhibit more viscous behaviour, and at other strain rate more elastic behaviour [13]. A visual presentation of a typical viscosity curve for polymeric melts is presented in Figure 5.

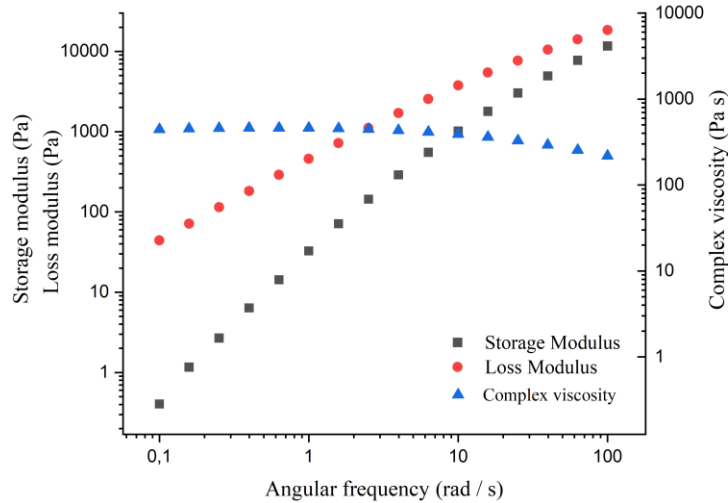


Figure 5: Typical viscosity curve of polymer melts.

As can be derived from Figure 5, both  $G'$  and  $G''$  increase with increasing angular frequency. It can be seen that the slope of the storage modulus is higher than the slope of the loss modulus, as both curves almost seem to cross at 100 rad/s. The slopes of both moduli are of utmost importance to characterize rheological properties of the analysed sample. The point where both curves cross, is known as the crossover point. Generally, the angular frequency of the crossover point corresponds to the longest possible relaxation time of the material, as result of the frequency dependency of the moduli. In addition, it can be derived that the viscosity decreases with increasing angular frequency. This is in direct relation to the distance between both moduli. The closer the storage modulus is to the loss modulus, the less viscous and the more elastic the material becomes. The viscosity is of utmost importance to enhance the processing behaviour of polymeric materials. Generally, the Cox-Merz equation (1) is used in combination with dynamic mechanical measurements to describe the relation between the complex viscosity ( $\eta^*$ ) and the angular frequency [16]:

$$|\eta^*| = \frac{|G^*|}{\omega} \quad (1)$$

For analytical purposes, the phase angle ( $\theta$ ) between both moduli is expressed to take the difference in both moduli into account.  $\tan(\theta)$ , also known as the loss factor, is analysed to gain a better understanding of the material behaviour. The phase angle is in tangential relation to the division of the loss and the storage modulus (equation (40)). From Figure 5 can be seen that for most polymeric materials the tangential of the phase angle decreases when the angular frequency is increased. From dynamic mechanical measurements, the plateau modulus ( $G_N^0$ ) can be determined. The plateau modulus displays the fully elastic, unrelaxed response of the material as a result from an induced flow transition.  $G_N^0$  is considered to be a frequency-independent storage modulus and can be expressed with equation (2). With this equation it is possible to calculate the molar mass of the filaments between crosslinks of the material [16] [17]. In practice the plateau modulus is of utmost importance due to it being one of the main characteristics for each polymeric material. But it is important to note that the temperature is of major influence on the rheological properties of a polymeric material (discussed in 2.3.1 (WLF)). The plateau modulus is a remarkably interesting material constant, which indicates the molecular structure of the analysed sample and is mainly influenced by the molecular entanglement weight ( $M_e$ ). Additionally, the plateau modulus is influenced by the molecular chain dimensions (e.g., gyration radius) [17].

$$G_N^0 = \frac{4 \rho RT}{5 M_e} = G'(\omega)_{\tan(\theta)_{min}} \quad (2)$$

It is important to note that thermoplastics generally show a very distinct plateau when the molecular weight distribution (MWD) is very low. Generally, the division of  $M_w$  to  $M_n$  is equal to approximately a value of 1 for very distinct plateaus. In this case, it is possible to estimate  $G_N^0$  by the value of  $G'$  obtained at the angular frequency resulting in the minimal value of the  $\tan(\theta)$  [16]. The  $M_n$  is the number average weight for a molecular blend, calculated with equation (3). Here,  $x_i$  is the fraction of total amount of chains and  $M_i$  is the molecular weight of a specific chain or a range of chains. On the other hand,  $M_w$  is the weight average molecular weight, calculated with equation (4). It is important to note that  $w_i$  is the weight fraction of the chain, not the numerical fraction as with equation (3) [18]. From Fujiyama et al. was concluded that for PP, a broader MWD resulted into a lower material melt flow index and higher shrinkage values in the flow direction. In the transversal direction of flow, the shrinkage behaviour remained constant at approximately 1.6% [19]. The material shrinkage behaviour is furtherly described in 2.3.5. MWD and molecular weight are especially important material characteristics, which majorly influence the material processability, as an example: the melt viscosity is greatly influenced by the molecular weight and distribution. A lower molecular weight or  $M_w$  result in a decrease of the melt viscosity, highly affecting the melt behaviour inside the injection moulding process [20].

$$M_n = \Sigma x_i M_i \quad (3)$$

$$M_w = \Sigma w_i M_i \quad (4)$$

To analyse the elastic portion of the material resulting from an applied deformation, creep tests are performed. With creep tests, a deformation is applied to the sample and subsequently removed. When the applied deformation is removed, the material will recover to its original state. Via analysing the recovery behaviour of the material it is possible to determine the elasticity of the material. Additionally, after obtaining the creep compliance of the material it is possible to calculate the zero-shear viscosity. This makes creep tests an interesting technique to analyse rheological properties. This is because via the analysis of several rheological properties such as the zero-shear viscosity, it is possible to examine several molecular properties of the material (e.g., molar mass, molar mass distribution, and long-chain branching) [16]. It is important to note that syndiotactic and isotactic PP (discussed furtherly) display the same degree of dependence regarding the zero-shear viscosity in relation to the molecular weight. However, generally the viscosity of syndiotactic PP can be ten times higher than the viscosity of isotactic PP, as resulted from a previously performed study [17].

Another important material characteristic is the glass transition point ( $T_g$ ) of the material. At this glass transition temperature an amorphous material shifts from being glassy and brittle to being more elastic, rubbery. This is due to the molecular rotation of single bonds being enhanced with increasing temperature, resulting in a rubbery-like material. On the other hand, crystalline materials do not exhibit one melting point, but rather a temperature range in which the material melts as result from their morphology (crystalline and amorphous regions (2.3.5)). The  $T_g$  of a material is influenced by several factors: the structure of the polymer (the presence of functional groups and branches (steric hindrance)), chain flexibility, intermolecular bonds, tacticity, and molecular weight. The presence of functional groups and branches results generally in steric hindrance. As a result, more energy is needed to generate molecular rotations, translating into an increased  $T_g$ . Logically, chain-backbone flexibility also majorly influences the  $T_g$ . An increased flexibility results in a lower  $T_g$ . The presence of intermolecular bonds (e.g., hydrogen bonds) causes an increase in the glass transition temperature, as more hindrance to the rotational movement is displayed. The tacticity of the chains is of utmost importance. Generally,

syndiotactic polymers display the highest  $T_g$ . On the other hand, isotactic polymers exhibit the lowest  $T_g$ . Lastly, the molecular weight has a crucial influence on the  $T_m$ , but no influence on the  $T_g$ . As mentioned prior, an increase in the molecular weight results into a higher melt viscosity. This translates into a more difficult rotational molecular movement, and thus an increase in the glass transition temperature [18] [21]. The isomeric structures of polymers (PP) are furtherly discussed in 2.1.2.

#### Enhancement of polymer melt

The mechanical properties of a polymer resin can be enhanced with the addition of filler components. But when using micro-moulding injection, traditional fillers, such as carbon fibres and glass are not applicable. The reason traditional fillers are not useable is that the small feature dimensions present in the mould cavities are too small for the fillers to penetrate. This translates to non-uniform rheological and optical properties of the product, located at these small feature dimensions, in comparison to the rest of the polymeric product. For microinjection moulding are nanofillers utilized, such as carbon nanotubes, polyhedral oligosilsesquioxanes (POSS), and exfoliated clay platelets. This specific type of filler is able to fully penetrate the micro mould cavities [22]. The polymer melt can also be coloured via the addition of pigments and altered with fibre reinforcements. The effects of fillers, pigments, and fibre reinforcements are further discussed in 2.3.5 [23].

### 2.1.2. Polypropylene (PP)

PP is known to be one of the leading plastics globally due to its significant mechanical properties, thermal and chemical resistance, versatile processability, and being a colour-free substance. Additionally, PP has the lowest material density among other plastics and is a relatively low-cost material. As a result, PP is used in a variety of applications, such as bottles, funnels, cleanroom and clinical appliances, door liners, etc [12]. In 2008 alone, the entire polypropylene market amounted to an estimated 245 million tons produced [24]. As mentioned prior, the characteristics of PP are influenced by the molecular weight of the polymer chain, the tacticity, and the grade of the structure. The tacticity of the structure has a major impact on the viscosity, which alters the physical and chemical properties of polypropylene. The structure of polypropylene can be divided into stereo-specific configurations: isotactic, syndiotactic, and atactic, presented below in Figure 6, Figure 7, and Figure 8. The polypropylene structure can be identified as a vinyl polymer bound to a methyl group [12] [25] [26].

The isotactic configuration of iPP has proven to be the most stable isomer of PP. As the methyl groups are bound to solely one side, steric hindrance averts the structure to crystallize in a zig-zag shape. IPP is known to crystallize in a more helical shape. As a result, the softening temperature of iPP is higher in comparison to the other two isomers. A higher softening temperature of a polymer translates to a higher melt viscosity. However, iPP is more susceptible to thermal and chemical degradation, compared with the other isomers. Nevertheless, iPP entails 90 – 95% of the total amount of PP produced [26].

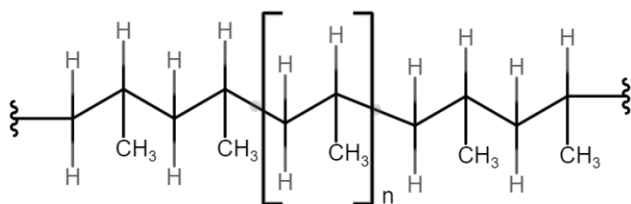


Figure 6: Molecular structure of isotactic polypropylene (iPP).

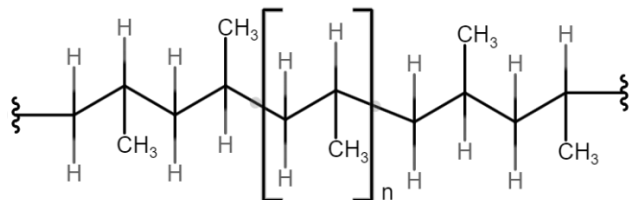


Figure 7: Molecular structure of syndiotactic polypropylene (sPP).

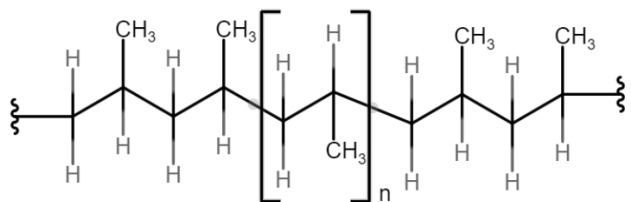


Figure 8: Molecular structure of atactic polypropylene (aPP).

Polypropylene is mostly manufactured through the Ziegler-Natta catalysed (e.g., titanium chloride) polymerization of olefin propylene monomers. PP (generally propylene gas) is polymerized in combination with a catalyst (Ziegler-Natta or metallocene), heat, and radiation to bind the monomers to form long chains [26] [27]. PP polymerization occurs through chain-growth polymerization in combination with the Ziegler-Natta catalyst; moreover, via head-to-tail incorporation of the PP monomers. Here, the head (active centre, C<sup>+</sup>) binds to the tail (CH<sub>2</sub>) of an unreacted propylene monomer. PP can be produced through four different pathways, such as bulk polymerization, gas-phase

polymerization, solution polymerization, and suspension polymerization [18] [26]. However, there are three distinct types of PP manufactured industrially. The first type of PP contains solely propylene monomers in a solid (semi-crystalline) form, also known as homo-polymer polypropylene (HPP). HPP is characterized as a two-phase system, with non-crystalline (amorphous) and crystalline zones in its structure. Important note, amorphous zones consist of both iPP and aPP, where the iPP will slowly crystallize. This translates to HPP almost completely consisting of iPP units along the chain. As a result, HPP exhibits a high melting point and stiffness but low transparency and impact strength. Today, HPP is the leading PP material for industrial and commercial uses, embodying 65 – 75% of the total market share [28].

The second type of PP is characterized by the implementation of a co-monomer in the PP chain. This type of PP is also known as random copolymer polypropylene (RCP). The utilized co-monomer is generally ethylene, which is present in the chain for 1 – 8% of the total weight. Here, the presence of ethylene decreases the uniformity of crystallinity in the structure, resulting in a lower crystal thickness. Additionally, the melting point also decreases. RCP structures are known to display improved impact strength and flexibility, but also a lower melting point. The third type of PP is known as impact copolymer (ICP) polypropylene. ICP is a mixture of HPP and RCP (approx. 40 – 65% ethylene). For ICP, the amount of ethylene embodies between 6 and 15% of the total polymer weight. ICP, preferably used at low temperatures (-20 °C), shows the highest impact resistance and decent stiffness. Important note, the impact resistance of ICP varies based on the distribution, shape, and size of the RCP particles used, also known as rubber particles. A general overview entailing the advantages and disadvantages of PP is presented in Table 1. The mechanical and thermal characteristics of PP, as well as a comparison between iPP and sPP, are presented in Table 2 [29] [28] [30]. These different properties are used during and after experiments to perform the necessary calculations, described in the next paragraph.

Table 1: Advantages and disadvantages of polypropylene.

	PP-type	Processability	Impact resistance	Stiffness	Food contact	Market share (%)
Advantages of polypropylene	HPP	Good	Good	Good	Acceptable	65 – 75
	RCP	High	High	Highest	Not preferable	5 – 10
	ICP	Highest	Highest	Lowest	Not preferable	20 – 30
Disadvantages of polypropylene		<ul style="list-style-type: none"> <li>• UV-degradation</li> <li>• Flammable</li> <li>• Degradation by chlorinated solvents and aromatics</li> <li>• Difficult to bond</li> <li>• Oxidative degradation is accelerated by metals</li> <li>• Poor low-temperature impact strength</li> </ul>				

Table 2: Mechanical and thermal properties of commercially sold polypropylene types (Novolen – Targor GmbH).

Property	HPP 1148TC	Random copolymer 3348SC	Block copolymer 2600TC
Melt flow ratio (g/10 min)	48	30	48
Tensile yield stress (MPa)	35	23	19
Tensile modulus (MPa)	1550	820	950
Haze (%)	60	7	95
Impact strength (23 °C) (kJ/m <sup>2</sup> )	103	No break	No break
Impact strength (0 °C) (kJ/m <sup>2</sup> )		190	170
Impact strength (-20 °C) (kJ/m <sup>2</sup> )		50	150

	Homo-iPP	Homo-sPP
Thermal conductivity (W/mK)	0.17	0.17
Available energy (MJ/kg)	46	46
Melt temperature (°C)	163	168
Crystallization grade (%)	40 – 60	30 – 40
Specific weight (g/cm <sup>3</sup> )	0.90 – 0.91	0.9 – 0.91
Tensile strength (N/mm <sup>2</sup> )	21 – 37	/
Elastic modulus (MPa)	16.5	61
Impact strength (-23 °C) (kJ/m <sup>2</sup> )	16	80
Opacity (%)	85	1.7

## 2.2. Injection moulding

In this chapter, an overview of injection moulding (IM) and microinjection moulding ( $\mu$ IM) is discussed. In the production of plastic parts, thermoplastic polymers are commonly used. They are known for their wide range of applications due to their unique characteristics regarding mechanical, thermal, and electrical properties. IM, also known as injection moulding, is the method mostly used to fabricate plastic components. The components made through IM vary from computer components to medical equipment [6]. Microscale and small parts have become increasingly popular in recent decades. As a result, the relevance and value of microsystems and miniaturization have increased. With the use of micro-scale processes, the process compatibility is improved, resulting in an expansion of materials and geometric forms which can be processed. Microinjection moulding ( $\mu$ IM) is the transmission of features in the (sub)micron range from a metal mould to a polymer melt [7]. IM is one of the leading processes, due to the comparably low production costs and ability to produce enormous quantities. Because the  $\mu$ IM process has proven to be widely applicable for moulding microparts, the demand for the improvement and research of  $\mu$ IM processes has also grown.

There are several types of injection moulding machines, based on the type of power source used: hydraulic, electrical, and a combination of both (hybrid). For this research, the Fanuc ROBOSHOT S-2000i30B injection moulding machine is used to perform experiments, as mentioned prior. This machine operates completely electrical. Electrical machines provide several advantages in comparison to hydraulic machines: electrical machines have proven to be faster and more precise in operation. Additionally, the power consumption is lower for electrical machines, as only electricity is consumed while operating. Hydraulic machines consume much more energy, due to the need of maintaining the hydraulic pressures at all times and cooling of the material. In comparison to hydraulic systems, the electrical systems require on average 33 – 40% of the amount of kWh to produce the same part and cools by nature. Additionally, that same part is produced 33% faster in comparison to the hydraulic system. Electrical machines also display a smaller start-up time, as there is no oil present in the system that needs to be heated, prior to operation. Last, the maintenance of electrical machine is easier and less frequent, as there is no risk of leakages. As a result, the use of an electric injection moulding machine provides a decrease of 50 to 70% in operation costs in comparison to the hydraulic alternative. To adjust and control the process conditions during operation, the machine is provided with a touch-screen control panel, as presented in Figure 20 ( 3.1)[31]. The disadvantages and advantages of both electrical and mechanical systems are presented in Table 3.

Table 3: Comparison between hydraulic and electrical injection moulding systems [31] [32].

System	Advantages	Disadvantages
--------	------------	---------------

Hydraulic	Lower construction cost	High consumption of electrical energy
	Higher energy delivery ≈ higher injection pressures	Degradation of viscous characteristics of oil after 9000 work hours
	Min. – Max. die height (= total mould height when closed)	High maintenance costs
		Negative environmental impact from oil replacement
Electrical	Consumes 50-55% less amount of electrical energy	Higher investment costs
	Greater efficiency	Extraordinary maintenance in case of motor failure
	Greater repeatability	Lower energy delivery
	Reduced noise	
	Shorter injection times ≈ shorter cycle times	
	Better product quality	
	Smaller start up time	

An injection moulding machine consists of two major systems: the injection unit and the closing unit of the machine, graphically presented in Figure 9. The injection unit consists of a motor, which powers the screw ram. The screw ram is implemented with a cylinder to limit the movement of the screw from a certain, fixed point inside the barrel. Without the cylinder, the screw would be able to move too far forward, with an increased risk of equipment breakage. The screw is implemented with grooves through which the polymer melt is transported as the screw rotates. The injection unit is also provided with a hopper in which the polymer pellets are deposited. The hopper is placed on top of the barrel. The barrel of the injection system is heated via multiple heating elements. After flowing over the screw, the melt will go through a nonreturn valve-system to ensure no fallback of the material inside the injection unit. The last component of the injection unit is the nozzle, through which the melt is injected into the mould.

The closing unit of the process consists of the actual mould and the clamping unit. The mould is placed inside the clamping unit. The mould consists of two mould halves, both fixed opposite to each other in the clamping unit. Additionally, the mould is equipped with an injection hole, through which the polymer melt is injected. The clamping unit consists of stationary and moveable plates. The injection hole of the mould is fixed between these stationary plates, as the mould preferably does not move mid-injection. Between the stationary and moveable plates are four tie rods. These tie rods make it possible for the moveable plates to move towards the stationary plates in a coordinated way. The result of this movement is pressing both mould halves onto each other. To generate high clamping pressures, the unit is equipped with a clamping cylinder and crosshead to apply the desired pressure uniform over the mould. Last, the clamping unit is also equipped with an ejector mechanism to expel the cast mould shape from the mould.

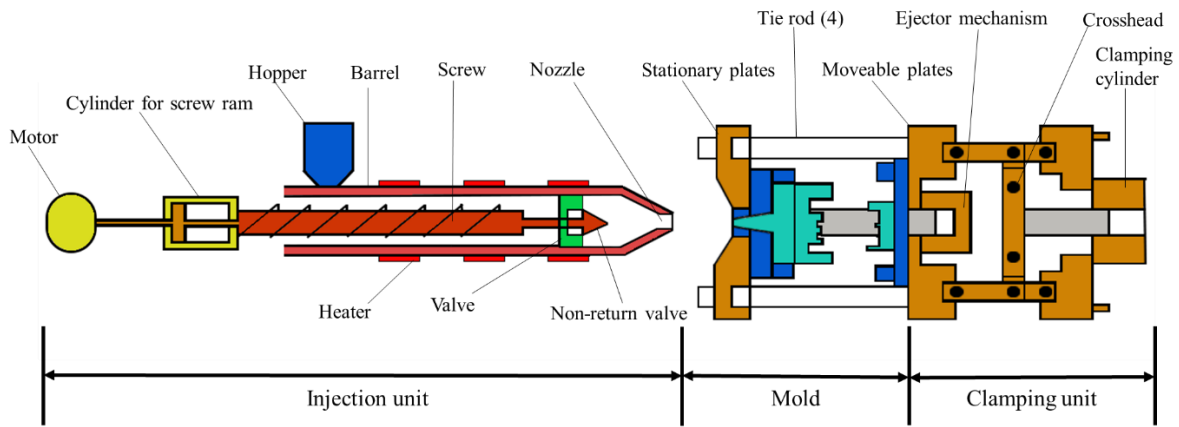


Figure 9: Schematic overview of an electrical injection moulding machine.

In general, the IM process consists of four main steps. First, the material is deposited into the hopper in the form of granules. Next, the material is transported to a plasticizer, where the material is molten and transported by the screw. Because the plasticizer is an independent system, a limitation of cycle times is permitted. Prior to the injection step, the mould is closed with pressure (clamping force) sufficient to prevent the mould from opening during the injection step. After the material is molten by the heated barrel, it is forced by a plunger through runners and gates, via a nozzle, inside a metal mould chamber and kept under high pressure. The moulding systems are divided into two categories: hot and cold runner moulds, described furtherly in this chapter. For conventional IM, a fixed temperature for the mould is applicable for temperatures lower than the glass transition temperature ( $T_g$ ) of the polymer. It is important to note that the mould temperature increases in relation to increasing aspect ratio of the mould. This translates into a microinjection process utilizing a mould temperature above the mould temperature of conventional IM. To obtain high aspect ratio micro characteristics, the temperature of the mould is generally kept close to the glass transition temperature of the polymer [6] [7]. During the injection step the melt will increase in temperature as it flows through the runners and gates. The reason for this is that while flowing through the runners, frictional energy is generated, resulting in an increase in temperature [33].

For a certain period, the polymeric melt is continuously exposed to the high pressure in the mould cavity, known as moulding-holding. In the injection step, around 98% of the required polymer is injected into the mould. This is done to compensate for the shrinking of material when cooled in the mould. While the melt is cooling under high pressure, the final amount of required material to completely fill the mould is dosed by means of the high holding pressure. When the melt has cooled down to a solid state, the polymer is extracted from the mould shape, this stage is known as the demoulding phase [6] [7]. A schematic overview of an elect injection moulding machine is presented in Figure 9, alongside the process cycle (Figure 10). The process cycle will be furtherly discussed in next chapter, alongside the process conditions and calculations suitable for each process step.

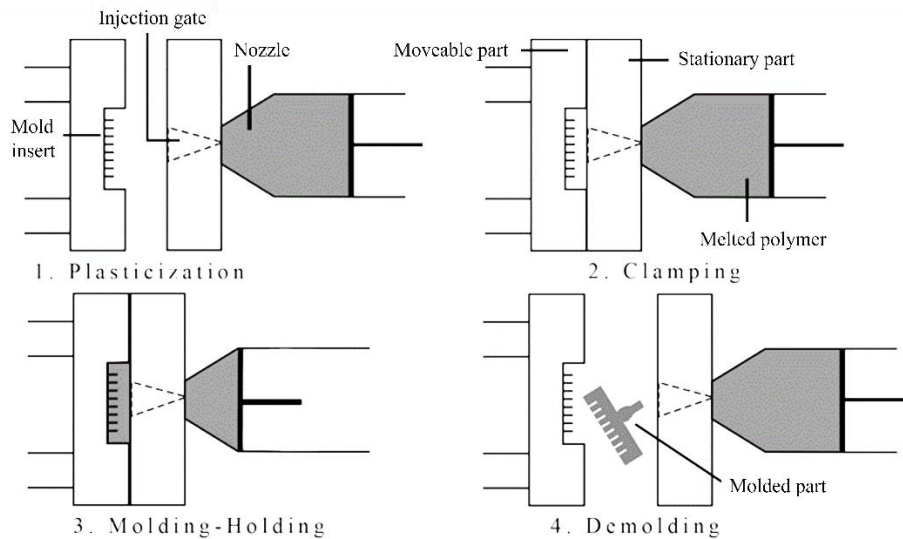


Figure 10: General injection moulding process steps.

From previous studies was concluded that the mould temperature is a crucial parameter to manufacture microparts [6]. The temperature of the mould can be controlled via two different methods: a fixed or a varying mould temperature. The variation of the mould temperature is also known as a variotherm process. In contrast to IM, microinjection moulding is performed with a mould temperature close to or above the glass transition temperature of the polymer. This is done to prevent short shots in the process. A variotherm process allows the reduction of both injection speed and injection pressure [6]. However, this does not apply to the actual polymer resin temperature during the plasticization phase. To properly melt the polymeric material, usually a much higher temperature is set to ensure complete melting of the polymer [34]. A visual presentation of the temperature profiles of variotherm and conventional injection moulding are given in Figure 11.

With a variotherm microinjection moulding process, the mould temperature is varied in the course of the melt injection cycle. Because the mould temperature is varied, a dynamic mould temperature control strategy needs to be utilized and is variotherm injection moulding also known as rapid thermal response (RTR) moulding or rapid heat cycle moulding (RHCM). With variotherm processes, the mould is heated to the glass transition temperature of the polymer, prior to injection in the mould cavity. While the mould is being filled, the temperature of the mould is kept above the  $T_g$ . This is done to eliminate the formation of a frozen layer near the mould cavity walls. Additionally, the flow behaviour of the melt improves from a temperature above  $T_g$ . At the end of the injection, the mould is cooled rapidly to the injection temperature of the melt. This is executed to solidify the melt and prepare the moulded part for the demoulding step. Next, the part is ejected from the mould. Now the mould is ready to be heated again for the next injection cycle. For variotherm processing, the heating and cooling power are major influences for the cycle time and/or the injection moulding efficiency [34]. The advantages and disadvantages of a variotherm process are presented in Table 4 [6] [35].

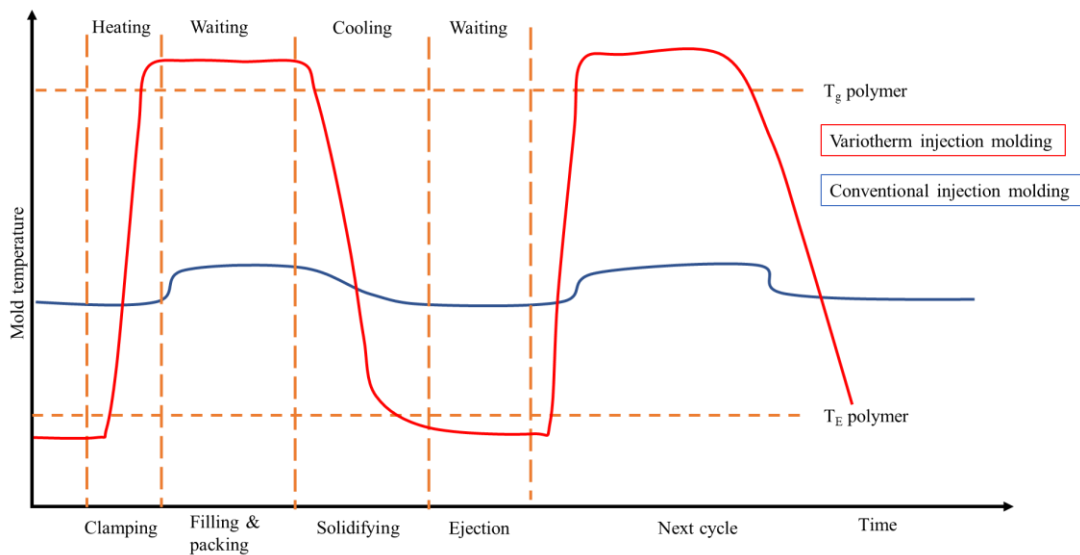


Figure 11: Variotherm and conventional injection moulding temperature profiles.

Table 4: The advantages and disadvantages of a variotherm process in comparison to a fixed temperature.

Advantages	Disadvantages
Prevents material degradation via a decrease in injection conditions	Increase in cycle time
Better control of cooling of the material	Increased mould degradation due to T-variation
Lower internal residual stresses	Process is still in development
Prevention of weld lines	
Prevention of short shots	

To successfully implement a variotherm system, the required cooling and heating power need to be determined, as well as the influence of the mould geometry and the cost. Today, the most effective variotherm solutions entail heating through induction or a gas flame. However, the implementation of a variotherm system is extraordinarily complex and delicate. Additionally, not every technique has the possibility to both heat and cool. Induction heating is the most viable method, as the entire material is heated. The gas flame method is only able to heat the surface of the mould, resulting in non-uniform heating of the resin. As previously mentioned, non-uniform heating of the resin is highly undesired, as it leads to poor material properties. Today, induction heating is used on an industrial scale for the fabrication of composite parts. However, for small and medium-scale applications, the used approaches are oil circulation, infrared heating, or electrical heating, disregarding the longer cycle time. Table 5 is a general overview of different systems to develop microparts [6]. Important note, another ground-breaking technique is becoming more interesting for commercial purposes, which is known as ultrasound injection moulding. Ultrasound injection moulding, moreover, ultrasonic plasticization microinjection moulding (UP $\mu$ IM) will be furtherly discussed in chapter 2.3.8.

Table 5: Systems for variotherm micro mould applications.

Heating equipment	Cooling equipment	Cycle time (s)	Temperature (°C)	profile	Tool surface (mm)
Gas flame	No	10	20 → 400		100 x 100 x 30

Rapid thermal response mould	No	11	20 → 250 → 50	72 x 25.4 x 12.7
Proximity heating (Induction system)	Air pockets	14	20 → 220 → 90	24.3 x 51
Electrical system	Water circulation	30	20 → 205 → 32	/
Infrared halogen lamp	No	20	20 → 208	180 x 180
Induction heating coils	Cold oil circulating system	/	/	7 x 4 x 0.05
Oil/electrical system combination	Water circulation	/	/	/
Special surface coating	Coolant circuit	/	/	/
Peltier device	Peltier device	Difficult T-control from power and response time		/

As said previously, frictional energy is generated between the melt and runners during the injection stage and the different mould systems are divided into two categories: hot and cold runner systems. The main purpose of the runners is to navigate the melt from the sprue to the mould cavity. But to be able to push the melt through the small runners, an extra amount of pressure is required. When small runners are used, the material efficiency will increase, as material wastage is decreased. However, via implementing small runners a larger injection pressure is required to push the melt into the mould cavity. On the other hand, large runners result in a lower required injection pressure. However, large runners lead to more material wastage, more frictional energy (requiring longer cooling time), and more required clamping force. These factors all make a proper runner and mould design of utmost importance. A proper runner system design leads to several advantages: minimalized material waste, easy injection, efficient energy consumption, proper melt-to-cavity transport, controlled cycle time, and balanced and proper filling of multiple cavities and multi-gate cavities [33]. The Fanuc ROBOSHOT is implemented with a cold runner mould, but to give proper insight into mould design, both runner types are furtherly discussed below.

Hot runner moulds, also known as runnerless moulds or hot-manifold moulds, are implemented with several temperature controlling devices. These temperature devices are in fact heating units, implemented to ensure the temperature of the runner is above the melting temperature of the injected polymer. This is done to uphold the molten flow in the runners and prevent blockage of the mould system. A hot runner mould is made up of a manifold system and multiple heated nozzles. The entire system is kept between two plates, which are heated by the manifold system. The manifold system is located inside one of the plates and directs the molten flow into the multiple heated nozzles. The use of hot runner systems provides several advantages: amazingly fast cycle time, increased component quality and repeatability, less waste in comparison to cold runners, very suitable to fabricate large parts, lower injection pressure, and more precise process control. Important note, two distinct types of hot runner systems exist: insulated and heated runners. Insulated runners are non-heated hot runners but ensure that the melt does not solidify in the runners. It is a low-cost solution, very suitable for colour changes, and ensures the same gate flexibility of a heated variant. However, insulated runners require significantly thick runner channels and large passages in the mould plate. This leads to lower applicable injection speeds and insulated runners not being suitable for a variety of materials [33].

The second type of hot runner system are the heated runners. Heated runners can be heated externally or internally. Generally, the heating is performed via coils, cartridges, heating rods, heating pipes, and heater bands. Externally heated runners make use of a cartridge-heated manifold system to swap cooled and hot manifolds cycle-wise. The use of a cartridge-heating system requires a highly insulated manifold

to decrease heat loss. The use of an externally heated runner system provides the lowest pressure drop of any runner system and is also the best method to perform colour changes. This is due to the colour being unable to solidify in the runner system. Additionally, the use of an externally heated system eliminates the sticking and deterioration of material to the heater surface, as it does not come into contact with any material. Internally heated hot runner systems are generally heated by a torpedo and probe in the passages. The heat loss is reduced by making use of the insulating effect of the polymer melt. However, internally heated hot runner systems are not suitable for heat-sensitive materials. This is due to the system requiring a higher moulding pressure, but also displaying difficulties with material deterioration and surface-stick. Additionally, internally heated runners are not suitable for colour changes [33].

Cold runner mould systems consist of two or three plates, all kept within the mould. Here, the polymer melt is injected into the mould cavity via a sprue and runners. The simplest design is the two-plate design in which both plates are separated by a parting line. When a part is made with a cold runner the sprue will be connected to it, leading to an excessive amount of wastage when fabricating small parts. For this study is made use of a two-plate mould design to fabricate small tensile bars. With the three-plate design, the mould will disconnect in three sections for the ejection of the part. With this separation, only the part requires ejection due to the runner being connected to a separate plate. This allows to simultaneously disconnect the sprue from the part, leading to a less intensive part production process. However, both cold runner mould types result in an extensive amount of material wastage due to the sprue, leading to the need of a recycling or regrinding step. This translates into an increased cycle time and material wastage in comparison to hot runners. But it is important to also mention the benefits of using a cold runner mould system: a low-cost production and maintenance, a suitability for a wide range of polymers, fast and easy colour changes, and improved cycle times for robotic systems. [33].

### 2.3. Microinjection moulding

Microinjection moulding encompasses the production of 3-dimensional parts in the sub-milligram masses and/or micro-scale surface characteristics.  $\mu$ IM has proven to be very suitable for the large-scale production of microscale complex components (>1000 parts per series) in combination with being widely applicable for several types of material, such as metals, ceramics, nanocomposites, but also polymers. Additionally,  $\mu$ IM has significantly low costs in comparison to other moulding techniques, such as batch processes (etching, lithographic techniques) and self-assembly of polymer structures [22]. It is important to note that micro injection moulding is not a simple scale-down of conventional injection processes. To achieve a sustainable  $\mu$ IM process, a complete redesign is required for each step of the process [6].

A micro moulded product usually is divided into three distinct categories based on the kind of microparts the product consists of: parts in the range of only a few milligrams, parts exhibiting features with dimensions in the micrometer range, and parts possessing tolerances based on dimensions in the micrometer range, without a dimension limit. In this research, the term microparts is used for three-dimensional parts, which show tolerance in the micrometer or nanometer range or exhibit at minimum one dimension. In previous studies, the fabrication of 3D parts has proven to be influenced by the thickness in relation to the lateral dimension. Generally, the ratio of the thickness/lateral dimension is generally higher than one. This translates to a dependency of the thickness of parts to the other dimensions [6].

From previously performed studies can be concluded that the conditions within a micro-moulding process are not similar to the conditions within a conventional moulding process. Due to large surface areas in comparison to product volumes, the melted material loses heat rapidly. As a result of this rapid

heat loss, micro-moulding entails extremely high temperature gradients. Furthermore, high injection speeds are required to prevent precocious solidification and incomplete products. Due to the high-speed injection of the material, stresses and strain rates can exceed those found in the traditional injection moulding technique, especially at the cavity's entrance, where shear strain rates often exceed  $10^6 \text{ s}^{-1}$ . These high stresses and strain rates result in unusual morphology and material integrity, such as cracks, porosity, inclusions, etc. [22]. For microinjection moulding, the realization of high aspect micro characteristics in the product is achieved with the use of a mould temperature in the range of the softening temperature of the polymer in combination with structures of the nanometre range [6].

The high injection speed and rapid heat loss result in a small range of operating conditions and variations in which the desired product can be fabricated. Small fluctuations in temperature, impurities, and material inconsistency result in below-par products, which cannot function as intended [22]. The temperature is of major importance to influence the viscosity and thus the flow behaviour of the polymeric melt. This relation can be calculated with the VFTH equation, furtherly discussed in 2.3.1.  $\mu\text{IM}$  techniques are in development since the 1990s, resulting in a variety of techniques applied to insert the polymer into the mould cavity. These techniques include the lithography process (LIGA), micro-electrical discharge machining ( $\mu\text{EDM}$ ), and laser micromachining. It is important to consider that the moulding of the polymer consists of several steps [6]. A schematic overview of the microinjecting moulding process is illustrated in Figure 10, in previous chapter.

In previous studies, two notions were investigated to decrease the amount of degradation of polymer and waste. The first notion entails the decrease of the dimensions of the screw and the barrel for a specific type of plasticizer, described further in this paragraph. Here, the diameters of both elements amounted to less than 20 millimetres. The reason for such small diameters is the minor amount of polymer required for the manufacturing of micro parts. The second notion entails the use of a separate plasticizer, as mentioned prior. The two-system process would be a plasticizer in combination with a separate injection unit. Today, two types of plasticizers exist. The first type of plasticizer is constructed with a plunger and a hot cylinder. The second type of plasticizer is constructed with a screw and a barrel. More importantly, the implementation of a screw and barrel type plasticizer results in a more uniform and efficient plasticization. This is due to the screw actualizing heat transport based on mechanical and thermal energy, in comparison to the first type of plasticizer, in which the plunger only provides mechanical energy. After melting the polymer, the melt is injected into the mould with the help of a plunger. By using a plunger, the control of the quantity injected polymer is very precise, as the same plunger displacement always is replicated. This translates into a favourable two-system process, initiated by a plasticizer (screw – barrel) and followed up by an injector unit (plunger). The size of the screw is usually limited to around twelve millimetres as a result of the standard bulk pellet diameter. Clamp forces are crucial in the microinjection moulding process to account for the material shrinkage and warpage, due to the small surface of the injected melt. A list of commercially sold microinjecting moulding machines, alongside their characteristics is presented in Table 29, located in the appendices [6] [36]. As derived from Table 29, a lot of different  $\mu\text{IM}$  are available, varying in injection capacity from  $0.082$  to  $10 \text{ cm}^3$ . The injection pressure varies between 1600 to 3500 bar, which is a significant amount. Additionally, the clamping force varies between values of 13.6 to 147 kN.

From the study of Packianather et al., the four main process influence parameters are derived: the mould temperature, the temperature of the barrel and melt, the holding pressure, and the injection speed. From these four parameters, the most influential are the mould temperature and holding pressure [9]. As a result, the mould temperature and holding and injection pressure will be examined, prior to the other process conditions.

### 2.3.1. Contaminations

The materials used for micro-moulding are monitored very strictly to ensure minimal to no contamination and uniform rheological properties. The existence of variations in rheological properties can result in significant fluctuations in process conditions, ensuing in unsatisfactory repeatability of experiments. It has to be noted that small, neglectable variations in the amount of contamination, like pellet-to-pellet variations, can result in the previously mentioned fluctuations. When contaminants enter the process it can have a detrimental impact on the rheology of the polymer, but also the fine structures present in the mould cavity have the risk of being damaged. Currently, micro moulded products are solely functional within very narrow optical and mechanical criteria. It is important to note that the aesthetics and tactile properties are considered to play a minor role in product evaluation and functionality [22]. A general overview of the different materials used in moulding and micro moulding injection processes is presented in Table 28. This table entails information about prior used temperatures of the moulds for (micro)moulding injection processes for each material, their applications, and the melt temperature of each material in micro moulding injection processes. Table 28 is constructed based on data, gathered from previous (micro) moulding injection studies.

However, the consequences of contamination not only include a change in rheology and damage to the mould cavity. As impurities are present in the polymer resin, the heat capacity of the resin also changes. The change in heat capacity translates to a change in the required amount of heating (plasticization) and cooling (moulding and holding step) during the microinjection moulding process. As a result, the formation of the microstructures of the mould is affected. It is important to note that the viscosity of the molten polymeric resin is mainly influenced by the temperature (and thus also less influenced by a change of the heat capacity due to contaminations) and the applied shear rate [6]. The temperature of the polymeric melt directly influences the kinetic energy of the resin and also the free molecular volume of the material. Via an increased temperature, the viscosity of the melt decreases, leading to an intensified purging of the material. This translates to a less required amount of material to fully purge the system. The actual volume of a material is known as the occupied volume ( $V_o$ ). The free volume ( $V_f$ ) is opted to be the movement/stretching room between molecules.  $V_f$  is crucial for molecules to be able to perform rotations and translations. As the temperature increases, the kinetic energy in the resin also rises, due to vibrations of the molecules. The vibration of molecules is related to the free volume. As a result, the total volume of a polymer or resin can be described as equation (5):

$$V(T) = V_o(T) + V_f(T) \quad (5)$$

The standard Arrhenius equation for most small molecule fluids with implemented temperature dependence is presented in equation (6):

$$\eta(T) = A \exp\left(\frac{E}{RT}\right) \quad (6)$$

For larger molecules, such as polymers, the Arrhenius equation can be adapted to accurately calculate the viscosity of larger molecules to equation (7):

$$\eta = A' \exp\left(\frac{B' V_o}{V_f}\right) \quad (7)$$

As the fractional free volume (f) is defined as the ratio of  $V_f/V$ , equation (X) can be simplified to equation (8):

$$\eta = A' \exp \left[ B' \left( \frac{1}{f} - 1 \right) \right] = A \exp \left( \frac{B'}{f} \right) \quad (8)$$

It is important to insert the temperature dependence of  $f$  into the equation when temperatures above the glass temperature of the polymer are used. this relation is presented in equation (9):

$$f = f_g + \alpha_f (T - T_g) \quad (9)$$

Here,  $\alpha_f$  presents the expansion factor for the free volume. When equation (7) is implemented into equation (6), following equation (10) is become:

$$\eta = A \exp \left( \frac{B'}{f_g + \alpha_f (T - T_g)} \right) \quad (10)$$

To simplify equation (10), two new parameters  $B$  and  $T_o$  are introduced. These calculations are presented in equation (11) and (12):

$$B = \frac{B'}{\alpha_f} \quad (11)$$

$$T_o = T_g - \frac{f_g}{\alpha_f} \quad (12)$$

When equation (11) and (12) are filled in equation (10), the Vogel-Fulcher-Tammann-Hesse (VFTH) equation (13) is become:

$$\eta = A \exp \left( \frac{B}{T - T_o} \right) \quad (13)$$

The VFTH equation is capable of describing the temperature dependence of the viscosity, as well as the temperature dependence of the relaxation time of any polymer chain. The VFTH equation can perform this calculation based on a chosen reference temperature ( $T_f$ ) for the viscosity of a polymer. This  $T_f$  is used to eliminate  $A$ . Additionally, the ratio of the viscosity to the viscosity of the polymer at the reference temperature is implemented. The altered VFTH relation is described by equation (14) below:

$$\ln \left( \frac{\eta}{\eta_r} \right) = B' \left( \frac{1}{f} - \frac{1}{f_r} \right) \quad (14)$$

Note that  $B'$  is an empirical constant, found in literature or determined through experiments and modelling. Next is the reimplementation of the linear temperature relation of  $f$ , described as equation (15), only now is chosen for a reference temperature ( $T_r$ ). This relation is only applicable if  $T_r$  is larger than  $T_g$ .

$$f = f_r + \alpha_f (T - T_r) \quad (15)$$

After implementing equation (14) with equation (15), a new equation is received, generally known as the William-Landel-Ferry (WLF) law. With the WLF law, the change in viscosity can be calculated for temperatures maximum 100 °C above the glass transition temperature. The WLF law is an empirical equation associated with time-temperature superposition, presented by equation (16):

$$\log \left( \frac{\eta}{\eta_t} \right) = - \frac{C_1 (T - T_t)}{C_2 + (T - T_t)} \quad (16)$$

$C_1$  and  $C_2$  are new parameters, specific for the WLF relation. These parameters are presented by equations (17) and (18):

$$C_1 = \frac{B'}{2,303f_r} \quad (17)$$

$$C_2 = \frac{f_r}{\alpha_f} \quad (18)$$

The fractional free volume ( $f$ ) is defined as the ratio of the available space ( $V_f$ ) to the space needed for the molecule ( $V$ ), as presented by equation (19) [37]:

$$f = \frac{V_f}{V} \quad (19)$$

For temperatures more than 100 °C above the glass transition temperature, the change in viscosity can be determined for polymer melts through an Arrhenius equation (20) [38]:

$$\eta_T = \eta_{T_0} \exp\left(\frac{E}{R}\right) \left(\frac{1}{T} - \frac{1}{T_0}\right) \quad (20)$$

### 2.3.2. Plasticization

During the plasticization step, the polymer pellets from the hopper are deposited onto a screw. While the polymer is being molten, the mould is pre-heated to the  $T_g$  of the polymer (this is prior to injection of the melt). Logically, the polymer melt is more rapidly cooled and heated for microinjection moulding in comparison to conventional injection moulding. This results into changes in viscosity, as mentioned prior (2.3.1), leading to defects in the microstructure of the moulded part. As a result, the mould temperature is generally kept close to the glass transition temperature ( $T_g$ ) or the melt temperature ( $T_{melt}$ ) of the polymer [22]. The temperature of the mould has proven to be of profound influence and needs to be precisely defined and fixed while operating the process. Equation (21) makes it be able to accurately calculate the required heating power to heat the mould, prior to injection. To perform equation (21) correctly, the heating time and mould characteristics (nature and dimensions) need to be considered. Important note, these parameters influence the type of heating device suitable for the process.

$$P = \frac{\rho \lambda V_p (T_f - T_i)}{t} \quad (21)$$

Generally, heating systems with low power densities are used for microinjection moulding processes, such as infrared heaters, electrical resistances, and induction heaters. This is a result of weak dimensions of the mould utilized for microinjection moulding, as a high-density power unit could result in breakage of the mould or material degradation. Induction heaters have proven to be the most efficient for  $\mu$ IM. However, the implementation of induction heaters into the process is usually more complex and costly in comparison to infrared heaters or electrical resistances. Additionally, the temperature difference is generally higher for  $\mu$ IM in comparison to conventional IM processes. The reason for this higher temperature difference is to ensure the melt completely fills the microstructures of the mould (high aspect ratio). As mentioned prior, the mould temperature for  $\mu$ IM is close to the  $T_g$  or  $T_{melt}$ , resulting in undesired, larger cycle times. However, the cycle time can be shortened via the implementation of a varying mould temperature, also known as a variotherm process, as discussed prior. A comparison between the power densities of these different heating systems is presented in Table 6 [6].

Table 6: Comparison of heater system power-densities.

Model	Power density (W/cm <sup>2</sup> )
Electrical resistance heater	0.5 – 6

---

A lot of mechanical excess energy is generated during the plasticization and injection step, which possibly leads to material deterioration. As a result, this excess energy needs to be extracted from the process. The effect of the excess mechanical energy is assessed by the Brinkman (Br) number. The Br is equal to the ratio of the thermal power dissipated by the flow of the melt, to the power transported through conduction. The Brinkman number relation is presented below in equation (22). For microinjection moulding processes, the Br number is generally greater than 1, as the temperature difference between the polymer melt and the wall of the mould is relatively small. A Brinkman number higher than one means a rather problematic air expulsion [6].

$$Br = \frac{P_d}{P_c} = \frac{\eta (\bar{v})^2}{\sigma (T_M - T_p)} \quad (22)$$

### 2.3.3. Injection

As previously mentioned, the viscosity of the polymer melt is influenced by the temperature and the shear rate. If the temperature and/or the shear rate are increased, the viscosity declines. The viscosity of a material is usually studied as a function of the applied shear rate. During the injection step, the temperature of the mould is kept at the  $T_g$  or  $T_{melt}$  of the polymer. The viscosity of the melt can be calculated through several theoretical laws in the function of the shear rate. It is important to note that each specific polymer type displays a certain viscoelastic response, which can be described by several empirical power laws. These laws, as well as their applications, are presented below in Table 7. The calculation of shear thinning behaviour of a polymer melt is performed with the Cross and/or Carreau law. Since a polymer melt is not a fully rigid plastic, the value of  $n$  is always higher than zero. However, most polymeric melts are known non-Newtonian fluids. As a result, the power-law index always amounts to a value between zero and one for polymeric melts [39]. During the injection phase, the melt flows through complex structures. While flowing through these microchannels, a wall-slip effect will occur [6] [39].

Table 7: Theoretical laws to describe the shear thinning behaviour of a polymer melt inside the mould.

Model	Rheological law equation	Applicable field
Cross	$\eta(\dot{\gamma}) = \frac{\eta_0}{(1 + \sigma \dot{\gamma})^{1-n}}$	$a = 1 - n$
Carreau	$\eta(T, \dot{\gamma}) = \frac{\eta_0(T)}{\left(1 + \left(\frac{\eta_0(T)}{t} \dot{\gamma}\right)^2\right)^{\frac{1-n}{2}}}$	$a = 2$
Carreau-Yasuda	$\eta(T, \dot{\gamma}) = \frac{\eta_0(T)}{\left(1 + \left(\frac{\eta_0(T)}{t} \dot{\gamma}\right)^a\right)^{\frac{1-n}{a}}}$	$a = 1$

Previous studies concluded that the rheological behaviour of a polymer is influenced by the size, shape, and roughness of the microchannels through which the melt flows, as this is in relation to the flow behaviour. Wall-slip is a common rheological issue, generally the result of large velocity gradients along the wall. Due to wall-slip, the viscosity of a melt is significantly reduced, in comparison to the rest of the material further away from the wall [40] [41]. Additionally, wall-slip increases with increasing melt temperature and decreasing micro-channel size. In a previously performed experiment, PP displayed unusual flow behaviour when injected into a mould with high aspect ratio structures. Here, PP exhibited affinity to form protrusions and nipples while being injected into a mould with an aspect ratio of six [42]. As mentioned prior, the temperature of the melt can also be changed for the injection step to increase the material performance. However, not every polymer is evenly strong influenced by a change in the melt temperature or even other process conditions. PP has proven to be less influenced by temperature than POM for example [7].

Due to the smaller channels in comparison to the conventional moulding process, the applied shear stress is higher for  $\mu$ IM. As a result of higher shear stresses, the decrease in melt viscosity is larger for  $\mu$ IM in comparison to IM. This translates to an increased influence of the applied shear on the viscosity of the polymer melt for  $\mu$ IM. As a result, the study of the viscoelastic nature of the polymer becomes more crucial for microinjection moulding processes. To avert premature solidification and ensure a good accuracy with  $\mu$ IM, polymers are used that display a low polymer melt viscosity and exhibit shear-thinning behaviour, such as LCP or PP [7]. The shear rate of the melt along the wall can be calculated with the help of the Poiseuille law, described in equation (23). It is important to note that the general

Poiseuille law still needs to undergo an adaptation, as equation (23) is only applicable for Newtonian fluids. The adapted form of the Poiseuille law (equation (24)) takes the pseudo-plastic behaviour of polymeric melts into account. As mentioned prior, is the  $n$ -parameter the power law of the material used in the calculation.  $n$  is equal to 1 for Newtonian fluids, and zero for rigid plastic structures [6] [43]. Additionally, can the shear stress be calculated via the use of equation (25) [30].  $R_c$  and  $L$  are the radius and length of the flow channel, both expressed in mm.  $\Delta P_r$  is the pressure drop occurring inside the channel, expressed in units of bar.

$$\dot{\gamma} = \frac{4Q}{\pi R_c^3} \quad (23)$$

$$\dot{\gamma}_p = \frac{3n+1}{4n} \frac{4Q}{\pi R_c^3} \quad (24)$$

$$\tau = \frac{R_c \times \Delta P_r}{2L} \quad (25)$$

Additionally, the injection speed is defined in terms of mm/s and more importantly, it is directly proportional to the shear rate. However, this is a relative interpretation of the speed of the melt. With the relative injection speed, the velocity is determined via the travel distance of the screw in function of the time. As mentioned prior, an increase in injection speed results in an increase of the injection pressure and the wall-slip. The enhancement of the wall-slip (friction) results in a temperature rise and thus a decrease in melt viscosity. This eventually translates to a change in the flow profile of the melt. However, the absolute velocity of the melt is determined via the absolute injected volume per unit of time, which gives a more accurate estimation of the melt velocity. The absolute injection speed of the melt can be determined with the relative injection speed and the diameter of the screw (equation (26)). It is important to note that for IM techniques, an injection profile is preferred, rather than a fixed injection speed. Usually, the injection speed is highest in the middle of the process. At the beginning and end of the injection phase, the velocity amounts to lower values. The use of an injection profile is not suitable for  $\mu$ IM, due to the small shot volumes [44].

$$v_{abs} = \frac{v_{rel} \times d_{screw}^2 \times \pi}{4000} \quad (26)$$

While the melt is injected into the mould, an internal pressure (cavity pressure) will develop that will apply forces to the cavity walls. As the internal pressure is in the opposite direction of the clamp forces, it results in a decrease of applied force to the melt, leading to possible material shrinkage. The applied clamp forces can be calculated with the use of equation (27), presented. However, the mean mould pressure is influenced by the material used, the thickness of the wall, and the maximum melt flow length. The pressure inside the mould cavity can be determined via the use of equation (28) [44]. Important note, the internal pressure of the system also affects the flow behaviour of the melt, resulting in friction between the melt and the cavity wall. The presence of friction in the system generates excess heat, which is absorbed by the melt. The temperature increase of the melt due to friction can be calculated with equation (29).  $\Delta P_r$  is the pressure drop inside the flow channel, expressed in units of bar.  $\rho$  is the density of the melt, expressed in kg per cubic meters.  $\lambda$  is the heat capacity of the melt, expressed in Joules per kilogram Kelvin. From a previously conducted study was derived that the mean temperature increase of the plastic melt is approximately the same as the amount of energy lost (as pressure loss) from the melt flowing inside the cavity [23]. Important note, this equation is only applicable for injection system, prior to contact between the hot polymer melt and cold mould wall.

$$\text{Clamp force (N)} = \frac{\text{surface (cm}^2\text{)} \times \text{mean mold pressure (bar)}}{1000} \quad (27)$$

$$\text{Mean mold pressure (bar)} = \frac{\text{pressure at nozzle exit (bar)} + \text{pressure at end flow length (bar)}}{2} \quad (28)$$

$$\Delta \overline{T}_M = \frac{\Delta P_r}{\rho \lambda} \quad (29)$$

In order to accurately calculate the viscosity of the polymer melt inside the injector, knowledge about the screw intensification rate (SIR) is required. The SIR, also known as the material pressure ratio, is characterized by the ratio of the injection pressure to the hydraulic pressure. This translates to the ratio of the pressure of the resin in front of the screw to the pressure of the piston in the injector cylinder (see Figure 9). The injection pressure is enforced directly onto the polymer resin via a ram. Due to the enforced injection pressure, resin flow is induced. The measurement of the injection pressure takes place in the nozzle, via a transducer. On the other hand, the hydraulic pressure is described as the pressure in the head supply line of the pump. The pressure induced in the head supply line results into movement of the ram. The hydraulic pressure is usually measured via a gauge, implemented into the hydraulic line. For hydraulic systems, the SIR generally amounts to a value of ten. Due to the microinjection moulding system being purely electric, the SIR value typically amounts to a value of unity. To give a better insight into the SIR calculation for hydraulic systems, a graphical presentation (Figure 12) of the parameters, as well the hydraulic ratio equation (30) are presented below this text. The usage of the SIR in the calculation of the melt viscosity inside the plasticizer is presented as equation (31) [8] [45].

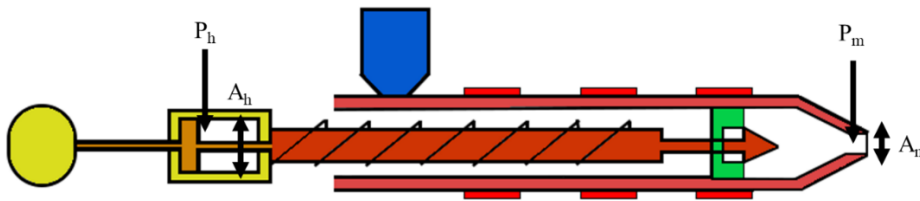


Figure 12: SIR parameters.

$$P_m = P_h \left( \frac{A_h}{A_m} \right) \quad (30)$$

$$\eta = \text{Peak injection pressure} \times \text{fill time mold (s)} \times \text{SIR} \quad (31)$$

#### Measuring the amount of injected product (metering size)

Additionally, the metering size needs to be defined and controlled very precisely. The metering size is based on the volume needed to fill the cavity and the volume needed to ensure the required holding pressure. To limit material shrinkage, the metering size must be very precisely calculated. When the amount of added volume is less than the required amount, not all cavities will be filled by the resin, leading to a defective part. When the mould gets over-filled, remarkably high injection pressures are generated inside the mould. However, over-filling is a less crucial parameter in comparison to under-filling, as pressure drops occur at corners inside the system, due to the complex geometry of the channels and the mould design. Usually, the injection of the melt is performed by a fixed plunger system, ensuring the same amount of injected melt for each rotation cycle of the plunger. The holding pressure inside the mould is also generated by this injection-plunger, leading to a packing effect, discussed furtherly in this chapter [6].

Measuring the weight of the injected product has proven to be an unsuitable method to control the process. However, measuring the pressure inside the system has proven to be more advisable to check

for process variations. With conventional IM is made use of the injection pressure to follow up the process. With  $\mu$ IM processes, control of the system via measuring the injection pressure is not suitable, as the injection pressure of  $\mu$ IM (200 MPa) amounts to ten times the injection pressure of conventional IM. Additionally, sub-milligram products ( $\mu$ IM) show high sensitivity towards changes in process conditions. When utilizing an immense pressure, such as 200 MPa, the smallest, neglectable change in conditions could possibly lead to an immense difference in injection pressure. Resulting in false assumptions regarding process control. For controlling  $\mu$ IM processes (and thus the amount of injected melt) of the pressure inside the mould cavity is used, via the implementation of a small pressure sensor directly inside the cavity. As mentioned prior, the injection pressure is in relation to the injection speed, as the injection speed increases, the pressure will increase as well. High injection speeds result in a reduction of the polymer viscosity and contact time between the hot polymer melt and the cold cavity wall. By reducing the contact time, the ability of the melt to solidify and short shots also decrease [6] [7].

#### Air presence in the mould cavity

It is important to mention the risks of the presence of air inside the cavity. The possible outcome of trapped air in the mould is material combustion. This phenomenon is also known as the Diesel effect. These defects are logically highly undesired. For conventional IM processes, the presence of air can be prevented via the implementation of air vents. However, air vents are not applicable to microinjection moulding processes. From previous studies was concluded that the geometry of the microparts and process conditions mainly influence the ability to accumulate air and combust, as the presence of air in the cavity was not always responsible for part abnormalities [6]. Alternatively, a vacuum or negative pressure is applied to the system when high injection speeds are utilized. As the injection speed is increased, the pressure of the air trapped inside the mould cavity also increases. As a result, the chance of material degradation and poor part performance is higher. By applying a vacuum to the system, complete elimination of air can be ensured, especially when the vacuum is applied pre-injection. However, the implementation of a vacuum setup results in more complex maintenance and higher manufacturing costs. Additionally, the implementation of a vacuum system to a decrease in mould temperature, potentially leading to insufficient melt filling. This situation mainly occurs for temperature-sensitive polymers, such as POM, and can be prevented via aligning microstructures adjacent to the parting line of the mould. The trapped air can escape the mould through these microstructures more easily [36].

### 2.3.4. Holding and cooling

During microinjection moulding, the polymer melt is cooled more rapidly in the mould compared to regular injection moulding. This is due to the enhanced contact surface of the polymer melt with the mould and its microstructures, in relation to the total polymer melt present in the mould. An improved cooling inevitably results in an increase in viscosity. The increased viscosity negatively impacts the flow pattern of the melt into the mould, leading to defects in the microstructure of the moulded part [42]. The holding pressure inside the mould cavity is generated via the movement of an injection plunger system towards the mould. The movement of the plunger has the possibility to result in a packing effect of the material. However, materials usually decrease in volume while being held and cooled in the mould. This can be solved by injecting a small dose of material in addition to the original amount of injected melt. The injection of an extra dose of polymer does not really solve the problem, but only accounts for it, even leading to longer cycle times. To resolve the material shrinkage can be made use of increased holding pressure, resulting in a denser material from the start. As the molecules are packed denser together, the possibility of molecule re-arrangement, and thus shrinking decreases. However, an increase in holding pressure results in higher internal residual stresses [6].

Important note, this method only applies to materials/melts showing a lower affinity to shrink. Materials with a high mould shrinkage (e.g., POM) cannot be packed denser with higher holding pressures. Important note, the packing effect does not only occur inside the mould cavity, but also in the injection system (barrel, nozzle, and screw). When sudden freezing of a channel occurs, a small, partial packing effect arises inside the channel. For a classical IM, the cooling time of the mould can be calculated via equation (32) [6]. In this equation,  $\delta$  is the symbol for the thermal diffusivity of the material ( $\text{mm}^2/\text{s}$ ). The thermal diffusivity can be described as the rate of transmission of a thermal disturbance, throughout the melt. The thermal diffusivity is calculated via the use of equation (33). However, equation (32) is only suitable for  $\mu\text{IM}$  if the mould temperature ( $T_w$ ) is lower than the melt temperature ( $T_M$ ) [6]. After several adaptations to (32), equation (34) is become, which correlates more to the different heat transport phenomena between the mould and the polymer melt [46]. Additionally, a rule of thumb has been created for some of the most common polymers to quickly estimate the required cooling time. However, this rule does not take the temperature of the mould into account, making this rule only suitable for quick estimations; Because no polymer specific characteristics are taken into account, such as molecular weight distribution (MWD), tacticity, etc., but they have a major influence on the solidification. This rule of thumb for several polymers is presented in Table 8 [44]. For an accurate estimation of the cooling time will still be made use of equation (34).

$$t_c = \frac{S^2}{\pi^2 \delta} \ln \left( \frac{4 (T_M - \bar{T}_W)}{\pi (\bar{T}_E - \bar{T}_W)} \right) \quad (32)$$

$$\delta = \frac{\text{Thermal conductivity } (\sigma)}{\text{Specific density } (\rho) \text{ Heat capacity } (\lambda)} \quad (33)$$

$$t_c = \frac{4S^2}{\pi^2 \delta} \ln \left( \frac{2\sqrt{2} (T_M - \bar{T}_W)}{\pi (\bar{T}_E - \bar{T}_W)} \right) \quad (34)$$

Table 8: Rule of thumb for the estimation of the cooling time for conventional plastics.

Polymer	Rule of thumb ( $t_c$ )
PP	$3.67 \times S_W^2$
PA6, LDPE, PBT	$2.64 \times S_W^2$
PA6.6, PS, ABS, SAN	$2.82 \times S_W^2$

PMMA, HDPE	$3.00 \times S_W^2$
PC	$2.17 \times S_W^2$
POM	$4.18 \times S_W^2$

Additionally, the temperature of the material is not uniform when cooled. The centre of the plastic takes significantly longer to cool and shrink in comparison to the surface. This is due to the low heat conductivity of polymeric materials. The centre temperature can be high enough to remelt the surface of the part after demoulding. The wall thickness of the part also is a crucial factor for the cooling. An increase in wall thickness will result in a higher core temperature. It is important to tune the cooling time very precise, as too short cooling times lead to significant material shrinkage and/or warpage. On the other hand, too long cooling times lead to longer cycle times and significant stress onto the moulded part, possibly resulting in part fractures [23].

### Polymer morphology

The skin-core crystalline morphology behaviour of the polymers has also proven to be of major importance. Polymer crystallinity translates into the packing rate of polymer chains to create an ordered structure, known as a crystalline region [18]. It is important to ensure the plastic inside the mould can transfer enough heat to prevent differential cooling of the melt. Otherwise, warping of the parts can occur, which is highly undesired. The skin-core crystalline morphology is used for macro-scale parts (IM) and is divided into two categories: the shish-kebab and the spherulitic structures. The shish-kebab structure results from flow-induced crystallization and is in the skin layer. The spherulitic structure is favoured when quiescent-induced crystallization occurs and is located in the core layer. Figure 13 is a graphical presentation of the skin and core layer of a microinjection moulded product. It is crucial to predict the skin and core layer of a polymer pre-moulding, as these structures dictate the tensile strength, tensile elastic modulus in stress direction, and impact strength perpendicular to the direction of the stress. The shish-kebab structure is known to improve the tensile strength and tensile elastic modulus, but to also decrease the perpendicular impact strength. By analysing the crystalline morphology behaviour, an adequate polymer selection can be executed for the microinjection moulding process, regarding the desired properties [7] [47] [48].

However, micro-scale parts (resulting from  $\mu$ IM) consist of a core-free morphology. No spherulitic structure is present at the centre, due to the high cooling rate and flow strength in  $\mu$ IM processes, resulting in a flow-induced crystallization. This translates to the creation of highly oriented structures and anisotropy in the micropart. Anisotropy are non-uniform properties (chemical, physical) of the part when measured in different directions. Logically, anisotropy is a highly undesired feature of the part, as this influences the overall characteristics, as well the shrinkage of the produced micropart. From a previously performed study was concluded that for PP, the spherulite size decreases with the reduction of microcolumn diameter [7]. As the name semi-crystalline implies, these materials consist of amorphous regions between crystalline regions. Due to these amorphous zones the density of the material is decreased as the zones are unoccupied volume in the material structure. These unoccupied volumes play a crucial role in the material shrinkage behaviour when cooled. This is because the amorphous zones are not able to pack as dense as the crystalline zones. As a result, the presence of amorphous zones leads to less shrinkage of the material. Semi-crystalline materials even show affinity to furtherly crystallize and shrink at room temperature, which can make the process very complex [23] [49]. Previous studies have proven pure PP (ZH500M) tends to shrink by approximately 1.6% [50]. Additionally, the cooling speed of the material is a crucial factor to influence the crystalline and amorphous zones. If the material is cooled at a fast rate the crystalline zones decrease in size and the

amorphous zones enlarge. To decrease the material shrinkage requires a low crystallization rate is required [23].

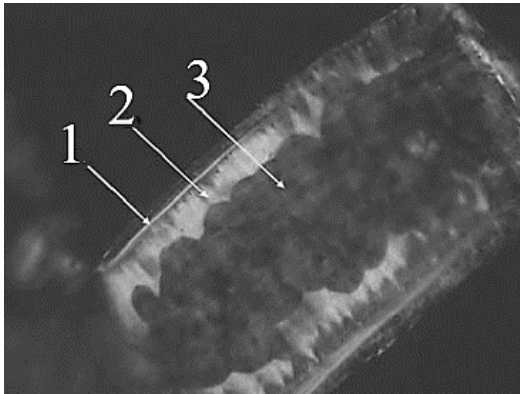


Figure 13: Micro column morphology. 1. Skin layer 2. Shear zone 3. Core layer [47].

### 2.3.5. Demoulding

The demoulding process of parts, especially parts comprised of microfeatures, can be exceedingly difficult and needs to be performed with the utmost caution. When parts with an aspect ratio above 1 are demoulded, it is generally opted to use demoulding surface agents. However, these surface agents are not suitable for medical appliances or microfluidic parts, as the parts have the possibility of contamination by surface agents. For traditional IM, the part is ejected from the mould with the use of ejector pins. Nevertheless, the use of ejector pins with microparts is highly prohibited, due to the chance of failures, cracks, breakage of microstructures, and deformations occurring in the micropart from the applied demould force. For demoulding the micropart, several concepts have risen over the last years, providing alternative solutions to demould the part, such as vacuum, ultrasonic ejection, and ejection by a mechanical robot arm [51].

From previously performed studies was concluded that each demoulding system must be altered for each specific geometry. Several factors determine the demoulding technique utilized in the process, such as the surface area of the parts, the surface roughness of the mould, and the shrinkage of the material. The material shrinkage is considered to be one of the crucial factors to impact the accuracy of the demoulding step. It is necessary to closely monitor and control the material shrinkage during every step of the process in order to provide greater accuracy. The shrinkage (*shr*) of the material is generally expressed in percentage and can be calculated via equation (35) [45] [52]. Table 9, presents a general overview of demoulding techniques, regarding the field of the appliance and limiting factors. An overview of the influence factors on in-mould shrinkage behaviour and usual shrinkage values of several semi-crystalline polymers are presented in Table 10 and

Table 11 [23]. Additionally, there is a technique to reduce the frictional coefficient of the mould wall, known as the electrorefining step during the fabrication of the mould insert [52].

$$shr (\%) = \left( \frac{Mold\ dimension - part\ dimension}{Mold\ dimension} \right) * 100\% \quad (35)$$

### The effect of fillers and reinforcements

Fillers are usually added to polymer resins to alter the mechanical properties of the polymer. For micro-scale parts nanofillers, such as carbon nanotubes, polyhedral oligosilsesquioxanes (POSS), and exfoliated clay platelets are generally used. These fillers are mostly inorganic materials and generally high-modulus fillers to increase the creep-resistance and stiffness of the polymer. A known disadvantage

of filler materials are the dissimilar properties in comparison to the polymeric resin, such as the thermal expansion coefficient (CTE). Fillers tend to shrink less than the polymer material. As a result from the addition of fillers, the resin displays non-uniform properties, resulting in differential shrinkage and warpage of the moulded part. This anisotropic shrinkage behaviour results from molecular fibre orientation and orientation-relaxation mechanism during the injection and holding and cooling phase. The fibre orientation is affected by several process conditions: injection rate, cavity thickness, viscosity (temperature, pressure, composition), and mould dimensions. During the injection phase, the polymeric melt will orient in the direction of the flow. The relaxation mechanism occurs during the cooling phase and results in a higher shrinkage of the material in the direction of the flow, compared to the cross-direction of the flow. However, the addition of fillers can decrease the overall shrinkage of the material [23].

For high aspect ratio fillers (e.g., fibres) the decrease in shrinkage is proportional to the concentration of filler in the resin. For lower-aspect ratio fillers (e.g., powders, beads, and flakes) anisotropic shrinkage of the material does not occur. The shrinkage is uniformly decreased in all directions. Another advantage of low-aspect ratio fillers is the enhanced dimensional control. Generally, the skin layer of the polymer is oriented randomly and is formed through instant freezing on the cavity wall post-injection. Inside the shear zone of the polymer the fibres are all oriented in flow direction. The core layer of the polymer consists of random fibre orientation. To orient the fibres located in the core zone of the resin high shear rates are required [23].

The problem of anisotropic shrinkage can be prevented via reinforcement of the polymer resin with glass fibres. With reinforced resins, the orientation-relaxation mechanism during the cooling step is blocked. Instead of relaxation, the orientation is frozen fixed during the cooling step. Because the filler material tends to shrink less than the polymer, the shrinkage is reduced in direction of the flow. However, the polymer shrinkage increases in the cross-direction of the flow. With an increased fibre concentration, the difference between shrinkage in both directions only increases. As a result, the fibre concentration needs to be very precisely determined to assure desired shrinkage behaviour. To prevent possible warpage due to the anisotropic shrinkage behaviour, a combination of fibre and flake reinforcements is used. The use of a hybrid composite results in a decreased and more isotropic shrinkage behaviour, but still provides the mechanical properties of the glass fibres [23].

### The effect of pigments

Generally, the addition of pigments results in an increased shrinkage of the material. The difference between the in-direction and crossflow shrinkage is also increased due to these pigments up to 300%. Most pigments are organic compounds and tend to act as crystal nuclei for the growth of crystals in the melt. Due to the increased crystallization rate and earlier initiation, the crystallinity of the product is enhanced, resulting in increased shrinkage. It is important to note that every pigment type behaves completely different from the other pigments. The concentration of the injected pigment also highly affects the shrinkage behaviour of the resin. When the concentration is increased, the shrinkage also increases [23]. However, pigments do not exhibit a significant influence on the shrinkage behaviour of PP (<1 %), as reported by several studies [53] [54].

*Table 9: Field of appliance and limiting factors of demoulding techniques.*

Technique	Limiting factor	Applicable field
Ejector pins	chance of failures, cracks, breakage of microstructures, and deformations	Microstructured parts with a large surface area
Demoulding agent	Pollution of microstructures and microparts	Parts with large surface area

Compressed air	/	Microstructured parts with a large surface area
Vacuum	Weak forces of vacuum	Microstructured parts with a large surface area
Ultrasonic ejection (dissimilar oscillation)	No improvement of demouldability	/
Mechanical robot arm ejection	The accuracy of the retraction arm is dependent on part geometry	/

Table 10: In-mould shrinkage influence factors.

Increased parameter	Shrinkage effect
Injection rate	Decrease
Injection pressure	Increase or decrease
Holding pressure	Decrease
Holding pressure time	Decreases
Melt temperature	Increase or decrease
Mould temperature	Increases
Chain branching	Decreases
Crystallization rate	Increases
Molecular weight	Increases due to higher viscosity, leading to more complex cavity filling
Clamping pressure	Low chance of decrease, no effect
Wall thickness	Usually increases
Melt flow rate	Decreases
Ejection temperature	Increases
Cooling time	Decreases
Gate dimensions	Decreases
Number of gates	Decreases
Filler amount	Decreases
Filler type	Increase or decrease
Post-ejection dead time (mould open)	Increase or decrease
Room temperature	Increases
Air humidity	Increases
Air flow	Usually decreases

Table 11: Shrinkage values of semi-crystalline polymers.

Polymer	Shrinkage (%)
Unfilled PP	1.0 – 2.5
PP – 40% talc filled	0.8 – 1.5
PP – 40% CaCO <sub>2</sub>	0.7 – 1.4
HDPE	1.5 – 4.0
Polyamide (Nylon 6)	0.5 – 1.5

Polyamide Nylon 6,6	0.8 – 1.5
Nylon – 30% glass fibre	0.3 – 0.5
Acetal	2.0 – 2.5

---

### 2.3.6. Purging

The execution of a purging step is crucial when the type of processed material is changed to a different polymer. The purging step is required to eliminate contaminations from the previous material. The presence of the old material on the screw would mix with the newly introduced polymer, leading to rheological and mechanical changes of the final product, which are highly undesired. Purging is known to consume significant amounts of product, time, and labour. To successfully purge a system of pigments can require over 100 kilograms of polymer material. However, not every material has the possibility to be ‘easily’ purged. For some applications, a disassembly of the screw is necessary to fully clean the system. These factors make purging a notorious, but a necessary phase when a change of material is desired. To successfully purge a system, several tips should be taken into account: always try to purge a less viscous material with a more viscous type, always try to purge a light colour with a darker colour, maintain the equipment, regularly clean the equipment, and (if necessary) use a transitional material to bridge the temperature difference between the purged and new material [55].

From previously performed studies it can be derived that to successfully purge a system, a high backpressure and screw rotational speed are crucial. The agitation and scrubbing of the material are maximized via maximizing the back pressure and screw RPM, resulting in a more intensified purge. Additionally, the screw needs to be kept completely forward to fix the agitation at the front end of the machine. The reason for this are the carbon and colour deposits, generally located in the nozzle of the injection unit. At this part of the machine, the purge is the most difficult. Via fixing a major part of agitation on the front end, the purge-efficiency is improved [2]. Purging can be performed via three different methods: via purging agents, disassembling and cleaning the machine, and via plastic resin flushing. With plastic flushing, no purging agent is added to the process, only unprocessed virgin material or already processed, ground material. With plastic flushing an immense number of shots are needed to ensure complete purge of the system and a lot of material is lost as waste. Industrial production processes generally make use of purging agents, due to time management being one of the major cost of operations. The use of purging agents results in an intensified purging step, leading to less material wastage and decreased in-between cycles time. Purging agents can be divided into three categories: mechanical, chemical, and virgin resins or regrinds, furtherly discussed in this chapter [56].

A purging agent is a plastic resin (type is dependent on type of material to purge) used to expel contaminants and clean the system. The usage of purging agents is especially beneficial to expel very difficult resins and contaminants (e.g., carbon deposit), but also for colour changes of the product. With the use of purging agents, the number of shots required to clean the system is drastically reduced. For the modern-day processing of thermoplastics, the use of purging agents is crucial to improve the processing efficiency, tool and die life, scrap rates, and equipment maintenance [56].

#### Mechanical purging

Mechanical purging expels contaminants via physical contact with the material. This technique uses abrasives or high viscosity plastics to scrape the contaminants from the barrel and screw. A mechanical purging agent is generally a thermoplastic blend, consisting of scrubbing granules and a carrier resin. The scrubbing granules are designed to be solid on the inside, but soft on the outside to protect the machine. Via the solid-soft configuration of the granules, only the metal surface is scrubbed securely, with low to no damage to the machine. Mechanical purging agents have been used widely in the industry and are safe to use. However, the use of mechanical purging agents also provides several disadvantages: limited ability to remove carbon deposit, limited temperature range due to possible melting of the granules, and damage to the barrel (wear) and mould (pitting). There are two main types of mechanical

purging agents: the mechanical abrasive and non-abrasive purge of the system. Both these purging agents are separately discussed.

The first type of mechanical purging agent are the abrasive purging agents. The abrasive compounds are constructed from low-viscosity abrasive minerals or glass. These abrasive materials have the ability to push the resin out the injection unit, while simultaneously scrubbing the metal surfaces. Depending on the type of mineral/glass particles sizes clogging may occur during the purge step. Additionally, the cost of the abrasive purging agents is determined by the type of carrier resin and filler. An example of an expensive, but outstanding purging agent is glass filled PC for the purge of PC from the system [56].

The second type of mechanical purging agent are the non-abrasive purging agents. The non-abrasive materials are known to be very stiff, due to a high viscosity. The non-abrasive compounds contain cleaning and release agents and are generally constructed from polyethylene (PE)-based materials. The non-abrasive purging agents are usually suitable for a larger temperature range, such as high-density polyethylene (HDPE). Because of the high viscosity of the agent, it is suitable to expel the resin from the system. The main advantages of the HDPE non-abrasive agents are the low cost, good push-ability, and wide temperature range. The disadvantage of HDPE is the need for disassembling the system post-purge to clean the residual HDPE in the system. This translates to the loss of the actual goal of using purging agents, which is to eliminate the requirement of disassembling the installation [56].

#### Chemical purging agents

With chemical purging agents the chains in the resin are depolymerized into components of a lower molecular weight. The result from chain-breaking is the decrease of resin viscosity, making it easier to be purged from the system. In comparison to mechanical purging, reactions are used to make the purge step easier, instead of applying physical force. A chemical purging agent consists of surfactants and a polymer resin with a low viscosity which penetrates the resin on the barrel. Via the penetration of the surfactant, it disperses into a purging melt. From this penetration the resin on the barrel and screw is loosened, making it easier to remove. The surfactant acts as an anionic or non-ionic active agent, which binds to the deteriorated original polymer resin to loosen the resin from the metal. To ensure maximal purge efficiency the purging melt resin should have a melt flow index equal to 0.1 or 0.3 times the melt flow index of the original resin. Generally, PP, PS, or acrylic cast is utilized as carrier purging resins [56]. The melt flow index (MFI) is a commonly used characteristic to describe the flow behaviour of thermoplastic polymers in a capillary. Moreover, the MFI is the resistance to flow, also known as viscosity, of a thermoplastic melt under a certain amount of time (usually 10 minutes), temperature, and applied force [57].

Today, chemical purging agents are mostly used due to the high mouldability rate of the waste material. The waste material is generally used to remould parts, making chemical purging very interesting for moulders. Additionally, chemical purging has proven to be more efficient and faster in comparison to mechanical purging, as a result from the reactions with the deteriorated resin and pigments. Commercial chemical purging agents are very cost efficient for companies, as less purging material is required, production costs are decreased, and machinery is maintained more properly in comparison to mechanical purging. However, chemical purging agents are very prone to deteriorate, not efficient for carbon removal, and take a longer interruption time due to the required soaking time. In addition, some chemical purging agents necessitate adequate mixing with the purging melt and accurate dosage measurement to ensure proper purging effectivity [56]. A general overview of recommended chemical purging agents and plastic changing profiles is presented in Table 12 and Table 13 below this paragraph [43].

## Virgin resins and regrinds

Pure, unprocessed resins, also known as virgin resins, can be used to purge a system. The usage of virgin material can be greatly beneficial for the removal of pigments and resins of the same type. However, virgin resin is less efficient, not suitable for carbon removal, and more costly in comparison to chemical purging agents. Generally, when using virgin material, an extensive amount of material is required to completely purge the machinery [56]. During this study virgin resin is utilized to purge the system to analyse the purging behaviour and subsequently intensify the purging step. This is done to decrease the amount of material required to ensure complete system purge. For research on newly developed specialty materials in the material development stage, the use of chemical purging agents is not appealing. This is due to the chemical reaction consuming tremendous amounts of material from the original, but also purging material. During the MDS the recovery of material is of major importance, as often not much material is available to perform experiments with. This makes purging with virgin material remarkably interesting for the MDS, as possibly most of the material can be recovered without any chemical changes due to surfactants.

For this study, the purging of the system is performed via injecting shots into the mould. Via this method the different process conditions influencing the injection moulding process can be studied, used, and tuned to enhance the purging process with virgin material. The number of shots required to purge the system will be analysed in the attempt to reduce the shot amount, translating into less material wastage.

*Table 12: Recommended purging agents.*

Material to remove	Purging agent
Polyolefins	HDPE
Polystyrene	Cast acrylic
PVC	Polystyrene, ABS, cast acrylic
ABS	Cast acrylic, polystyrene
Nylon	Polystyrene, low-melt-index HDPE, cast acrylic
PET polyester	Polystyrene, low-melt-index HDPE, cast acrylic
Polycarbonate	Cast acrylic, polycarbonate grind
Acetal	Polystyrene
Engineering resins	Polystyrene, low-melt-index HDPE, cast acrylic
Fluoropolymers	Cast acrylic followed by polyethylene
Polyphenylene sulphide	Cast acrylic followed by polyethylene
Polysulfone	Ground polycarbonate, extrusion-grade PP
Polysulfone/ABS	Reground polycarbonate, extrusion-grade PP
PPO	Polystyrene, cast acrylic
Thermoset polyester	Material of similar composition (no catalyst)
Filled and reinforced materials	Cast acrylic
Flame-retardant compounds	Immediate purging with natural, non-flame-retardant resin with 1% sodium stearate

Table 13: Recommended plastic changing profiles.

Material to remove	Material to change to	Rapid purge and soak material	Temperature bridging material	Final material
ABS	PP	ABS	/	PP
	SAN	SAN	/	SAN
	Polysulfone	ABS	PE	Polysulfone
	PC	ABS	PE	PC
	PBT	ABS	PE	PBT
Acetal	PC	Acetal	PE	PC
	Any material	PE	/	New material
Acrylic	PP	Acrylic	/	PP
	Nylon	Acrylic	/	Nylon
TPE	Any material	PE	/	New material
Nylon	PC	PC	/	PC
	PVC	Nylon	PE	PVC
PBT	ABS	PBT	PE	ABS
PC	Acrylic	PC	/	Acrylic
	ABS	PC	PE	ABS
	PVC	PC	PE	PVC
PE	Ryton	PE	PE	Ryton
	PP	PP	/	PP
	PE	PE	/	PE
	PS	PS	/	PS
PETG	Polysulfone	PETG	/	Polysulfone
Polysulfone	ABS	Polysulfone	PE	ABS
	ABS	Cracked acrylic	/	ABS
PP	ABS	ABS	/	ABS
	Acrylic	Acrylic	/	Acrylic
	PE	PE	/	PE
	PP	PP	/	PP
PS	PP	PP	/	PP
PVC	Any material	LLDPE or HDPE	/	New material
	PVC	LLDPE or HDPE	/	PVC
PPS	PE	PPS	PE	PE
San	Acrylic	Acrylic	/	Acrylic
	PP	SAN	/	SAN

### 2.3.7. Mould insert production techniques

The utilized moulds in the  $\mu$ IM process are crucial to manufacture plastic, microstructure components. To be able to transfer the desired microscale shape to the polymer melt, the mould needs to be produced very precisely. After production, the shape of the mould is examined to be within the allowed tolerance. The moulds used in  $\mu$ IM can differ in shape, size, cost, aspect ratio, and material, which is specific for each application. For the production of distinct types of moulds, different techniques are available. These different mould production types are listed in Table 14. The different mould insert production types can be divided into six main categories, but only the LIGA technique will be discussed, as it is the most commonly used technique [6]:

1. LIGA based methods involving lithography, electroplating, and moulding
2. Ultrashort pulse lasers and excimer laser erosion
3. 3D micro machines using ultrashort pulses:
  - a. Micro electrical discharge machine ( $\mu$ EDM)
  - b. Electrochemical machine (ECM)
  - c. Micro mechanical milling
4. Silicon wet etching
5. Thick deep UV resists
6. Deep reactive ion etching (DRIE)

Table 14: The different processes for mould fabrication [6].

Technology	Structure size	Tolerance	Aspect ratio	Wall roughness	Materials	Geometry
Ion beam LIGA	0.1 – 0.5 $\mu$ m	0.02 – 0.5 $\mu$ m	1	/	/	2D
Focused ion beam	0.2 $\mu$ m	0.02 $\mu$ m	/	/	Any	2D/3D
X-Ray LIGA	0.5 $\mu$ m – 1 mm	0.02 – 0.5 $\mu$ m	10-100	<20 nm	Electroformable materials: Cu, Ni, Ni-alloy	2D
Electron beam LIGA	0.1 – 0.5 $\mu$ m		1 – 2	/	Electroformable materials	/
UV-LIGA	2 – 500 $\mu$ m		1 – 10	/	Electroformable materials	2D
Femto-second laser	1 $\mu$ m	<1 $\mu$ m	1 – 10		Any	2D/3D
Excimer laser	6 $\mu$ m	<1 $\mu$ m	1 – 10	1 $\mu$ m – 100 nm	Polymer, ceramics, metal to a lower extent	2D/3D
Ultra-short pulses ECM	Few micrometres	<1 $\mu$ m	8			2D/3D
$\mu$ EDM	10 – 25 $\mu$ m	3 $\mu$ m	10-100	0.3 – 1 $\mu$ m	Conductive materials	2D/3D
Micro milling	25 $\mu$ m	2 $\mu$ m	10 – 50	Few microns	PMMA, aluminum, brass, steel	2D/3D
Deep UV resists	/	2 – 3 $\mu$ m	22	1 $\mu$ m	/	/
Deep reactive ion etching	/	<1 $\mu$ m	10 – 25	2 $\mu$ m	Silicon	/

The LIGA technology (lithography, electroplating, and moulding) is a process, performed in several steps. This technology is reportedly suitable for industrial-scale production and is commonly used in the manufacturing of sub-micronic structures. In addition, LIGA techniques are the leading method for the fabrication of mould inserts with a high aspect ratio. It is a very flexible technique, in which the mechanical properties of the metal can be altered by changing the current density. Usually, the surface roughness of the mould is lower in comparison to other mould fabrication techniques. However, LIGA

techniques are known for exhibiting long fabrication times and to be unsuitable for conventional tool materials, such as diamonds, steel, and ceramics. Another drawback of LIGA techniques is the necessity of draft angles to decrease the chance of damage to the microstructures. The draft angles are also crucial for the demoulding process. It can be a complicated process to implement draft angles in the microinjection moulding process, as the draft angles need to be controlled with the use of the specific angle of the x-rays emitting [6].

The first stage, also known as the lithographic stage, is the coating of the substrate surface with seed layers of a certain conductive material, such as silver, copper, and aluminium. The substrate surface used is generally one constructed of silicon wafers. Next, a polymer is conveyed onto the layer of coating. Take note that UV or X-ray sensitive polymers are used, such as PMMA or SU8 epoxy. A mask membrane, which contains the required pattern design, is fixed between the irradiation source and the resist layer. The irradiation process can now begin. While exposing the polymeric resist to radiation, the material will chemically modify, or even completely disintegrate, replicating the mask membrane pattern. Be aware of the noteworthy influence of the LIGA conditions on the accuracy of the shape pattern, as not only the mask membrane is of importance. The next step is the placement of an anode and cathode in an electrolytic bath, also known as the electroforming step. In this step, metal ions are reduced at the cathode and the metal will deposit onto the microstructure. The metal deposition is followed by the stripping of unirradiated resist, on which the metal first was deposited. Now, an almost full-functional metal mould is created with a very precise, micro metallic structure. It only needs to be attached to a glove plate with an injection hole. Now the moulding process can start. After moulding, a second electroforming process is performed, now to clean the mould of leftover polymer resin [6][58].

LIGA processes are greatly influenced by the kind of used radiation. As can be derived from Table 14, ion or electron beam, x-ray, and UV lithography are the leading LIGA techniques. When is opted to use X-rays, these rays are usually produced by a synchrotron, which is an extremely powerful and expensive generator for X-rays [6]. However, X-ray lithography has proven to encounter some limits in aspect ratio, which are presented in Table 15 [58]. The UV-LIGA technique is known to be limited, regarding inserts of a high aspect ratio between 20 and 500. Other more complex, but more efficient LIGA techniques exist, such as extreme UV, synchrotron radiation LIGA, electron beam LIGA, and ion beam LIGA. These complex techniques are not furtherly discussed in this thesis [6].

*Table 15: Aspect ratio limits of deep x-ray lithography.*

Structure type	Aspect ratio	Restriction
Self-standing polymer columns	50	Mechanical stability polymer
Holes in polymer	70	Diffusion transport behaviour
Detailed	500	Mask distortions

### 2.3.8. Ultrasound microinjection moulding techniques

The application of ultrasound power is known to be a very promising approach to fabricate a variety of polymeric microparts in order to enhance the performance of the microinjection moulding process. The implementation of ultrasound into microinjection processes is generally performed via two different approaches; The microinjection moulding process is either assisted with ultrasound power (UA $\mu$ IM), or fully operated with only ultrasound power (UP $\mu$ IM).

#### Ultrasound assisted microinjection moulding (UA $\mu$ IM)

Ultrasound assisted microinjection moulding is suitable for the fabrication of macro-scale components with surficial micro or nano functional structures and is an already existing process. The already existing UA $\mu$ IM process is constructed in such way that polymer melt flow is induced into the micro or nano cavities. The ultrasound power is used as an auxiliary, external field of energy to enhance the melt flow and is applied to- and transmitted by the mould itself to the mould cavities and the melt. Due to the indirect power transmission, a high-power ultrasonic energy field is required. This is necessary to overcome the low energy efficiency of the system, but translates into a significant power consumption. However, the use of ultrasound assisted microinjection moulding results in a reduced energy consumption of the process in comparison to conventional injection moulding. This is due to the auxiliary effect of the ultrasound power resulting in a decrease in the required process conditions to successfully fabricate a part. Ultrasound power is dissipated more easily in comparison to conventional heating techniques (Table 6), which makes it a very feasible technique. Due to the ultrasonic power being focused on solely the microchannels, a minimal heat storage is required. This results into a reduction of the required cooling time in comparison to conventional heating techniques, ultimately leading to a decrease in complete cycle time. UA $\mu$ IM processes have proven to be thrice as efficient, compared to conventional microinjection moulding techniques, based on production efficiency. The production costs are also decreased via UA $\mu$ IM processing. This is because the mould temperature, pressure, and viscosity drop are reduced with ultrasound power implementation [59].

Additionally, ultrasound assisted microinjection moulding has proven to be beneficial for the filling rate, but results in a slower cooling rate, prevents material wall-stick, excessive forces and flow resistance, and results in a decreased condensate layer thickness. These factors translate to an increased flow length and part weight. It is important to note that due to the decreased resistance to the flow, the pressure loss is decreased. From a previously performed study resulted that the pressure loss of ultrasound assisted microinjection moulding only amounts to 27% of the generated pressure loss with conventional microinjection moulding. In addition, the number of short shots is influenced by the set amount of ultrasound power. As the amount of ultrasound power is increased, the number of short shots will decrease. On the other hand, a higher mould temperature is beneficial to reduce the cooling rate and shear stresses in order to improve the filling efficiency. The implementation of ultrasound also improves the reproducibility of the process. From a previously performed study it was found that the reproducibility was increased from 84 to 95% with the usage of ultrasound vibrations. Additionally, the surface accuracy increased by approximately 25%, the filling area was increased by approximately 7%, and the symmetric deviation was decreased by approximately 15.6%. A general comparison of the process conditions of UA $\mu$ IM and a conventional variotherm microinjection moulding process is presented in Table 16 [59].

Table 16: Comparison of variotherm and ultrasound assisted microinjection moulding techniques.

Technique	Mould temperature (°C)	Injection Speed (mm/s)	Packing pressure (MPa)	Production cycle (s)	Part height ( $\mu$ m)	Standard deviation
-----------	------------------------	------------------------	------------------------	----------------------	------------------------	--------------------

UA $\mu$ IM	70	102	123	11.86	36.46	0.75
Variotherm $\mu$ IM	108	131	150	45	31.12	0.73

### Ultrasound plasticization microinjection moulding (UP $\mu$ IM)

In order to decrease the plasticization time can be made use of ultrasonic power, also known as UP $\mu$ IM. It is very suitable for the fabrication of micro-scale components. Reportedly it is possible to process injection volumes between 5 to 300 mg with UP $\mu$ IM, which is a significantly low amount. The UP $\mu$ IM process is remarkably similar to the conventional  $\mu$ IM: first the material is fed to the process in the feeding stage. During the feeding stage the sonotrode is moved from the mould to open the feeding channel. After the material is dosed into the mould the sonotrode is placed back into the mould to perform a certain amount of compression on the material. The sonotrode will transmit high-frequency ultrasound energy onto the material to perform the plasticization step. Next, the injection and holding step are performed through an induced downward displacement of the sonotrode to apply a certain force onto the melt. After the material is cooled and ejected from the mould the cycle can restart again. But it is important to mention that the UP $\mu$ IM process is specifically designed to melt lesser amounts of materials in a singular shot. With this technique, only one moulding cycle of raw material is necessary to perform the moulding process, making it very suitable for the material development cycle [59].

In comparison to conventional microinjection moulding, UP $\mu$ IM does not make use of a plasticizing screw, barrel, heaters, and other pieces of equipment. Due to the decreased amount of heated equipment, the thermal load onto the material is decreased, decreasing the chance of degradation. This technique even has the possibility to eliminate the necessary system purge step for material switches. These factors make UP $\mu$ IM a very feasible technique to analyse the processing behaviour of newly developed materials during the material development stage. In addition, UP $\mu$ IM results in a decreased residence time of the material inside the system. This reduces the amount of material degradation for sensitive materials, as the residence time is of utmost importance. With UP $\mu$ IM, between 20 to 70% of the sprue volume can be decreased via ultrasound implementation. This translates into a significant amount of material wastage decrease. More importantly, this technique is feasible to fabricate parts of high quality. In conventional microinjection mould processes approximately 40% of total energy consumption is from the plasticization step. However, with UP $\mu$ IM the efficiency of the plasticizing step is increased from 10 to 50%. Here, the efficiency of the process increases with increasing ultrasound power. Additionally, the use of UP $\mu$ IM for the fabrication of microparts requires lower pressure [59].

Several UP $\mu$ IM systems are currently used in the material development cycle: the Sonorus 1G system is limited to a maximum amount of 2 grams per shot, making it a very interesting processing application to fabricate the tensile bars. From previously performed studies was concluded that with the use of the Sonorus 1G the energy consumption is decreased with approximately 90% in comparison to conventional microinjection moulding processes [58]. With this method is made use of air pressure to inject the melt into the mould cavity. But this is an unpredictable method as the air pressure method is very unstable. However, it is possible to alter this machinery to process slightly larger shot sizes. On the other hand, the second version of the system (Sonorus S210) can process shot sizes of 5 grams per shot. With this device is made use of a servo drive instead of air pressure to perform the injection step. Through this method a much more precise pressure control and injection is achieved. This makes the Sonorus S210 an interesting approach to test newly developed specialty materials [56].

## 2.4. Analysis techniques

### 2.4.1. Rheometry

Rheological or flow characteristics are necessary by manufacturers, compounders, processors, and machinery fabricators to make a good selection of materials in relation to processability and properties. The simplest method to analyse material uniformity for thermoplastics, is via the melt flow index. In function of the material development stage and the processing characterization, complete analysis of the polymeric melt is of utmost importance. Via rheometrical analysis it is possible to foresee several processing problems (e.g., die swell) through the analysis of the viscoelastic nature of the material [60]. There are two main distinct types of existing rheometers. The first type are the rotational rheometers. The second type of rheometer are the extrusion methods, such as capillary and orifice. The extrusion methods are suitable for the characterization of pastes. During this study is made use of both, a rotational and a capillary rheometer. Rheology is the study of flow and deformation behaviour, stated in the laws of viscosity (Newton) and elasticity (Hooke). Flow behaviour is divided into three different components: Shear flow, extensional flow, and elastic behaviour. The shear and extensional flow are distinguished by their related viscosities. Elastic behaviour is defined as different moduli or swell ratios [14].

With capillary rheometry it is possible measure the slip velocity of the melt with the capillary wall in addition to the rheological properties of the melt. As mentioned prior, the rheological properties are significantly influenced by the material of the wall. While shear is being applied, friction energy is generated and transported to the bulk material. However, while the shear is applied, the region between the wall and melt will develop unique characteristics in comparison to the bulk material. The shear rate is influenced by the position in the melt shear zone, which can give false measurements. The main advantages of the capillary rheometer are the suitability of the technique to determine the rheological properties of polymeric melts with a high-volume fraction and also in a broader shear rate range [14] [26] [61]. The rotational rheometers are not suitable for these high-volume fractions and shear rates. But in comparison to capillary rheometers, rotational rheometers have an independency of the shear rate of the position of the fluid in the shear zone. Due this independency, the rotational rheometer is a very accurate method to measure the rheological properties of a melt in the lower shear rate range. Rotational rheometers are the most viable method to determine the molecular structure and processing characteristics of the polymer melt. Via measuring the viscoelastic characteristics, this technique provides information regarding the average molecular weight and molecular weight distribution [61] [62].

Important note, the flow geometries are not equal for capillary and rotational rheometers. However, to compare the values of both rheometers is feasible when several assumptions are implemented, such as: steady laminar flow behaviour, incompressible material, no end effects, no wall-slip effect, and a constant viscosity. But it is important to mention that a previous study concluded results obtained via either capillary or rotational rheometers are very similar regarding results and experimental errors [62]. The combination of both techniques makes it possible to analyse several rheological properties for a wide range of materials, over a wide shear rate range [13] [61][60].

#### Rotational rheometer (rotational compact disk rheometer)

As mentioned prior, the shear rate is assumed constant throughout the whole sample material by a rotational rheometer. A rotational rheometer is commonly known as a viscometer and is used for the measurement of shear viscosity and elasticity in a lower shear rate range. With rotational rheometry, a sample is heated until molten and furtherly fixed between a rotor and a stator, such as two plates. A variety of rotational rheometers exist, such as the plate and cone rheometer, the plate-plate rheometer, etc. During this research is a rotational compact disc rheometer used (described furtherly). As a result,

only the theoretical background regarding the rotational compact disc rheometers is discussed. With the compact disk rheometer, shear stress is generated between a fixed lower plate (stator) and a rotating upper plate (rotor). Through the measurement of shear behaviour, it is possible to identify structural changes of materials [10]. The shear rate and shear stress are calculated via equation (36) and (37) [14] [61]. A graphical presentation of the rotational compact disk rheometer is given in Figure 14.

$$\dot{\gamma} = \frac{\Omega r}{h_p} \quad (36)$$

$$\tau = \frac{T}{2\pi r^3} \left[ 3 + \frac{d \ln(T)}{d \ln(\Omega)} \right] \quad (37)$$

With the compact disk rotational rheometer, it is possible to measure the viscoelastic properties of a sample via two methods. This can be performed at a constant shear rate or via oscillatory shear rate tests. For oscillatory tests, a small amplitude oscillatory, sinusoidal shear is applied to the sample in function of the time. Via this method, the rheological properties of the sample can be measured at different frequencies, also known as a frequency sweep test. Oscillatory testing reduces experimental time consumption and provides greater understanding of the material rheological behaviour. The shear and stress are defined as sinusoidal equations (38) and (39). The shear amplitude of the oscillation is defined as  $\gamma_0$ . This method is particularly useful for the measurement of viscoelastic materials, such as polymer melts. This is due to the dependency of the viscoelastic materials to the measurement frequency. For viscoelastic materials, the rheological properties are significantly influenced by the applied frequency, such as the storage ( $G'$ ) and loss ( $G''$ ) modulus, as well the complex viscosity ( $\eta^*$ ). The phase angle ( $\theta$ ) is the shift between the applied shear and resulting shear stress of the viscoelastic material, resulting from the frequency sweep. The loss factor is the tangent of the phase angle, which is generally used to study material properties. The loss factor and phase-shifted signal of the stress amplitude ( $\tau_0$ ) can be calculated from the moduli via equation (40) and (41). For equation (41),  $|G^*|$  is the significance of the complex modulus  $G^*$ .  $G^*$  is generally calculated via equation (42), here  $i$  presents the imaginary part of the equation [61] [63] [64].

$$\gamma = \gamma_0 \sin(\omega t) \quad (38)$$

$$\tau = \tau_0 \sin(\omega t + \theta) = \gamma_0 [G' \sin(\omega t) + G'' \cos(\omega t)] \quad (39)$$

$$\tan(\theta) = \frac{G''}{G'} \quad (40)$$

$$\tau_0 = \gamma_0 |G^*| = \gamma_0 \sqrt{G'^2 + G''^2} \quad (41)$$

$$G^* = G' + iG'' \quad (42)$$

It is important to note that rotational rheometers are suitable for the detection of the glass transition temperature of polymeric materials. For these experiments, the applied shear and frequency are set to a constant value (e.g., 1% and 10 Hz). The moduli of the material are studied on a log scale in function of a linear temperature scale. Generally, a large drop of the storage modulus can be derived as the temperature increases. In addition, a significant rise of the loss factor is displayed. In practice, the peak of the loss factor curve is mostly used to determine the glass transition temperature [65].

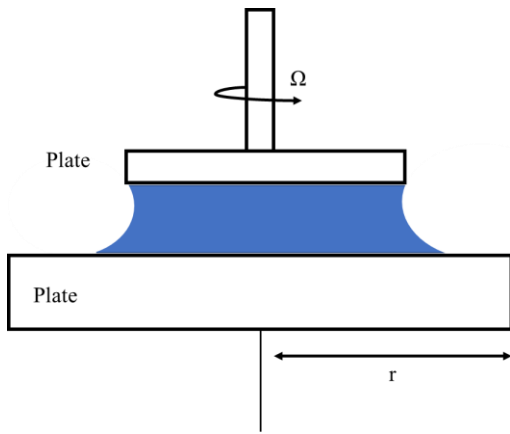


Figure 14: Compact rotational disk rheometer schematic presentation.

### Capillary rheometer (extrusion)

A capillary rheometer comprises of a cylindrical ram with a smooth surface. The cylinder is filled with the sample. The ram will move at a constant speed inside the cylinder to measure the shear rate. During the movement of the ram, the sample will flow through the capillary, located at the other side of the cylinder. For the capillary rheometer the shear rate laterally to at the wall is calculated via equation (23). The volumetric flow rate can be determined via equation (43). Eventually the shear stress located at the capillary wall can be calculated via equation (25) [13] [61] [62] [66]. A graphical example of a capillary rheometer is presented in Figure 15.

$$Q = \pi R_r^2 v_r \quad (43)$$

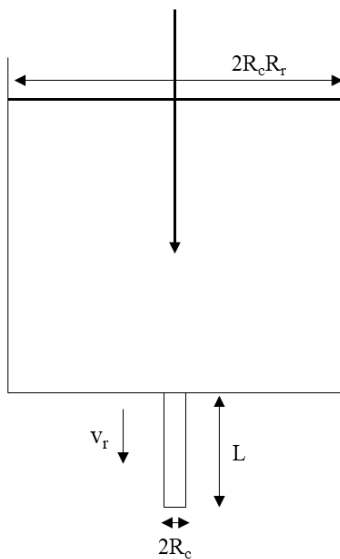


Figure 15: Capillary rheometry schematic presentation.

### 2.4.2. Differential scanning calorimetry (DSC)

Differential scanning calorimetry (DSC) is one of the leading techniques to analyse the crystallinity of semi-crystalline polymers (e.g., PP). DSC is a thermoanalytical method in which the amount of heat required to heat a sample is compared to a reference, both in function of the temperature. During experiments, the temperature of both samples is kept at equal values. DSC is mainly used for the analysis of phase transitional behaviour, such as: melting, glass transition, and exothermic decompositions. These transitions are characterized by energy or heat capacity changes. However, via DSC it is possible to detect these changes with a high sensitivity. Generally, DSC is used to analyse the composition,

melting point, and glass transition temperature of polymeric materials. Via this analysis it is possible to identify polymer degradation (e.g., lower melting point) [67]. Additionally, it is possible to uncover the percent crystallinity in the sample. As mentioned prior, the percentage crystallinity influences several polymer characteristics, such as: stiffness, toughness, brittleness, creep behaviour, gas transfer resistance, stability, and optical clarity [11] [68].

The use of DSC provides several benefits: low cost, easy operation, the ability to process many samples at once (+ 40), high performance regarding sensitivity and resolution, and consistent and reproducible measurements. To measure the polymer, a small sample of approximately ten milligrams is precisely weighed and put into the DSC machine. For DSC, a pre-determined temperature profile is run through. The initial temperature of the sample is generally room temperature (20 °C). The material is then heated to a temperature of approximately twenty to thirty degrees above the melting temperature of the polymer. The heating time, also known as heating rate, is set to a preferred value (e.g., 10 °C/min). Additionally, the amount of purge gas is determined (e.g., 10 mg) [68] [11].

The melting and cooling heat are calculated by integrating the areas under the heating and cooling peak. The heat flux is defined in terms of Joules per gram sample. It is important to note that for some polymers a cold crystallization exothermic peak is not observed via DSC. However, this does not include PP. The crystallinity percentage can be calculated via equation (44).  $\Delta H_{r^\circ}$  is defined as the reference melting heat value for a certain polymer if it is 100% crystalline. For PP,  $\Delta H_{r^\circ}$  amounts to a value of approx. 207.1 J/g [11]. An example of a typical DSC curve is graphically presented in Figure 16, below this paragraph. In this graph, the x-axis represents the temperature, defined in degrees Celsius. The y-axis represents the heat flow (W/g) [11]. On this curve, exothermic reactions (e.g., crystallization) are presented as a positive heat flow (upwards direction of transitional peak). On the other hand, endothermic reactions (e.g., melting) are presented as a negative heat flow (downwards direction of transitional peak). The width of the melting peak is a generally observed material property, which gives information about the size of the crystals and their perfection [18].

$$\% \text{ Crystallinity} = \frac{\Delta H_h - \Delta H_c}{\Delta H_{r^\circ}} 100\% \quad (44)$$

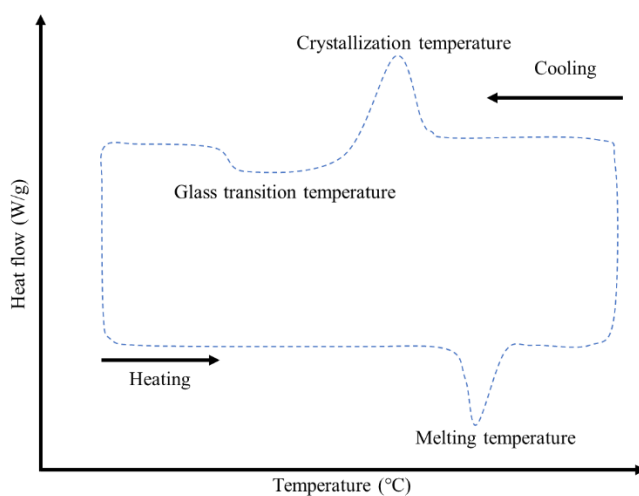


Figure 16: Typical DSC curve (exemplary).

### 2.4.3. Mechanical testing

Polymer characteristics as well as its processing define the final material properties such as tensile strength, compression, flexural stress, shear stress, melting point, yield stress, wettability, etc. As a result, changes in tensile characteristics are remarkably interesting and viable to determine material deterioration [60]. Therefore, it requires testing them not only on rheological properties and crystallinity, but also on mechanical properties [69]. Generally, tensile properties are of crucial importance for a proper quality-control examination [60]. The mechanical testing of a sample includes tests regarding tensile strength, compression, flexural stress, and shear stress. These tests can generally be performed with a mechanical testing machine, after adaptation for each specific test. For each test, a sample (e.g., tensile bar or rectangular shape) is inserted into the load cell. Grips are used to fix the sample into the cell. Additionally, an extensometer is required when measuring the elongation modulus. To measure the dimensions of the test piece is typically made use of a micrometer or a dial gauge [69].

#### Tensile strength testing

The tensile strength testing is the leading material testing technique. The tensile test provides information regarding several properties related to material deformation and strength, such as the tensile stress and strain properties. These properties are calculated by applying a force to the material, to rip the sample apart. The required force, as well the deformation of the material (deformation rate) are measured. The force and displacement are then furtherly used in the calculation of the stress and strain properties. The stress and strain are calculated via equation (45), (46) and (47). Important note, the stress is measured for the original sample dimensions, pre-tensile testing. When force is applied to the sample, it will stretch and become less thick in comparison to the original shape. The result of material stretch is an increased stress. However, this is not the calculation of the true material stress. The true material stress is calculated via the comparison of the original material stress (pre-test) and the measured material stress. Here, the difference between the stretched ( $l_s$ ) and original sample length ( $l_o$ ) provides the true displacement of the sample.

$$\alpha = \frac{F}{Area (mm^2)} = \frac{F}{hb} \quad (45)$$

$$\varepsilon = \frac{l_s - l_o}{l_o} \quad (46)$$

$$\varepsilon (\%) = \frac{l_s - l_o}{l_o} 100\% \quad (47)$$

$$E_E = \frac{\alpha}{\varepsilon} \quad (48)$$

Generally, the relation between stress and strain is linear until a certain breaking point, also known as failing point. The relation between stress and strain is constant and expressed as the elastic modulus of the material. The elastic modulus is presented by equation (48) [69]. A graphical example of a typical stress versus strain curve for a perfect elastic solid is presented in Figure 17. However, polymeric materials are non-linear. Their stress and strain properties can be very differently and are divided into four categories: yield stress greater than failure stress, yield stress less than failure stress, equal yield and failure stress, and brittle materials. A visualisation of the stress-strain curve for each type of polymer is presented in Figure 18.

Commercially, only two types of tensile testing machines are utilized: the electromechanical and servohydraulic testing machine. Generally, the allowed tolerance of tensile strength tests is between

approximately ten to twenty percent. Important note, plastic samples with a thickness of less than one millimetre are not suitable for this type of test. To obtain accurate results, the samples are fixed by grips and measured in each direction five times. The samples need to be very precisely aligned to the axis of the machine. A proper alignment additionally ensures the prevention of pre-stresses, which is highly desired. The testing speed of the machine is determined based on the type of material tested. The general testing speeds are between 5 to 300 millimetres per minute. If a sample bends or breaks outside the applied pressure zone, the test sample should be rejected. This point is known as the failure point of the material. The result from a tensile strength test is a force-elongation curve. From this curve, the stress, strain, and moduli curves can be calculated [69].

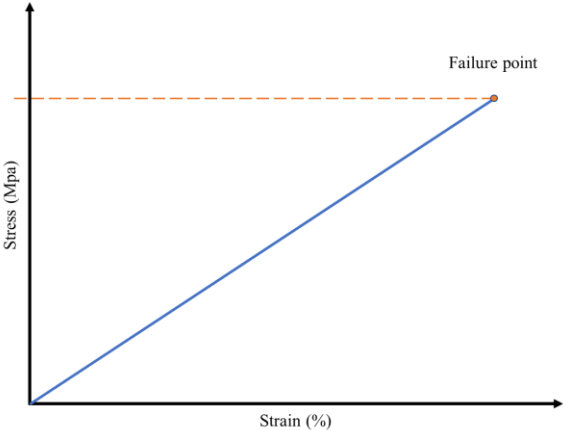


Figure 17: Typical stress-strain curve for perfect elastic solids.

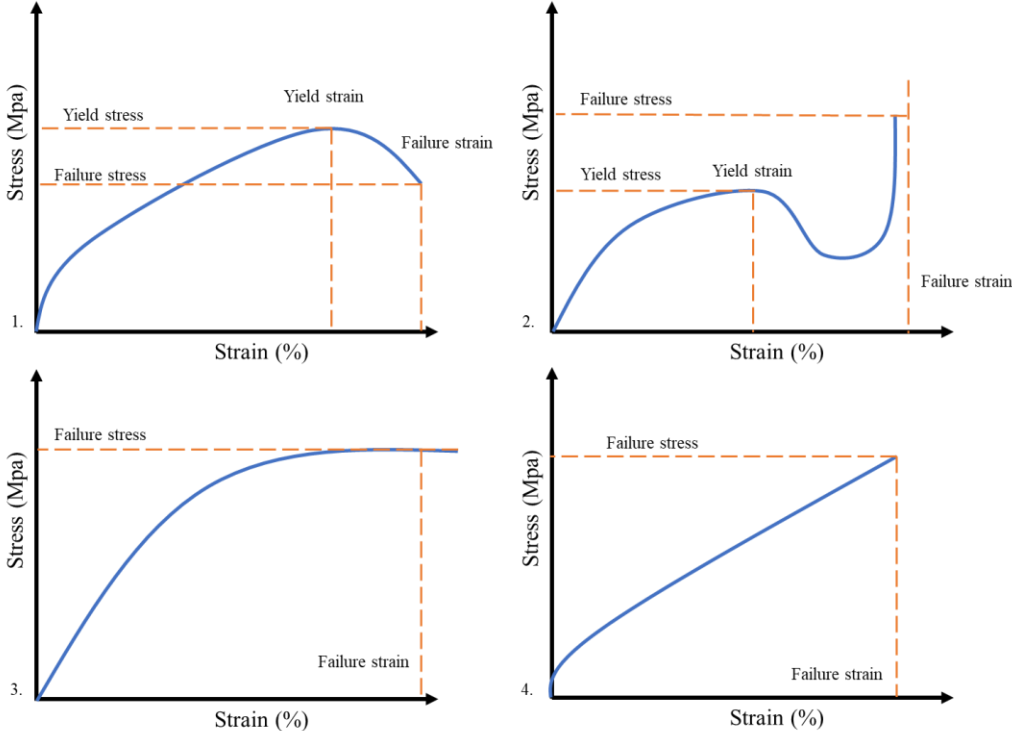


Figure 18: Typical stress-strain characteristics: 1. Yield stress > failure stress 2. Yield stress < failure stress 3. Yield stress = failure stress 4. Brittle materials.

## Flexibility testing

The flexural properties of a material are almost of the same importance as the tensile properties. For flexibility testing a rectangular sample is measured, instead of a tensile bar. The rectangular samples are easier to manufacture and test, what make flexibility testing an easier to perform technique. Additionally, the probability of gripping problems is neglectable due to the rectangular shape. The flexibility stress and strain properties of the material are measured by applying a force onto the sample. The applied force will result in the sample to flex and displace. With flexibility tests, the sample exhibits a maximum tensile force on one side of the sample. The other side of the sample exhibits a compressive force. Important note, the same properties are measured as with the tensile tests. However, with flexibility tests, the stress and strain are the maximum outer fibre stresses, as the sample is analysed on its outer layer. The pressure projected onto the sample can be realised via three different setups: a three-point, four-point, and simple cantilever loading methods. For this research is made use of the most common technique (three-point) to measure the samples. With three-point loading the force is applied to the sample at three points: one centre point and two outer supporting points [69]. A visualisation of the three-point loading of a sample is presented in Figure 19.

The sample is fixed onto two supporting rods, located at both ends of the sample. The force is applied at the centre of the sample via a loading rod. To measure the applied force and the induced displacement, the central loading rod is equipped with a force transducer and displacement measuring device. Nevertheless, to obtain feasible data, the force and displacement need to be transformed to provide the stress-strain characteristics of the sample. For a rectangular sample is made use of several equations to calculate the flexural stress (49) and flexural strain (51). However, the value of  $s$  in equation (49) is neglectable small in comparison to the length ( $l$ ). As a result, this formula is adapted to be more accurate for the calculation of the stress to equation (50). From the stress and strain expressions, the flexibility modulus can be calculated via equation (52). With this modulus, the slope is characterized by the force-deflection curve between reference strain-values. For a standard test sample, the test speed is generally set to a value of 2 millimetres per second [18] [69].

$$\alpha_f = \frac{3Fl}{2bh^2} \left( 1 + \frac{4s^2}{l^2} \right) \quad (49)$$

$$\alpha_f = \frac{8Fl}{\pi D^3} \quad (50)$$

$$\varepsilon_f = \frac{6hs}{l^2} \quad (51)$$

$$E_f = \frac{4l^3}{3\pi D^4} \text{ slope} \quad (52)$$

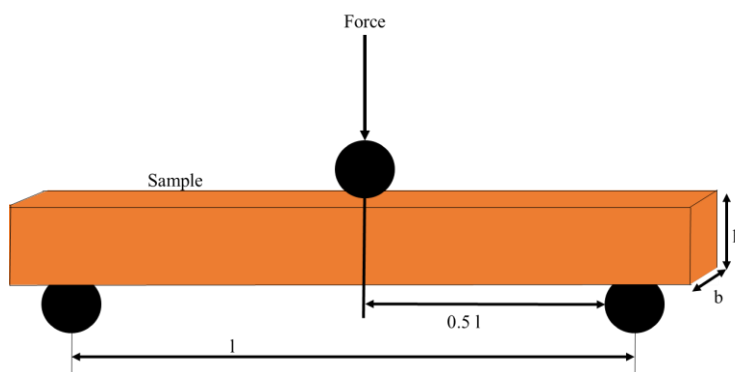


Figure 19: Three-point loading of a polymer sample (flexibility test).



### 3. Materials and methodology

#### 3.1. Microinjection moulding machine

For this research is made use of the Fanuc ROBOSHOT S-2000i30B to perform the experiments, presented in Figure 20. The machine is implemented with an IS525/330/240 injection unit. The screw has a diameter of 14 mm. A specific overview of the mechanical and environmental specifications of the machine is presented in Table 17. The mould is cooled via an external cooling system from HB-THERM (HB-180Z2), presented in Figure 21. During experiments, the amount of cooling water is kept at a value of approximately 5.7 l/hr. Technical dimensions of the Fanuc ROBOSHOT are presented in Figure 45 in the appendices.



Figure 20: Fanuc ROBOSHOT S-2000i30B [70].



Figure 21: Thermo-5 (HB-180Z2) cooling unit (HB-THERM).

Table 17: General overview of the mechanical and environmental specifications of the Fanuc Roboshot S-2000i30B [70] [71].

Unit	Process part	Mechanical specification	
Clamp unit	Clamping mechanism	Double toggle	
	Tonnage force of the clamp	300	kN
	Min. – Max. die height (= total mould height when closed)	150 – 330	mm
	Clamping stroke	230	mm
	Locating ring diameter	100	mm
	Tie bar spacing (H x V)	310 x 290	mm
	Platen size (H x V)	440 x 420	mm
	Minimum mould size (H x V) (a smaller mould can limit the clamp force)	175 x 165	mm

	Ejector stroke		60						mm
	Max. ejector force		8						kN
Injection unit	Nozzle touch force		9						kN
	Screw diameter		14	16	18	20	22		mm
	Injection stroke		56	56	75	75	75		mm
	Max. injection volume		9	11	19	24	29		cm <sup>3</sup>
	Injection speed 525 mm/s (IS525/330/240)	Max. injection pressure (high pressure filling mould)	/	/	300	270	220		MPa
		Max. injection pressure	250	250	230	200	180		MPa
		Max. pack pressure	250	250	210	180	160		MPa
		Max. injection rate	80	105	133	164	199		cm <sup>3</sup> /s
		Max. injection speed	525						mm/s
		Max. screw rotational speed	450						min <sup>-1</sup>
		Machine weight	Approx. 1.88						tonnes
		Required current to machine	50						A
	Injection speed 700 mm/s (IS700/500)	Max. injection pressure (high pressure filling mould)	/	/	300	270	220		MPa
		Max. injection pressure	250	250	230	200	180		MPa
		Max. pack pressure	250	250	210	180	160		MPa
		Max. injection rate	107	140	178	219	266		cm <sup>3</sup> /s
		Max. injection speed	700						mm/s
		Max. screw rotational speed	450						min <sup>-1</sup>
		Machine weight	Approx. 1.95						tonnes
		Required current to machine	60						A
Screw barrel	and	Amount of pyrometers	Barrel	3					
			Nozzle	1					
		Total heater wattage		2.4	2.8	3.1	3.5	3.8	kW
Nozzle for transparent polyolefins	Length		Short			Long			
	Shape penetration		35			65			mm
Cooling water	Flux		> 3.0						l/min
	Pressure		0.15 – 0.49						MPa
	Connection diameter		9						mm
Dry air for ejector	Req. air pressure		0.5						MPa
	Flux		> 200						l/min

Complete machine	Input power source	3-phase AC200V±10% 50/60Hz±1Hz		
	Earth grounding resistance	3-phase AC220V±10% 60Hz±1Hz < 100Ω		
	Environment conditions	Temperature	0 – 40 (20 – 25 is recommended)	
		Humidity	< 75%	
		Vibrations	< 0.5G	
Atmosphere	No presence of corrosive gases			

### 3.2. Rotational rheometer (MCR302L, Anton Paar)

The used rotational rheometer to perform analyses is a compact disk rotational rheometer, as discussed prior. This rheometer is connected to a computer with the Anton Paar software to analyse and save the measurements. Two different probes are used for analyses: the PP25 (79044) and the much smaller PP08 (5681) probe. Visual presentations of the MCR302e and the probes are presented in Figure 22 and Figure 23, below this paragraph. The specific dimensions and properties of both probes are presented in Table 18 [10].



Figure 22: MCR302e Rotational Compact Disk rheometer (Anton Paar).



Figure 23: PP25 (79044) parallel plate probe (left) and PP08 (5681) (right).

Table 18: PP25 (79044) and PP08 (5681) specifications.

Property	PP25 (79044)	PP08 (5681)	Unit
Plate diameter	24.999	7.996	mm

Torsional compliance	0.00113	0.00156	rad/Nm
Active length	100	100	mm
Positioning length	100	100	mm
Trim position	25	25	μm
Min. temperature	-200	-200	°C
Max. Temperature	620	620	°C

---

### 3.3. Differential scanning Calorimetric analysis machine (2920 TA, TA Instruments)

The used DSC machine is the DSC autosampler (2920 TA), from TA Instruments. A photo of this machine is presented in Figure 24 **Fout! Verwijzingsbron niet gevonden.**, below this paragraph. To perform experiments, several types of DSC pans can be utilized. However, for this study are aluminium pans used, which are applicable in a temperature range between -180 to 600 °C [67]. These experiments are performed for several types of PP ( $T_m = 160$  °C). As a result, a maximum allowable temperature of 190 °C is set.



Figure 24: DSC Autosampler (TA Instruments).

### 3.4. Tensile testing machine (Quasar 50kN, Galdabini)

The used tensile testing machine is the Quasar 50kN, from Galdabini. A photo of this machine is presented in Figure 25. To perform tensile strength measurements with the Quasar, the tensile bar needs to be fixed between the clamps of the moving and fixed part. After pressing start, the machine will pull the tensile bar until breakage and the measured data is sent to a computer [72].



Figure 25: Quasar 50 kN tensile testing machine.

### 3.5. Flexibility testing machine

To evaluate the suitability of conventional flexibility techniques for the analysis of small samples is the ZwickRoell 1486 (ZwickRoell GmbH. & Co. KG) and a three-point loading setup, as discussed previously (2.4.3). The ZwickRoell 1486 and the three-point loading setup are graphically presented in Figure 26. The applicable measurement range of this machine is from 1 to 500 Newton. In addition, the adjustment tensile and adjustment compression amount to 1.006920 and 1.007070.



Figure 26: ZwickRoell 1486 flexibility testing machine (ZwickRoell GmbH. & Co. KG).

### 3.6. Polymeric materials

To perform experiments, two main types of PP are used. Both these materials are commercially produced and sold by the company Sabic, located in the Netherlands, Geleen. These polymers are PHC31-81, referred to as simply PHC31 in this thesis, and 515A. The PHC31 is described as a PP impact copolymer, displaying very high stiffness and impact strength. PHC31 is said to exhibit particularly good flow properties, and is UV stabilized [73] [74]. The 515A is described as a PP homopolymer, displaying remarkably high flow and rather wide molecular weight distribution. 515A is said to contain anti-gas stabilization and is generally used for filaments run continuously (e.g., tri-colour carpet yarn). This material is not validated yet regarding safety for usage in medical applications [75]. Sabic has provided datasheets of these materials, which are presented below this paragraph in Table 19 and Table 20. It is important to note that both of these materials are sold as pelletized granules [73] [74] [75].

Table 19: PHC31-81 datasheet.

Properties			Units
	Melt flow rate (230°C, 2.16 kg)	15	dg/min
	Density	905	kg/m <sup>3</sup>
	Part shrinkage (24h post-injection)	1.6	%
Mechanical properties			
Tensile test	Yield stress	25	MPa
	Yield strain	5	%
	Stress at break	17	MPa
	Tensile modulus	1300	MPa
Izod notched impact	At 23 °C	11	kJ/m <sup>2</sup>
	At 0 °C	7	kJ/m <sup>2</sup>
	At -20 °C	5	kJ/m <sup>2</sup>
Charpy notched impact strength	At 23 °C	12.5	kJ/m <sup>2</sup>
	At 0 °C	8	kJ/m <sup>2</sup>
	At -20 °C	5	kJ/m <sup>2</sup>
Hardness shore D		65	
Thermal properties			
Heat deflection temperature	At 1.80 MPa	55	°C
	At 0.45 MPa	80	°C
Vicat softening temperature	At 10 N	149	°C
	At 50 N	74	°C

Table 20: 515A specification sheet.

Properties			Units
	Melt flow rate (230°C, 2.16 kg)	24	dg/min
	Density	905	kg/m <sup>3</sup>
	Isotacticity	Medium	
Mechanical properties			
Tensile test	Yield stress	37	MPa
	Yield strain	8	%
	Stress at break	17	MPa
	Tensile modulus	1700	MPa

In order to determine the minimal amount of material required to perform a single shot with the Fanuc ROBOSHOT is a powdered material used instead of pellets. The used material was a standard Ziegler-Natta based PP with broad MWD ( $M_n=50$  kg/mol, PDI = 6). As a real case study to validate the efficacy of the developed protocols, two novel lab-scale PP materials developed by an external company have also been tested (grade 1 and grade 2). This material is processed as powdered material (pure), as well as granules (pure) and granule blends. To accurately determine the real processing behaviour of the powdered grades, these pellets were constructed to fully characterize the behaviour of the material and to eliminate the limitations and possible difficulties of the Fanuc injection moulding machine in combination with powdered material feed. These filaments were fabricated via putting 25 grams of PP powder (grade 1 or 2) and 62.5 mg stabilizer in liquid acetone in order to have a proper stabiliser dispersion. The utilized stabiliser was 2,6-di-tert-butyl-4-methylphenol (99%). This stabilizer was added to the grades to improve the thermal resistance of both materials in an attempt to make them more suitable for injection moulding processing. After evaporating the acetone, both grades of the pure PP powder were processed into filaments via extrusion at 150 °C (Mini-REX). Additionally, two polymeric blend filaments were fabricated. Each blend consists of 5 grams of grade 1 or 2, mixed with 20 grams of the powdered polymer from Sabic and 62.5 mgs of stabilizer. The same steps (acetone mixing – evaporation – extrusion – cutting) are followed in the process to make these filaments. The complete procedure which was followed to produce these filaments are graphically presented in Figure 27.

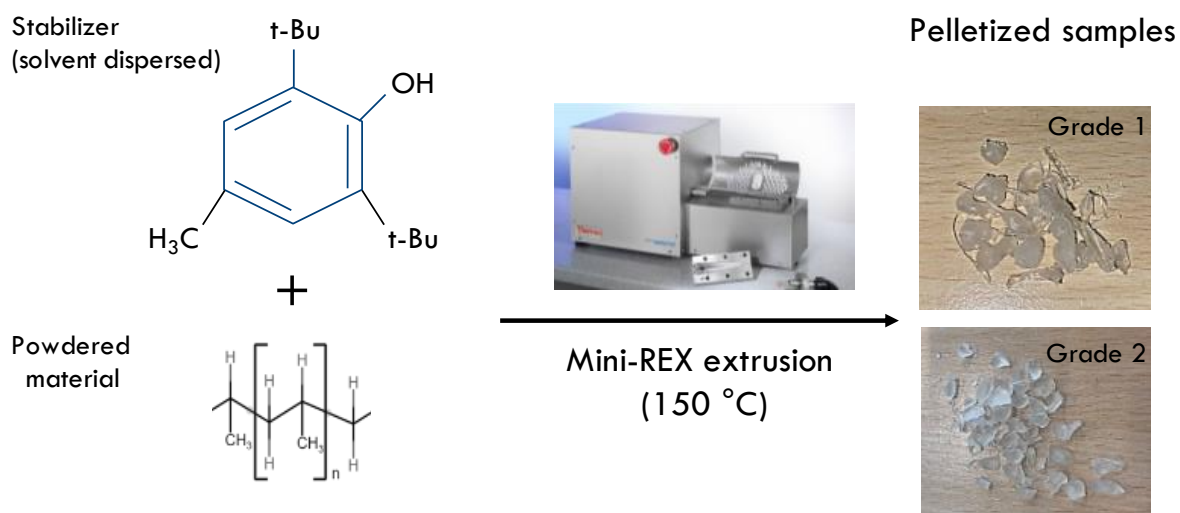


Figure 27: Pelletization procedure.

### 3.7. Viscosity curve of the microinjection moulding machine

As mentioned prior is it of the utmost importance to analyse the viscosity curve of the machine. This is to identify the Newtonian behaviour region of the melt. In this chapter the different steps are given which are required to accurately develop the viscosity curve of the microinjection moulding machine [8] [45]:

1. Tune the melt temperature to the recommended value given by the manufacturer. If the recommendation is in a range, set the temperature to the centre value of this range.
2. Deactivate the holding phase by setting the holding phase parameters to zero. This translates to solely melt injection by the machine
3. Fix the injection pressure to the maximum recommended value.
4. Set the cooling time large enough to ensure complete part cooling to the desired ejection temperature, before opening the mould.
5. Set a low injection speed to manufacture a short part, make sure that the mould cavity only is filled for 50% by adjusting the position of the transfer.
6. Increase the injection speed stepwise until the maximum injection speed of the machine. Adjust the transfer position of the mould to ensure that approximately 95% of the mould cavity gets filled.
7. Perform five new injection shots while monitoring the fill time and peak pressure necessary to fill the mould cavity.
8. Lower the injection speed in small amounts, while monitoring the peak injection pressure and fill time (e.g., 100 to 90%).
9. Repeat step 6 to obtain the lowest possible injection speed
10. Find the SIR of the screw (=1)
11. Calculate the viscosity via equation (31)
12. Plot the viscosity curve

The influence of the temperature is studied for three different temperature profiles of the injection system. These profiles are presented as Tlow, Tmid, and Thigh. The temperature beneath the hopper is kept at a value of 60 °C. The temperature of the mould is set at a value of 45 °C. A visual presentation of the temperature profile, as well as the data is presented in Table 21 and Figure 28.

Table 21: Temperature profile of the injection system (°C)

Profile	H	B3	B2	B1	N
Tlow	60	175	200	210	210
Tmid	60	175	210	220	240
Thigh	60	215	250	260	280

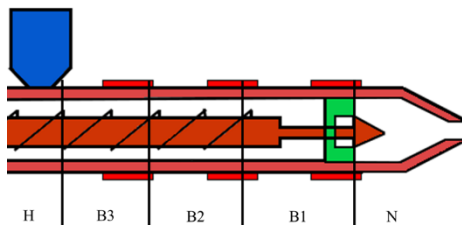


Figure 28: Temperature profile of the injection system.



## 4. Results

This chapter entails the results from the several performed experiments. As mentioned, to improve the microinjection moulding process, it is crucial to study, comprehend, and define the capabilities, limitations, and influence parameters of  $\mu$ IM. The first goal was to examine the Newtonian region of the melt in the machine. The injection speed range of the machine is limited to only the Newtonian region, as in this region small variations in process conditions do not result in significant rheological changes in the melt, such as flow behaviour and viscosity. Next, the microinjection moulding process was observed regarding the influence of the different process conditions on the material properties, part properties, and part dimensions. Here, the degree of influence of the mould temperature, the barrel and melt temperature, the injection speed, the injection and holding pressure, and the cooling time will be studied [9]. After gaining a better understanding regarding the influence of the different parameters, the following experiments will be conducted only within the Newtonian zone in order to decrease the required amount of purging material.

As mentioned, the  $\mu$ IM process will naturally lead to small-scale samples that cannot be characterized using conventional procedures. Therefore, it will be required to develop special material testing methods. However, for small scale components the mechanical and rheological testing is often limited to a small number of properties, such as tensile tests and yield kinetics for mechanical testing. For this study, the rheological properties of the moulded part and virgin material were examined via the Rotational Compact Disk rheometer from Anton Paar (MCR 302e). The difference in physical properties of the small, moulded part and conventional part size were examined via tensile strength and flexibility testing. This is performed to analyse possible material deterioration from the microinjection moulding process regarding mechanical properties.

### 4.1. Viscosity curve of the Fanuc ROBOSHOT

#### 4.1.1. Influence of the screw RPM

First is the influence of the rotational speed of the screw analysed regarding the flow behaviour of the melt. Both 515A and PHC31 are analysed separately. It is crucial to study the influence of the screw RPM as a change in the rotational movement speed of the screw leads to change in the generated frictional energy between the system and polymer melt, eventually leading to a change of the melt temperature and thus a change of the melt viscosity. However, the degree of influence of the screw RPM can differ for different injection moulding systems in combination with different types of materials. The graphical visualisation of the viscosity in function of the injection speed is presented in Figure 29. From these tests can be derived that the Newtonian region is located at an injection speed equal to or higher than 400 mm/s; For 515A, the viscosity amounts to a value of 22.48 Pa s with the screw rotational speed set to 100 RPM. When the screw rotational speed is increased to 450 RPM, the material displays a viscosity of 25.64 Pa s at an injection speed of 400 m/s. It was expected that the viscosity of the material would be lower for higher rotational speeds as more friction is generated in the system, resulting in an increase in temperature. However, one possible explanation is that due to this extra friction, the material does not increase enough in temperature to obtain the desired decrease in viscosity, but exhibits more resistance to the rotation of the screw. At an injection speed of 400 mm/s, the viscosity difference between both analysed rotational speeds is only 14%. When the injection speed is increased furtherly, it can be derived that influence of the screw RPM is decreased. At a value of 525 mm/s, the viscosity difference between both screw RPMs is only 8.3%. It is believed that if the injection would be furtherly increased, the influence of the screw RPM would reduce even more. However, the Fanuc ROBOSHOT injection moulding machine is limited to a maximum injection speed of 525 mm/s.

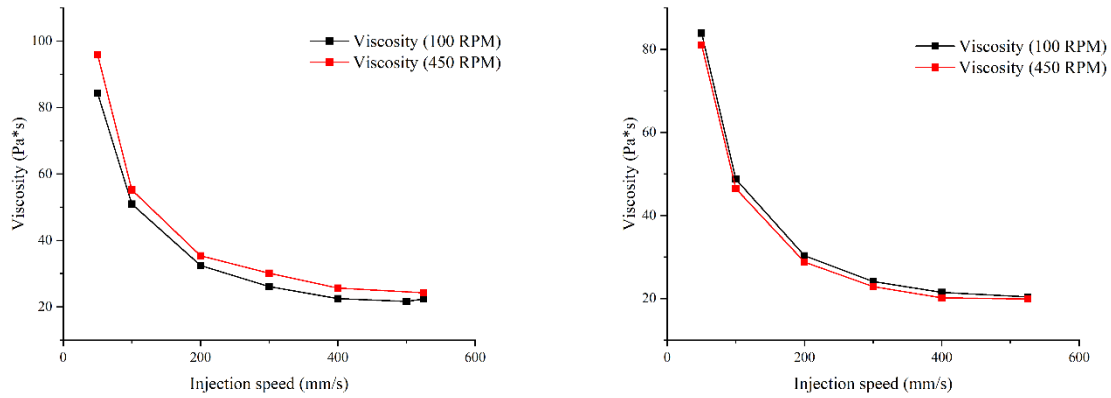


Figure 29: RPM influence 515A (left) and PHC31 (right) ( $T_{mid}$  temperature profile).

For PHC31, the viscosity amounts to a value of 21.48 Pa s with the screw rotational speed set to 100 RPM. When the screw rotational speed is increased to 450 RPM, the material displays a viscosity of 20.20 Pa s at an injection speed of 400 m/s. Here, the increase of the screw RPM results in a decrease of the melt viscosity. At an injection speed of 400 mm/s, the viscosity difference between both analysed rotational speeds is only 6.4%. When the injection speed is increased furtherly, it can be derived that influence of the screw RPM is decreased. At a value of 525 mm/s the viscosity difference between both screw RPMs is only 2.4%. It is believed that if the injection would be furtherly increased, the influence of the screw RPM would reduce even more.

#### 4.1.2. Influence of the temperature

Next is the influence of the melt temperature analysed regarding the flow behaviour of the melt. Both 515A and PHC31 are analysed separately. The graphical visualisation of the viscosity in function of the injection speed is presented in Figure 30. From these tests can be derived that the Newtonian region is located at an injection speed equal or higher than 400 mm/s, but also the major importance of the melt temperature. When the temperature is increased, it can be derived that the viscosity of each material reduces. This can be highly beneficial, but it is important to take material degradation into account when increasing the melt temperature. For these experiments, the screw rotational speed is set to a value of 450 RPM. For 515A, the viscosity amounts to a value of 25.64 to 25.22 Pa s for Tmid and Tlow at an injection speed of 400 mm/s. When the temperature of the melt is increased to the highest value the material displays a decrease in viscosity to a value of 15.44 Pa s. This translates to a decrease of approximately 39%. It was expected that the viscosity of the material would be lower for higher melt temperatures as discussed previously. When the injection speed is increased furtherly, it can be derived that the difference in viscosity between Thigh and Tlow is less significant in comparison to lower injection speeds. At a value of 525 mm/s the viscosity difference between both temperatures is decreased from 39 to 28%. However, this is still a major difference. It was expected that the viscosity of the melt would decrease in relation to the temperature. However, at the highest injection speed, the viscosity of the Tmid experiments have proven to be higher than for the lowest analysed temperature. The difference is between Tmid and Tlow amounts to 12.3%. A proper explanation for this behaviour cannot be given.

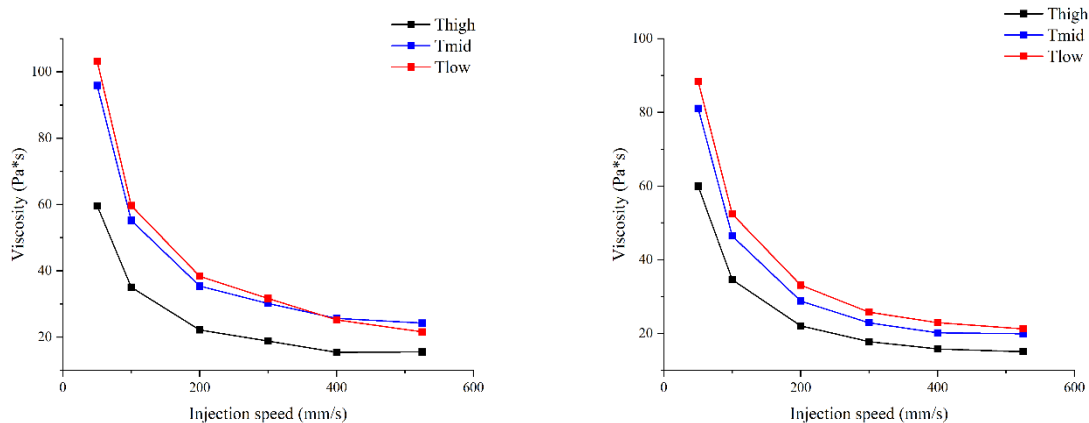


Figure 30: Temperature influence 515A (left) and PHC31 (right) (450 RPM).

For PHC31, the viscosity amounts to values of 20.20 and 22.91 Pa s for Tmid and Tlow at an injection speed of 400 m/s. When the temperature of the melt is increased to the highest value the material displays a decrease in viscosity to a value of 15.79 Pa s. This translates to a decrease of approximately 31% from Tlow to Thigh. It was expected that the viscosity of the material would be lower for higher melt temperatures as discussed previously and this can also be concluded from Figure 30. For injection speeds above 400 mm/s, it can be derived that the difference in viscosity between Thigh and Tlow remains constant at approximately 30%. Important note, both PHC31 and 515A are different types of PP. From these experiments can be concluded that to perform reproduceable, smooth processes and experiments, a minimal injection speed of 400 mm/s needs to be respected with both 515A and PHC31. With an injection speed lower than 400 mm/s the chance of significant fluctuations in the melt processing behaviour and thus experiments increases as the injection speed is furtherly increased, as mentioned prior (1.4). As a result, the different experiments regarding the purging of the injection moulding system are performed with an injection speed of 400 mm/s in order to analyse the absolute limits of the injection moulding system and system purging; But with reproduceable results. In addition, to characterize the

rheological analysis, tensile strength, and flexibility testing method, the utilized specimens are fabricated with this injection speed to obtain uniform specimen properties. These uniform specimen properties result in an increased accuracy of the determination of the suitability of these different analyses techniques for small specimens.

## 4.2. Minimal required amount of material to perform one single shot with the Fanuc ROBOSHOT

In order to explore the limitations of the Fanuc ROBOSHOT regarding the minimal required amount of virgin material to perform a singular shot, several experiments were conducted with a powdered type of PP. Generally is made use of pellets instead of powdered material for injection moulding, but in order to find the absolute minimal amount was opted to use powdered material. As mentioned, the reduction of the required amount of material is very interesting for the material development stage in order to reduce the research costs and time as much as possible. However, due to the feed material being a powdered form, the optimal process conditions can differ for this type of material in comparison to the pelletized variant. Powdered material is known to result in difficulties during the dosage phase of the material onto the heated, rotating screw. In addition, powdered material is known to have the possibility to form clogs inside the injection unit. In order to decrease possible system clogage, a different injection speed, screw RPM, or even injection pressure can prove to be more suitable.

For these experiments, the powdered PP from Sabic was used in order to analyse minimal required amount of material to perform a singular shot with the Fanuc ROBOSHOT injection moulding machine. These experiments were performed with an injection speed of 200 mm/s, an injection pressure of 100 bar, a screw RPM of 300, a holding pressure of 150 bar for 9 seconds, a cooling time of 11 seconds at 45 °C, and the “Tmid” temperature profile of the injection unit. After obtaining the minimal amount of material with these settings, the screw RPM and injection pressure were observed in order to furtherly decrease the amount of required material. With these settings it was possible to process a singular shot with 4 grams of powder. This already is a significantly low amount of required material. However, this value represents the amount of material required, after purging the system with virgin powder. To perform experiments during the MDS stage will require more amount of material, due to the required purging step.

After analysing the influence of both the injection pressure and the screw RPM, an ideal configuration of the process was obtained. A screw RPM of 450 and injection pressure of 100 bar (in combination with the previously mentioned process conditions) resulted in a minimal required amount of approximately 3 grams powder to perform a singular shot. Only with these settings it was possible to perform a single shot with 3 grams. When the injection pressure is set to a value of 200 bar, 3 grams was insufficient to perform a singular shot. The screw rotational speed has proven to be of crucial importance to process powdered material. From these experiments can be concluded that an increase of screw RPM has a beneficial effect on the processability of powdered materials. In contrast to the screw RPM, the injection pressure has proven to exhibit a non-beneficial effect on the processability of low amounts of powdered material. An increase in injection pressure resulted in an increase of required amount of material to perform a single shot. A possible explanation cannot be given.

Lastly, an estimate is presented of the minimal required amount of material to perform a single shot, at any process conditions configuration. To perform a single shot with complete certainty, approximately 8 to 10 grams of PP powder is required. In order to validate the developed protocol using a real-case study, experiments were performed with the newly developed materials (grade 1 and 2) from the external company (discussed previously) present on a very small scale. However, to successfully perform processing experiments with any material, a suitable temperature profile needs to be set with the Fanuc in order to negate the possibility of material deterioration. The study and use of the correct temperature profile is based on the melting temperature and thermal behaviour of each specific material type (generally analysed via DSC). Only when the temperature is set to a desired profile (suitable for the specific material type), it is possible to fully analyse the real processing behaviour of a certain type of

material; otherwise, the occurrence of material deterioration leads to non-representative and inaccurate results.

From DSC analysis it was concluded that the melting temperature of the powdered material amounted to approximately 140 °C (grade 1) and 135 °C (grade 2). The received DSC curves are graphically presented in Figure 31. The material exhibited a lot of difficulty being dosed onto the screw; no material was taken into the system from the rotational screw movement. However, it was possible to fabricate not-completely filled deteriorated specimens with a melt temperature of 150 °C. The other settings of the system were set the same as with the powdered PP from Sabic, except the cooling time (300 s). The injection pressure and screw RPM were set to a value of 100 bar and 450 RPM. These not-completely filled specimens were obtained with 5 grams of material per shot. But it is important to mention that at 150 °C, material degradation was observed to a relatively large amount in each specimen. At a temperature lower than 150 °C, the material solidified inside the injection system, completely clogging the machine. Since it was impossible to completely fill the entire cavity shape with these settings, a higher mould temperature can possibly enhance the filling efficiency. It is expected that the material cools significantly fast inside the mould system, possibly solidifying inside the runners and gates, mid-injection.

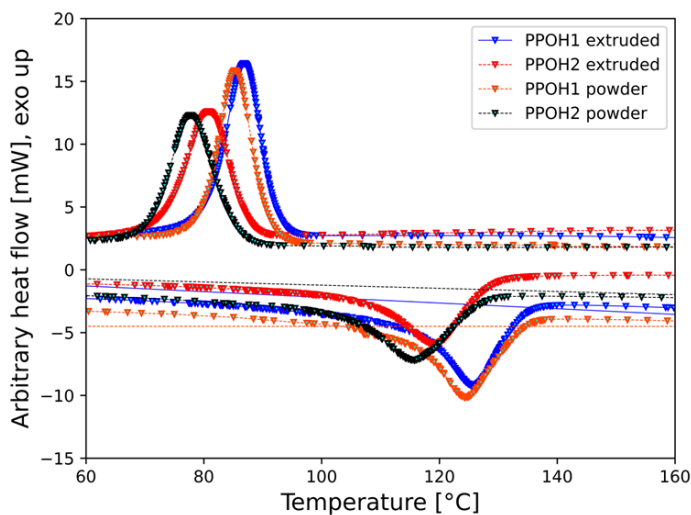


Figure 31: DSC curves powdered grades (PPOH1 = grade 1, PPOH2 = grade 2).

In addition, the material is extremely brittle; The moulded part tends to break at multiple locations every time the mould is opened. The main breakage points are connection between the sprue and the rest of the part shape and the corners of the part. It is important to note that during these experiments, the part breakage eventually led to complete clogging of the sprue and entrance point of the mould cavity. A system clogage necessitates complete mould disassembly to effectively remove these material clogs. In order to furtherly examine the processing behaviour of this newly developed PP and overcome the dosage problems, polymer filaments were fabricated and cut to reflect real pelletized processing behaviour. Injection moulding machines are generally designed to process pellets and not powdered material.

From these experiments it was concluded that even after pelletization the material exhibited a lot of difficulty being processed with microinjection moulding. In addition, a lot of clogging occurred, especially with processing temperatures below 150 °C. It was possible to complete a single shot with both pure, stabilized grades. But due to the difficulty of material it was considered to be a risk to the injection moulding system. As clogging occurred in a significant matter, system breakage was a real

risk. As a result no further experiments were performed with the pure grades. Due to the very low viscosity of the material it was opted to use an injection speed of 200 mm/s and a lower injection pressure of 100 bar. The screw RPM was set to a value of 450 RPM with a relative large amount of material to successfully dose the material onto the screw. A cooling temperature of 45 °C and cooling time of 120 seconds was set. These experiments were performed with a temperature profile of: H = 60 °C, B1 = 130 °C, B2 = 140 °C, B3 = 152 °C, N = 152 °C.

On the contrary, the polymeric blend filaments with grade 1 were very suitable for injection moulding. These experiments were performed with a temperature profile of: H = 60 °C, B1 = 150 °C, B2 = 160 °C, B3 = 170 °C, N = 180 °C. An injection speed of 200 mm/s and a lower injection pressure of 100 bar were utilized. The screw RPM was set to a value of 450 RPM with a relative large amount of material to successfully dose the material onto the screw. A cooling temperature of 45 °C and cooling time of 120 seconds was set. It was possible to perform a singular shot with approximately 3 grams of material, which displays system consistency for suitable materials. However, the second grade blend was yet again very difficult to process. The settings were kept the same as with the first grade blend, but the same difficulties as with the pure, stabilized grades occurred. Of each filament type, one moulded part was obtained and furtherly analysed regarding the molecular orientation.

### 4.3. System purging experiments

These experiments are performed with PHC31 and 515A. The determination of a complete system purge is performed via rheological analysis; moreover frequency tests of the viscoelastic behaviour. Since there is some deviation occurring between different measurements with the PP25 probe and possible material degradation, a threshold of maximum 15% compared to the Carreau – Yasuda fit is accepted in order to determine material purity after the processing step. In case the material viscosity is within the 15% deviation threshold, a complete system purge is concluded. In order to have a good reference viscosity, both materials (virgin) are thrice tested regarding their rheological properties and a mean complex viscosity is calculated for each angular frequency. The complex viscosities of both materials are graphically presented in Figure 32.

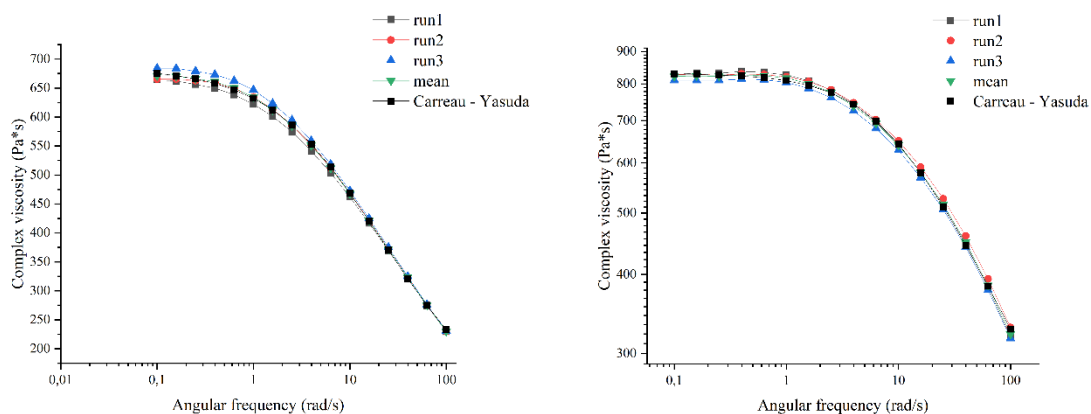


Figure 32: Complex viscosity of 515A (left) and PHC31 (right) in the function of the angular frequency (230 °C).

#### 4.3.1. RPM influence in combination with maximum injection pressure

##### 4.3.1.1. More viscous (PHC31) change to less viscous (515A)

In this paragraph, the results of the system purging experiments are discussed for a switch from a more viscous to a less viscous material. The experiments are performed with an injection pressure of 200 bar, a cooling time of 11 seconds, a mould temperature of 45 degrees Celsius and an injection speed of 400 mm/s. The combinatorial influence of the temperature and the RPM is studied via performing

experiments at different temperature profiles, as specified in 3.7. The results from these experiments are visually presented in Figure 33. As can be seen from Figure 33, a change in RPM does not significantly influence the required amount of purging material. However, it can be derived that a high screw RPM is beneficial in order to decrease the amount of purging material as much as possible. The least amount of purging material is obtained at the highest temperature profile (Thot) in combination with a screw RPM of 450. A complete system purge was completed with only 14 grams of virgin material or 7 shots, making it very viable for material research purposes. The combination of the Thot temperature profile and a lower screw RPM than 450 resulted in an increase of the required purging material. With a screw RPMs lower than 450, the required amount of purging material amounts to 18 grams or 9 shots. This translates to an increase of 28.6% of the required amount of material.

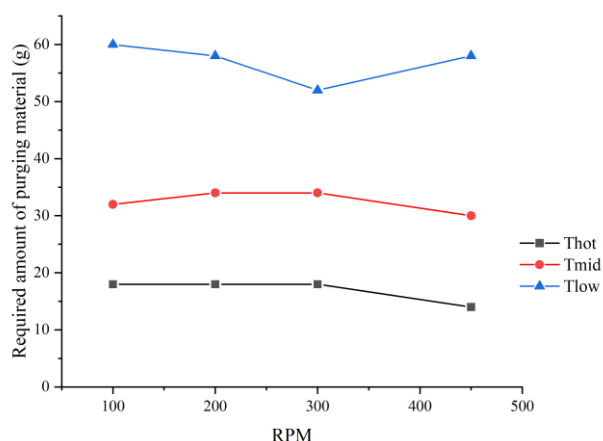


Figure 33: PHC31 to 515A (high pressure) in the function of the screw RPM.

When the temperature profile is switched to Tmid or Tlow, an increase in the required amount of purging material was derived. With the Tmid profile, a similar trend is concluded as with the Thot profile. However, this resulted in the required amount of purging material being between 30 and 34 grams of material. This translates to an increase of approximately 114% of the required amount of material in comparison to the Thot profile. When the overall temperature is furtherly decreased to Tlow, the amount of material is between 52 and 60 grams, which is a substantial amount and highly undesired. In contrast to the Thot and Tmid profile, the least amount of material required was obtained at a screw RPM of 300 for the Tlow temperature profile. When the screw RPM is decreased or increased, the amount of material increases.

#### 4.3.1.2. *Less viscous (515A) change to more viscous (PHC31)*

In this paragraph, the results of the system purging experiments are discussed for a switch from a less viscous to a more viscous material. The experiments are performed with an injection pressure of 200 bar, a cooling time of 11 seconds, a mould temperature of 45 degrees Celsius and an injection speed of 400 mm/s. The results from these experiments are visually presented in Figure 34. As can be seen from Figure 34, a change in RPM does not significantly influence the required amount of purging material. However, it can be derived that a low screw RPM is beneficial in order to decrease the amount of purging material as much as possible in combination with the Tlow profile. On contrary, a high screw RPM is more beneficial in combination with the Thot profile. The least amount of purging material is obtained at the lowest temperature profile (Tlow) in combination with a screw RPM of 100. A complete system purge was completed with only 12 grams of virgin material or 6 shots, making it yet again very viable for material research purposes. The combination of the Tlow temperature profile and a higher screw RPM than 100 resulted in an increase in the required purging material. At screw RPMs higher than 100, the required amount of purging material amounted to 14 grams or 7 shots. This translates to an increase of 16.67% of the required amount of material.

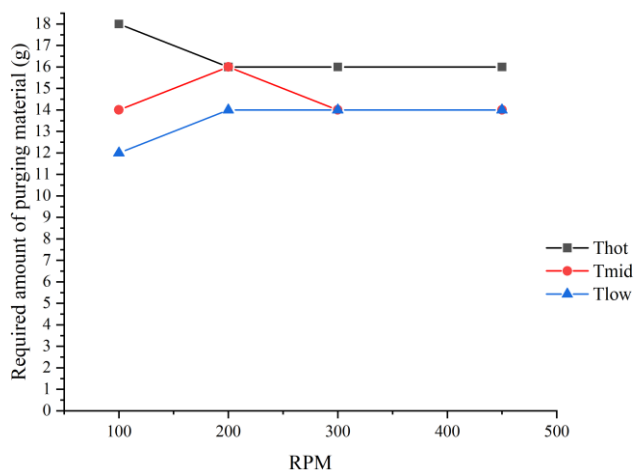


Figure 34: 515A to PHC31 (high pressure) in the function of the screw RPM.

When the temperature profile is switched to Tmid or Thot, an increase in the required amount of purging material was derived. With the Tmid profile, the required amount of purging material is between 14 and 16 grams of material. When the overall temperature is furtherly increased to Thot, the amount of material is between 16 and 18 grams. In contrast to the Tlow and Tmid profile, the most amount of material required was obtained at a screw RPM of 100 for the Thot temperature profile. It is believed that a lower temperature profile is beneficial when is switched from a less viscous to a more viscous material. With a lower temperature, the desired scraping effect of the newly introduced virgin material is enhanced, resulting in a more efficient purging process. On the other hand, a high temperature is beneficial when is changed from a more viscous material to a less viscous virgin material. With an increased temperature, both viscosities of the materials are decreased. However, this results eventually in a decreased scraping effect of the more viscous material but enhances the ‘flushing’ behaviour during the purging step.

#### 4.3.2. RPM influence in combination with low injection pressure

##### 4.3.2.1. *More viscous (PHC31) change to less viscous (515A)*

In this paragraph, the results of the system purging experiments are discussed for a switch from a more viscous to a less viscous material. The experiments are performed with an injection pressure of 50 bar,

a cooling time of 11 seconds, a mould temperature of 45 degrees Celsius and an injection speed of 400 mm/s. The combinatorial influence of the temperature and the RPM is studied via performing experiments at different temperature profiles, as specified in 3.7. The results from these experiments are visually presented in Figure 35. As can be seen from Figure 35, a change in RPM does not significantly influence the required amount of purging material. However, it can be derived that a high screw RPM is beneficial in order to decrease the amount of purging material as much as possible. The least amount of purging material is obtained at the highest temperature profile (Thot) in combination with a screw RPM of 450. A complete system purge was completed with 40 grams of virgin material or 20 shots, which is a substantial amount compared to the amount of required purging material with a high injection pressure. When both injection pressures are compared, an increase of 26 grams or 186% of the required purging material is derived when the injection pressure is set to 50 instead of 200 bar. The combination of the Thot temperature profile and a lower screw RPM than 450 resulted in an increase of the required purging material. At a screw RPMs of 100, the required amount of purging material amounted to 48 grams or 24 shots. This translates to an increase of 20.0% of the required amount of material.

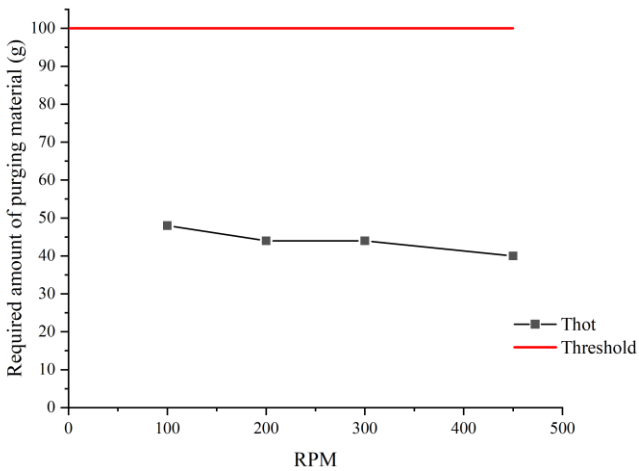


Figure 35: PHC31 to 515A (low pressure) in the function of the screw RPM.

When the temperature profile is switched to Tmid or Tlow, an increase in the required amount of purging material was derived. The threshold for the maximum allowable amount of purging material is set to a value of 100 grams. For both temperature profiles, no complete system purge was achieved at this value. For this reason, both temperature profiles are not included in Figure 35, nor are these values determined.

#### 4.3.2.2. *Less viscous (515A) change to more viscous (PHC31)*

In this paragraph, the results of the system purging experiments are discussed for a switch from a less viscous to a more viscous material. The experiments are performed with an injection pressure of 50 bar, a cooling time of 11 seconds, a mould temperature of 45 degrees Celsius and an injection speed of 400 mm/s. The results from these experiments are visually presented in Figure 36. As can be seen from Figure 36, a change in RPM does not significantly influence the required amount of purging material. However, it can be derived that a low screw RPM is beneficial in order to decrease the amount of purging material as much as possible in combination with the Tlow profile. On contrary, a high screw RPM is more beneficial in combination with the Thot profile. The least amount of purging material is obtained at the lowest temperature profile (Tlow) in combination with a screw RPM of 100. A complete system purge was completed with only 12 grams of virgin material or 6 shots, making it yet again very viable for material research purposes. The combination of the Tlow temperature profile and a higher screw RPM than 100 resulted in an increase in the required purging material. At screw RPMs higher than 100, the required amount of purging material amounted to 14 grams or 7 shots. This translates to an increase of 16.67% of the required amount of material.

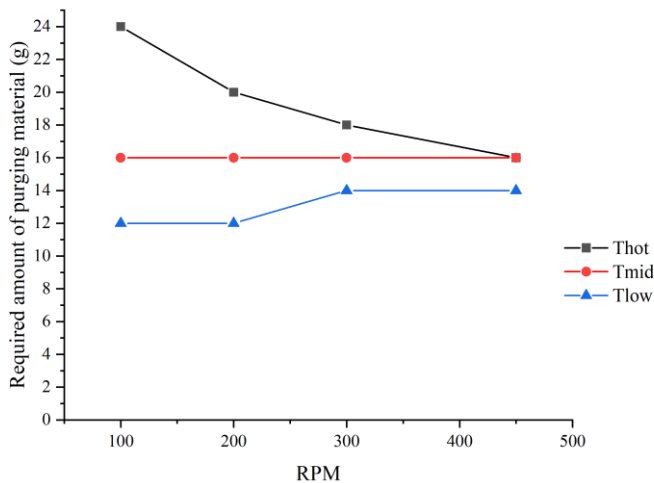


Figure 36: 515A to PHC31 (low pressure) in the function of the screw RPM.

When the temperature profile is switched to Tmid or Thot, an increase in the required amount of purging material was derived. With the Tmid profile, the required amount of purging material is 16 grams of material, with no influence of the screw RPM. When the overall temperature is furtherly increased to Thot, the amount of material is between 16 and 24 grams. Similar to the experiments performed with a high injection pressure, the most amount of material required was obtained at a screw RPM of 100 for the Thot temperature profile. It is believed that a lower temperature profile is beneficial when is switched from a less viscous to a more viscous material. With a lower temperature, the desired scraping effect of the newly introduced virgin material is enhanced, resulting in a more efficient purging process. On the other hand, a high temperature is beneficial when is changed from a more viscous material to a less viscous virgin material. With an increased temperature, both viscosities of the materials are decreased; resulting in a decreased scraping effect of the more viscous material, but enhancing the ‘flushing’ behaviour during the purging step.



### 4.3.3. P influence in combination with low screw RPM

#### 4.3.3.1. More viscous (PHC31) change to less viscous (515A)

In this paragraph, the results of the system purging experiments are discussed for a switch from a more viscous to a less viscous material. The experiments are performed with screw RPM of 100, a cooling time of 11 seconds, a mould temperature of 45 degrees Celsius and an injection speed of 400 mm/s. The combinatorial influence of the temperature and the pressure is studied via performing experiments at different temperature profiles. The results from these experiments are visually presented in Figure 37. As can be seen from Figure 37, a change in pressure does significantly influence the required amount of purging material. However, it can be derived from all the experiments performed that a high injection pressure is beneficial in order to decrease the amount of purging material as much as possible. The least amount of purging material is obtained at the highest temperature profile (Thot) in combination with an injection pressure of 200. A complete system purge was completed with only 18 grams of virgin material or 9 shots, making it very viable for material research purposes. The combination of the Thot temperature profile and a lower pressure than 200 bar resulted in an increase of the required purging material. At an injection pressure of 150 bar, the required amount of material amounts to 34 grams. This translates to an increase of 89%. If the injection pressure is furtherly lowered to a value of 100 bar, a small increase of 2 grams required purging material was derived.

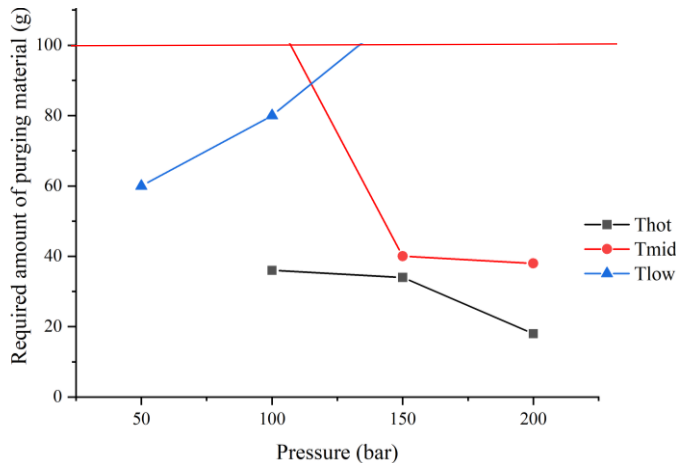


Figure 37: PHC31 to 515A (low RPM) in the function of the pressure.

When the temperature profile is switched to Tmid or Tlow, an increase in the required amount of purging material was derived. With the Tmid profile, a similar trend is concluded as with the Thot profile. However, this resulted in the required amount of purging material being between 38 and 100 plus grams of material. At an injection pressure of 100 bar, no complete system purge was performed with 100 grams of material. However, at an injection pressure of 150 bar, a significant decrease can be derived, as only 40 grams was necessary. If the injection pressure is furtherly increased to 200 bar, a small decrease of 2 grams can be derived. When the overall temperature is furtherly decreased to Tlow, the amount of material is between 60 and 100 plus grams, which is a substantial amount and highly undesired. In contrast to the Thot and Tmid profile, the least amount of material required was obtained at an injection pressure of 50 bar for the Tlow temperature profile. When the injection pressure is increased, the amount of material increases. At an injection pressure of 100 bar, 80 grams of material was required to achieve a complete system purge. If the injection pressure is furtherly increased, the required amount of material exceeds the threshold of 100 grams.



#### 4.3.3.2. *Less viscous (515A) change to more viscous (PHC31)*

In this paragraph, the results of the system purging experiments are discussed for a switch from a less viscous to a more viscous material. The experiments are performed with screw RPM of 100, a cooling time of 11 seconds, a mould temperature of 45 degrees Celsius and an injection speed of 400 mm/s. The results from these experiments are visually presented in Figure 38. As can be seen from Figure 38, a change in pressure does not significantly influence the required amount of purging material. However, it can be derived that a low injection pressure is beneficial in order to decrease the amount of purging material as much as possible in combination with the Tlow profile. On contrary, a high injection pressure is more beneficial in combination with the Thot and Tmid profile. The least amount of purging material is obtained at the lowest temperature profile (Tlow) for either screw RPM, as well for the Tmid profile with an injection pressure equal to or above 150 bar. A complete system purge was completed with only 12 grams of virgin material or 6 shots, making it yet again very viable for material research purposes.

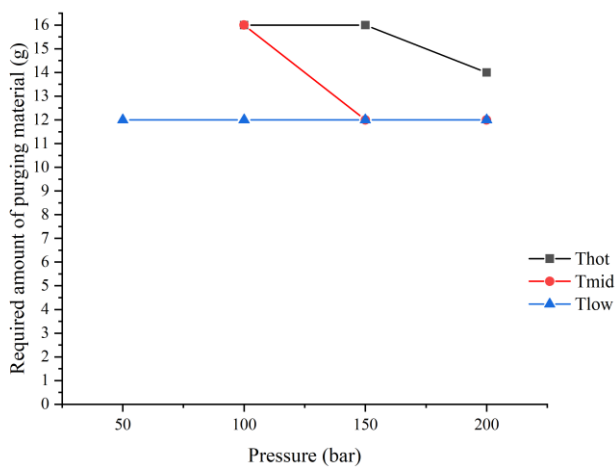


Figure 38: 515A to PHC31 (low RPM) in the function of the pressure.

When the temperature profile is switched to Tmid or Thot, an increase in the required amount of purging material was derived. With the Tmid profile, the required amount of purging material is between 12 and 16 grams of material. When the overall temperature is furtherly increased to Thot, the amount of material is between 14 and 16 grams. In contrast to the Tlow profile, the most amount of material required was obtained at a screw RPM of 100 for the Thot and Tmid temperature profile. It is believed that a lower temperature profile is beneficial when is switched from a less viscous to a more viscous material. With a lower temperature, the desired scraping effect of the newly introduced virgin material is enhanced, resulting in a more efficient purging process. On the other hand, a high temperature is beneficial when is changed from a more viscous material to a less viscous virgin material. With an increased temperature, both viscosities of the materials are decreased. However, this results eventually in a decreased scraping effect of the more viscous material but enhances the ‘flushing’ behaviour during the purging step.



#### 4.4. Determination of the accuracy and reproducibility of the conventional PP25 and smaller PP08 probes (MCR302e)

As mentioned, in order to decrease the amount of consumed material per analysis is the suitability of an alternative, smaller probe analysed. The decrease of material per analysis would be beneficial for the material development stage. With less material consumption for each material analysis step, the overall costs and required research time would be decreased. This chapter entails the results of the comparison between the two different probes in combination with the MCR302e rotating disk rheometer. The two different probes are the conventional PP25 and smaller PP08 probes, both specified previously in 3.2. Overall, both probes are compared regarding their suitability utilizing two different materials: PHC31 and 515A. The analyses are performed at a temperature of 230 °C. The rheological data is visually presented in several graphs, discussed separately. To properly evaluate the obtained results, a model fit (Carreau – Yasuda) was performed on the data of PHC with the PP25 probe. The obtained data of both the probes is compared regarding the deviation to the Carreau – Yasuda fit. In addition, a time-temperature superposition (TTS) is performed with the data resulting from the analyses with PHC31 for direct comparisons of the data sets. A Carreau – Yasuda fit was constructed for the entire temperature range with the PP25 probe and properly shifted to evaluate the constructed TTS to a model fit. Via the TTS method, it is possible to measure the rheological properties of these specific materials at one certain temperature and make estimates of the data at higher temperatures. The obtained master curves are analysed based on the deviation in order to determine the accuracy of both probes at different temperatures. Via analysing materials at a lower temperature, the viscosity of the polymeric melt is lower in comparison to higher temperatures. As a result, more torque is generated during a frequency sweep test, resulting in more accurate measurements; Possibly, leading to improved accuracy of both probes in combination with accurate estimates of their rheological properties over a wide temperature range.

##### 4.4.1. 515A

These measurements are performed in sets of three in order to determine the deviation of measurement data resulting with both probes, as well the accuracy of the PP08 probe in comparison to the PP25 probe. The measured data is graphically presented in Figure 39. The x-axis presents the angular frequency, expressed in radials per second. The y-axis presents the measured complex viscosity, expressed in mPa\*s. The overall deviation is determined by splitting each frequency sweep experiment into two separate ranges: from high to low angular frequency and vice-versa. The mean deviation of each separate probe, as well as the viscosity difference at the highest and lowest angular frequencies of both probes, is presented in Table 22. It is important to note that for the Carreau – Yasuda fit only the data resulting from the experiments from high to low frequency are processed in order to reduce noise between data. As can be derived from Table 22, the PP25 is a very accurate probe to determine the rheological properties of thermoplastics. Between three different analyses, the mean deviation of the PP25 probe amounts to approximately 1.34 percent (high to low frequency) and 1.71% (low to high frequency), which is a significantly low amount. On the contrary, the deviation of the PP08 amounts to significantly high values between 32.53 and 36.25%. More importantly, when both probes are compared regarding their results, the viscosities from the PP08 experiments differ between 1.74 and 9.34% from the Carreau – Yasuda fit. Compared to the difference occurring with the PP25 probe (< 0.01%), a significant difference is obtained with the PP08. However, due to the values differing less than 10% from the

theoretical model, the PP08 probe is considered to be a relatively good measurement technique to gather a first insight of the properties of a new, less available material.

Table 22: PP25 and PP08 comparison 515A.

Experiment	PP25 mean deviation (%)	PP08 mean deviation (%)	$\eta_{\infty}^*$ difference to Carreau - Yasuda (PP25) (%)	$\eta_0^*$ difference to Carreau - Yasuda (PP25) (%)	$\eta_{\infty}^*$ difference to Carreau - Yasuda (PP08) (%)	$\eta_0^*$ difference to Carreau - Yasuda (PP08) (%)
High to low frequency	1.34	36.25	0.001	0.0005	1.74	9.34
Low to high frequency	1.71	32.53	/	/	/	/

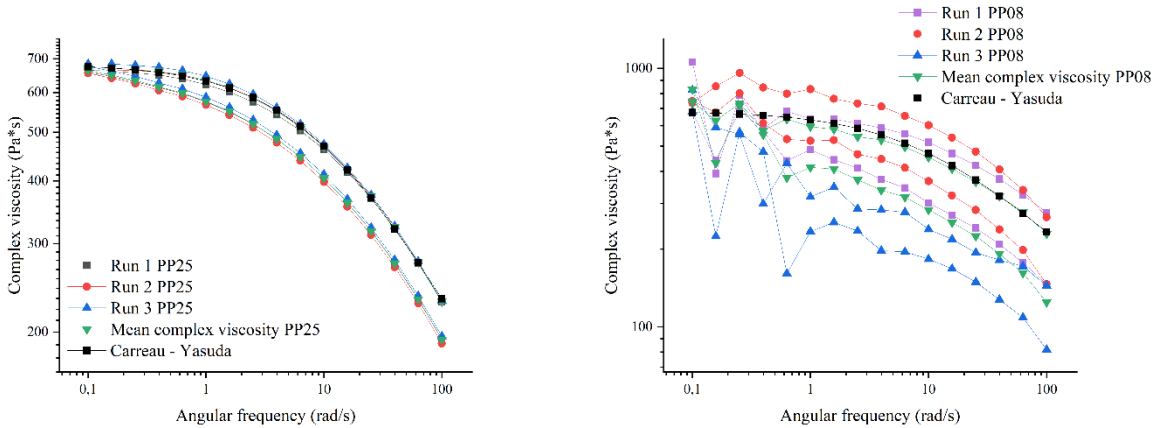


Figure 39: Comparison of PP25 (left) and PP08 (right) probes (515A).

#### 4.4.2. PHC31

These measurements are performed in sets of three in order to determine the deviation of measurement data resulting with both probes, as well the accuracy of the PP08 probe in comparison to the PP25 probe. The measured data is graphically presented in Figure 40. The x-axis presents the angular frequency, expressed in radials per second. The y-axis presents the measured complex viscosity, expressed in mPa\*s. The overall deviation is determined by splitting each frequency sweep experiment into two separate ranges: from high to low angular frequency and vice-versa. The mean deviation of each separate probe, as well as the viscosity difference between the measured values of both probes, is presented in Table 23. It is important to note that for the Carreau – Yasuda fit only the data resulting from the experiments from high to low frequency are processed in order to reduce noise between data. As can be derived from Table 23, the PP25 is a very accurate probe to determine the rheological properties of thermoplastics. Between three different analyses, the mean deviation of the PP25 probe amounts to approximately 1.67 percent (high to low frequency) and 1.27% (low to high frequency), which is a significantly low amount. On the contrary, the deviation of the PP08 amounts to significantly high values between 10.37 and 15.67%. More importantly, when both probes are compared regarding their results, the viscosities from the PP08 experiments differ between 12.33 and 18.14% from the Carreau – Yasuda fit. Compared to the difference occurring with the PP25 probe (< 2%), a significant difference is obtained with the PP08. In comparison to the experiments performed with 515A, larger deviation values, as well as larger differences to the Carreau – Yasuda fit were obtained.

Table 23: PP25 and PP08 comparison PHC31.

Experiment	PP25 mean deviation (%)	PP08 mean deviation (%)	$\eta_{\infty}^*$ difference to Carreau – Yasuda (PP25) (%)	$\eta_0^*$ difference to Carreau – Yasuda (PP25) (%)	$\eta_{\infty}^*$ difference to Carreau – Yasuda (PP08) (%)	$\eta_0^*$ difference to Carreau – Yasuda (PP08) (%)
High to low frequency	1.67	10.37	0.84	1.88	18.14	12.33
Low to high frequency	1.27	15.67	/	/	/	/

Noticeably, both probes display less overall deviation but more difference to the Carreau – Yasuda fit when PHC31 is measured instead of the less viscous 515A. A possible explanation for this is that PHC31 is more viscous than 515A, generating more torque during the rheological measurement. As a result of more generated torque, the measurements are more accurate, leading to less deviation in the measurement. However, the values resulting from the PP08 display a non-neglectable deviation. In order to increase the generated torque was opted to decrease the utilized melt temperature. The reduction of the measurement temperature was performed with both probes and utilized to construct time-temperature superposition curves in order to determine the most accurate measurement temperature for the smaller PP08 probe. Through the TTS it is possible to determine the accuracy of both probes at different temperatures and it is possible to measure a material at a lower temperature and estimate the viscoelastic properties based on shift factors at different, higher temperatures.

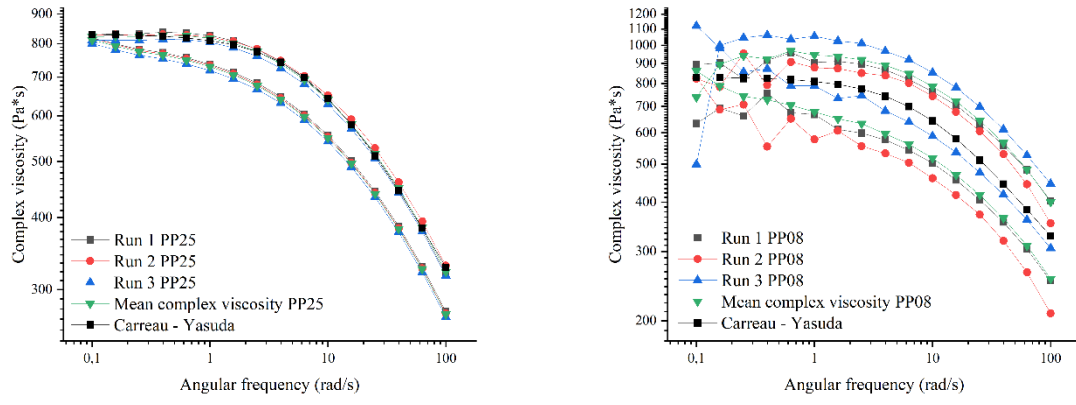


Figure 40: Comparison of PP25 (left) and PP08 (right) probes (PHC31).

#### 4.4.3. Time/frequency-temperature superposition of PHC31

The construction of the master curve through a time-temperature superposition is performed with the PHC31 type PP from Sabic. This is done for both probes (PP08 and PP25). The PP25 probe is known to provide more accurate data. As a result, the reference data (measured at 190 °C) is the data resulting from the PP25 probe used, as well as for the construction of the master curve of the PP08 probe. The rheological analyses are performed in a temperature range of 190 to 230 °C. In addition, only the data resulting from high to low angular frequency is utilized to reduce the overall noise between the data. For the construction of the master curve two shift factors need to be taken into account: the horizontal shift factor ( $a_t$ ) and the vertical shift factor ( $b_t$ ). The horizontal shift factor can be calculated from the zero-shear viscosities measured at two temperatures. Generally, the zero-shear viscosity of a higher temperature is divided by the zero-shear viscosity at the reference temperature, in this case, 190 °C (equation 53). The calculation of the vertical shift factor is generally performed by dividing the maximum loss factor measured at the higher temperature by the maximum loss factor measured at the reference temperature (equation 54). However, for most entangled polymer structures the vertical shift factor amounts to a value of one, neglecting a possible shift in loss moduli [76].

$$a_t = \frac{\eta_0(\omega, T)}{\eta_0(\omega, T_{ref})} \quad (53)$$

$$b_t = \frac{G''(\omega, T)}{G''_{ref}(\omega, T_{ref})} \quad (54)$$

$$\frac{a_t}{b_t} \eta_0(\omega, T_{ref}) = \eta_0(\omega_{reduced}, T) \quad (55)$$

After obtaining data at four or five different temperatures, the prediction of the rheological properties can be performed by predicting the horizontal shift factor over a wider temperature range. Subsequently, the predicted viscosity at a certain temperature can be performed via equation 55. To graphically construct the master curve, the viscosity values are multiplied by the shift factors as presented in this equation. In addition, the angular frequencies obtained at a different temperature than the reference temperature are multiplied by the horizontal shift factor to obtain a reduced angular frequency. The loss and storage moduli are not multiplied by any shift factor but are presented in the function of the reduced angular frequency, rather than the normal angular frequency. This is due to the temperature shift resulting in a difference in the generated torque during analyses, resulting in a reduced induced angular frequency. This data is generally plotted on a double logarithmic scale, as presented in Figure 41 and Figure 43. Both probes are analysed regarding the deviation between measurements at different temperatures. The accuracy of the PP08 probe is then subsequently determined by comparing the values of the PP08 master curve to the values of the PP25 master curve [76]. In addition, the results from both probes are compared to a constructed and properly shifted Carreau – Yasuda fit, performed for each temperature.

First, the results of the PP25 probe are discussed. The data from these experiments is plotted in Figure 41. Here, the viscosities and loss and storage moduli are plotted in function of the reduced angular frequency. Since both shift factors are material characteristics and not measurement properties, they are determined with the PP25 probe and furtherly used to analyse the accuracy of the PP08 probe. The accuracy of the PP25 probe is determined by comparing the data calculated with the shift factors and reference temperature, to the data obtained from an actual measurement at this temperature with the PP25 probe. In addition, the viscosities obtained at the maximum and minimum angular frequency are compared to the calculated values resulting from the Carreau – Yasuda fit. The results are presented in Table 24. Due to the experiments being performed separately as frequency sweeps, the deviation of each

measurement fluctuates in a certain absolute range in function of the angular frequency. This range is presented as the ‘*deviation range (%)*’ column. The mean deviation is calculated for each temperature to study the influence of the temperature (and thus melt viscosity) on the accuracy of measurements.

Table 24: TTS PP25 deviation results.

Temperature (°C)	$\eta_{\infty}^*$ difference to Carreau – Yasuda (%)	$\eta_0^*$ difference to Carreau – Yasuda (%)	Mean deviation (%)
190	1.40	0.52	/
200	0.00	0.00	6.29
210	0.00	0.00	8.79
220	0.00	0.00	13.89
230	0.00	0.00	17.02

As expected, with an increased temperature (and thus lower viscosity), the accuracy of measurements decreases due to the less generated torque. However, as can be derived from Table 24 at each temperature the mean deviation ranges from 6.3 to 17.02%. The measured and calculated data with 0 percent deviation are obtained at the lowest angular frequency measured of 0.1 radials per second. In this region, the melt displays Newtonian behaviour (zero-shear viscosity). As a result, the lower the angular frequency, the less deviation between measurements with the PP25 probe. In addition, the highest angular frequency (100 rad/s) measured resulted in the highest obtained deviation for each temperature. Overall is expected that the mean deviation of measurement will furtherly increase if a temperature is set above 230 °C. The highest obtained mean deviation of 17.02% at 230 °C is yet a relatively low value. As a result the PP25 is considered to be a relatively accurate measurement tool to analyse the viscoelastic behaviour of polyolefin melts.

Compared to the Carreau – Yasuda fit, the viscosities differ less than 1.5% for the PP25 probe. Noticeably, the only values differing more than 0.01% were obtained for the experiments performed at the lowest (reference) temperature. At any higher temperature the viscosity difference is less than 0.01%, which is a significant low amount. It was expected that the accuracy would decrease with higher temperatures. A proper explanation for this behaviour can not be given. However, at the lowest temperature the highest obtained viscosity difference only amounts to 1.40% (infinite shear), which is still a significantly low amount.

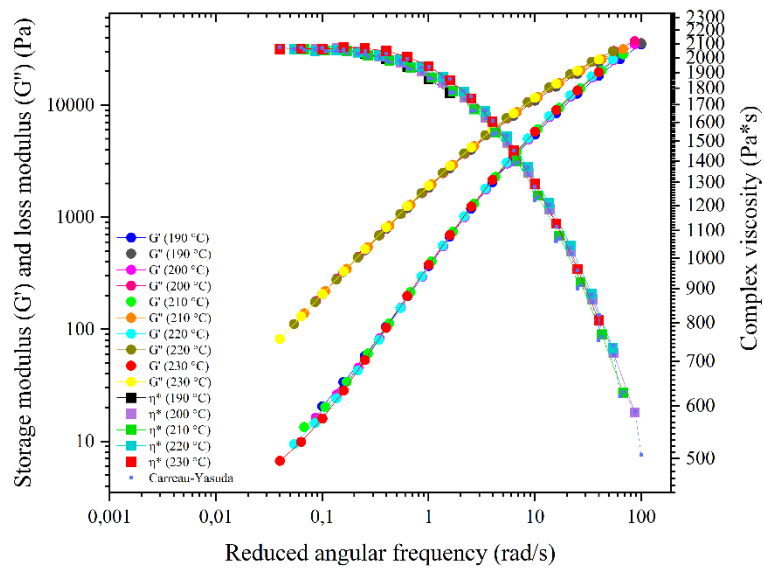


Figure 41: PP25 master curve ( $T_{ref} = 190^{\circ}\text{C}$ ).

As mentioned, the vertical shift factor is equal to one. The horizontal shift factor is determined in function of the temperature. This data plotted in Figure 42. The x-axis presents the temperature, expressed in Kelvin. The y-axis presents the horizontal shift factor. The most optimal fit for this data displays an R-squared value of 0.9962, which is a relatively accurate fit. The estimation of the horizontal shift factor over a wider temperature range is performed with following equation (56).

$$a_t(T) = -0.0153(T) + 8.0837 \quad (56)$$

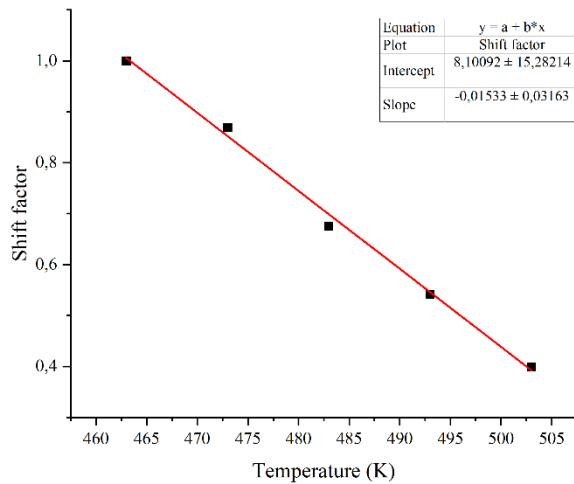


Figure 42: Horizontal shift factor in function of the temperature (PHC31) using PP25.

Next, the master curve of the PP08 probe is discussed. The processed data resulting from experiments is graphically presented in Figure 43. As mentioned, due to the shift factors being material properties, the data is processed with the obtained shift factors from the PP25 probe. As can be seen in Figure 43, no proper master curve is obtained. It was not possible to completely shift the curves towards the reference temperature values in combination with the obtained shift factors. The obtained PP08 master curve is calculated with values resulting from experiments with the PP08 probe and shift factors

resulting from experiments with the PP25 probe. In addition, the PP08 master curve is compared to the constructed Carreau – Yasuda master curve (PP25, 190°C). To properly compare both probes, the absolute difference range and mean difference of the PP08 values compared to the PP25 values are presented in Table 25. In order to reduce the noise between the different datasets, the biggest outliers (higher temperatures) were removed from the figure.

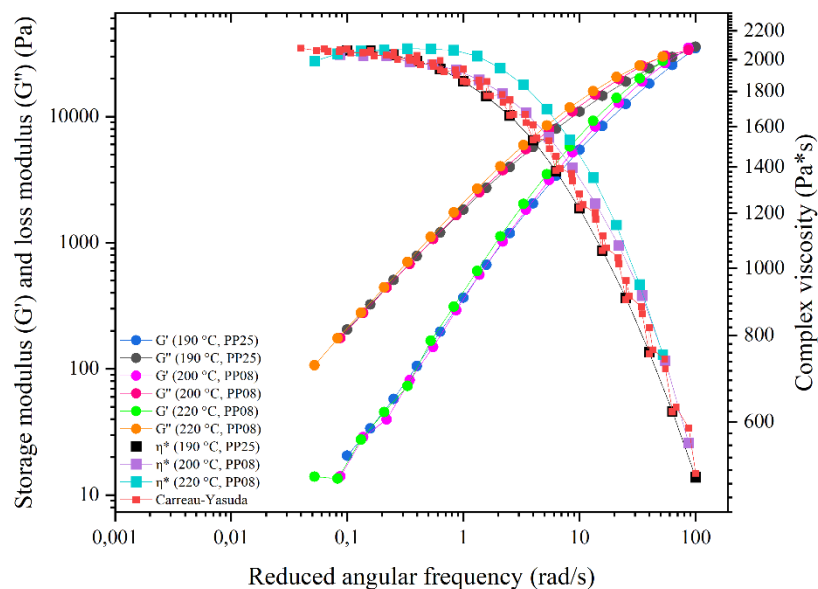


Figure 43: PP08 master curve ( $T_{ref} = 190^{\circ}\text{C}$ ).

Table 25: PP08 master curve deviation results and compared difference to the PP25 probe master curve.

Temperature (°C)	$\eta_{\infty}^*$ difference to Carreau – Yasuda (%)	$\eta_0^*$ difference to Carreau – Yasuda (%)	Mean deviation (%)	Mean difference to PP25 master curve (%)
190	0.57	0.02	/	/
200	0.00	0.00	9.08	2.75
210	0.00	0.00	42.15	29.09
220	0.00	0.00	25.93	6.37
230	0.00	0.00	48.03	19.04

As expected, with an increased temperature (and thus lower viscosity), the accuracy of measurements decreases due to the less generated torque. The measured and calculated data with the lowest percent deviation are obtained again at the lowest angular frequency measured of 0.1 radials per second. In this region, the melt displays Newtonian behaviour (zero-shear viscosity). As a result, the lower the angular frequency, the less deviation between measurements with the PP25 probe. In addition, the highest angular frequency (100 rad/s) measured resulted in the highest obtained deviation for each temperature. Overall is expected that the mean deviation of measurement will furtherly increase if a temperature is set above 230 °C. Compared to the PP25, the PP08 displays significantly large mean deviation percentages. But when the difference between both probes is analysed, the mean difference is lower than expected. However, at 210 degrees Celsius the highest mean difference percentage was obtained of 29.1%. On the other hand, at 200 degrees Celsius, the mean difference only amounted to 2.75%, which is a significantly low value.

Compared to the Carreau – Yasuda fit, the viscosities differ less than 0.6% for the PP08 probe. Noticeably, the only values differing more than 0.01% were obtained for the experiments performed at the lowest (reference) temperature. At any higher temperature the viscosity difference is less than 0.01%,

which is a significant low amount. It was expected that the accuracy would decrease with higher temperatures. A proper explanation for this behaviour can not be given. However, at the lowest temperature the highest obtained viscosity difference only amounts to 1.40% (infinite shear), which is still a significantly low amount.

But overall can be concluded that the use of the PP08 probe results in a relatively large deviation and difference in comparison to the conventional PP25 probe. It is recommended to use the PP08 at relatively low temperatures in relation to the analysed material, since here relatively accurate values are obtained. At higher temperatures it is recommended to use the PP25, as only a maximum mean deviation of 17.02% is present, compared to 48.03% with the PP08, both at 230 degrees Celsius (70 degrees above  $T_{melt}$ ). For the analysis of the zero shear and infinite shear viscosities, the PP08 probe provided relatively accurate results (<20% difference to the Carreau – Yasuda fit).

#### 4.5. Tensile analyses

This chapter entails the analysis and validation of the conventional tensile strength measurement for conventional sized and small sized samples. As mentioned, this measurement technique is designed for conventional sized specimens. In order to reduce the amount of material consumption during the processing step was opted to fabricate smaller sized parts in comparison to the conventional sized parts. Due to the constant demand for process, part, and material consumption minimalization, the suitability of the tensile strength measurement needs to be analysed for small sized samples. This is to ensure correct and accurate material characterization (post-processing) for smaller samples. Via a correct measurement technique it is possible to accurately assess the suitability of newly developed materials for the microinjection moulding process or other processing techniques in which a small tie-rod specimen or sheet foil is manufactured. Via the material minimization of both the processing step and the analyses, it is possible to reduce the total costs and required research time of any newly designed material during the material development stage.

For both sample sizes, the complete general test procedure is followed and the data from these experiments is presented in Table 26 and Figure 44. For conventional sized tensile bars, a mean E-modulus of 1212 N/mm<sup>2</sup> was obtained for PHC31. The tensile strength of the samples amounts to approximately 25.3 N/mm<sup>2</sup>. The average yield strength (Rp) at 0.2 amounts to 9.73 N/mm<sup>2</sup>. Overall, the deviation of the tensile strength analysis has proven to amount to only 0.77% deviation (based on the tensile strength). This is a substantially low amount, making this technique very suitable for the analysis of conventional sized parts. On the other hand, the deviation of the tensile strength of the small samples in comparison to conventional sized samples amounts to approximately 7%. This is a relatively low amount, making this technique interesting to examine the tensile strength of smaller components.

Table 26: Tensile strength analyses results.

Sample size	Thickness (mm)	Width (mm)	Section (mm <sup>2</sup> )	E-modulus (N/mm <sup>2</sup> )	Rp 0.2 (N/mm <sup>2</sup> )	Rm (N/mm <sup>2</sup> )	Elongation (%)	Stdev (%)	Rm
Conventional	4.13	10.04	41.47	1171	9.74	25.04	121.2	0.77	
Conventional	4.06	10.05	40.8	1162	9.67	25.38	147.8		
Conventional	4.05	10.01	40.54	1255	9.76	25.5	115.4		
Conventional	4.04	9.99	40.36	1261	9.72	25.28	107.1		
Small	0.99	1.56	1.55	/	/	26.77	82.45	1.15	
Small	0.99	1.56	1.54	/	/	27.05	68.31		
Small	0.99	1.54	1.51	/	/	27.39	96.59		

However, as can be derived from Table 26, no E-moduli and Rp values were obtained for the smaller samples. To obtain plausible characteristics, each test needs to be terminated after obtaining the elongation peak. This is due to a secondary elongation mechanism occurring only for the small samples. This secondary elongation mechanism can be derived as a secondary elongation peak, usually exhibiting a higher stress than the first peak. When this secondary elongation mechanism is taking place, the sample stretches at the undesired ends of the part instead of the analysed middle section. When the complete test procedure is followed, all the obtained parameters are completely false and significantly lower than in reality. To overcome this problem, it is possible to stop a test after obtaining the first elongation peak of the material. This results into viable tensile strength values (only 7% deviation from conventional sized parts), but no E-modulus or Rp values are obtainable. It is important to note that the tensile strength deviation of the small parts only amounts to 1.15%, which is still a significantly low amount. This makes the tensile testing technique a very viable method to examine the tensile strength of a moulded micropart, but unsuitable for the examination of the E-modulus and the Rp of the material. A visual presentation of the analyses of the stress in function of the part elongation is given in Figure 44 for both the conventional and small samples.

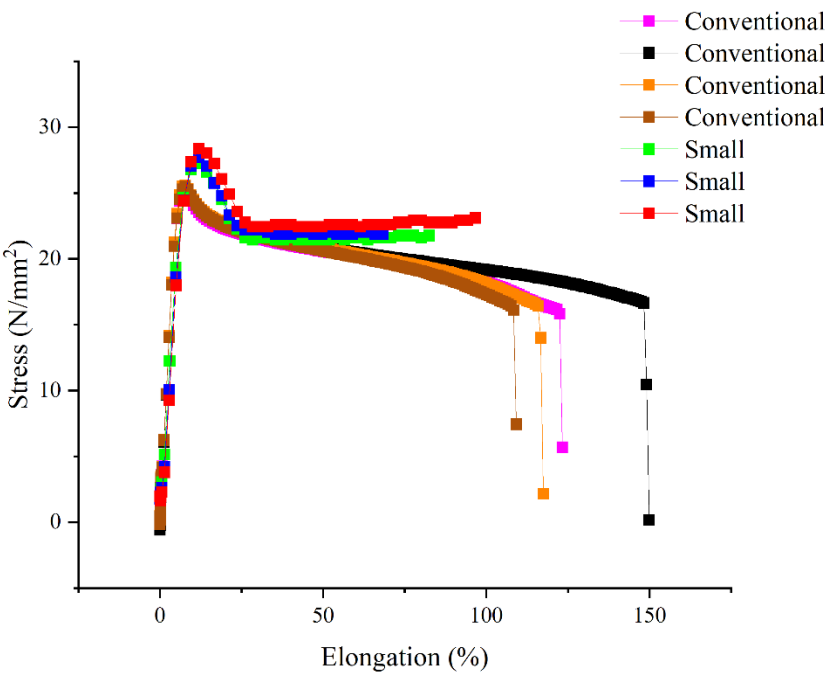


Figure 44: Tensile strength tests in function of the percentage elongation.

#### 4.6. Flexibility analyses

Due to the constant demand for process, part, and material consumption minimalization, the suitability of the flexibility measurement needs to be analysed for small sized samples. This is to ensure correct and accurate material characterization for smaller samples. Via a correct measurement technique it is possible to accurately assess the suitability of newly developed materials for the microinjection moulding process or other processing techniques in which a small tie-rod specimen is manufactured.

The data resulting from the flexibility analyses is presented in Table 27. With conventional sized samples it can be seen that the three-point loading flexibility testing is a very accurate result for the analysis of the E-modulus, as the deviation between the measurements only amounts to 3%. On the other hand, the measurement of small samples resulted into a deviation of 9%, which means it is still a very accurate measurement technique. However, from Table 27 can be derived that this method is less viable for the measurement of the Rp, tensile strength, and maximum force. Between these values a significant difference can be derived regarding conventional and small parts. As a result, the flexibility testing method is very suitable for the determination of the E-modulus of both conventional and small samples. When the deviation of the mean E-modulus obtained from the small sample size is compared to the conventional sample size, only a 2.73% difference was concluded. However, for smaller parts, more measurements are required to acquire an accurate mean E-modulus, due to the larger deviation of the analyses.

Table 27: Flexibility analyses results.

Sample size	A (mm <sup>2</sup> )	E-modulus (N/mm <sup>2</sup> )	Rp (N/mm <sup>2</sup> )	0.2 Rm (kN/mm <sup>2</sup> )	E <sub>r</sub> max (%)	Stdev E-modulus (%)	Mean E-modulus
Conventional	40	1243	/	0.02	1.33		
Conventional	40	1212	/	0.02	1.32	2.99	1247
Conventional	40	1286	/	0.02	1.31		
Small	1.444	1185	23.52	0.04	4.99		
Small	1.444	1146	20.5	0.02	1.92		
Small	1.444	1179	29.32	0.04	4.87		
Small	1.444	1090	32.77	0.04	4.85		
Small	1.444	1179	30.18	0.04	4.87		
Small	1.444	1053	29.89	0.04	4.87	9.00	1213
Small	1.444	1207	26.96	0.04	4.85		
Small	1.444	1382	26.61	0.05	4.86		
Small	1.444	1427	28.63	0.05	4.87		
Small	1.444	1215	30.46	0.04	4.86		
Small	1.444	1188	29.31	0.04	4.87		
Small	1.444	1301	28.6	0.04	4.87		

It is important to note that the alignment and possible part warpage needs to be taken into account. As the small parts tend to remain stuck inside the mould cavity after the ejection phase, material warpage is present in most of the parts. The material warpage is generally derived as a curved tensile bar. However, this altered shape needs to be aligned properly with the flexibility measurement machine. It is important to place the curve of the shape downward to obtain accurate results. When the curve is aligned upwards, false measurements are obtained as the contact of the bar with the three-point loading alignment is not uniform at both sides, possibly leading to movement of the shape mid-testing.

As said previously, this method is less viable for the measurement of the  $R_p$ , tensile strength, and maximum force. When the  $R_m$  and  $R_p$  values are compared to the values presented in Table 26, it can be derived that the flexibility testing provides inaccurate results. The accuracy of the  $R_p$  measurements is difficult to determine due to the units being presented in  $kN/mm^2$ . For the conventional sized parts, the error is expected to amount to a maximum of 20%, which is still a relatively high amount. However, for smaller parts this error is significantly larger, even possibly reaching an amount of 100%. Regarding the  $R_p$  measurements, no accurate conclusion can be derived as with the flexibility testing, the  $R_p$  for conventional parts cannot be determined; and with the tensile testing, the  $R_p$  for small parts cannot be determined. However, when both conventional (tensile) and small (flexibility) parts are compared regarding the  $R_p$  value a difference of approximately 200% is derived from both tables. It is more plausible that for the smaller parts (flexibility) an overestimation is made during these tests, as the same is derived from the  $R_m$  values.

## 5. Conclusions

The goal of this study was to improve the material efficiency for material processing step and several analyses techniques. As mentioned, microinjection moulding was chosen for this research for the material processing step. With improved material efficiency, the overall costs and research duration for newly developed materials decreases. The microinjection moulding process was analysed regarding the actual processing of the material, as well as system purging. The analyses techniques studied include rheological and mechanical characterization techniques.

First, the Fanuc microinjection moulding machine was analysed regarding its minimal required amount of material to perform a singular shot. This was analysed in order to maximally reduce the amount of material consumed to perform a processing experiment. After analysing the influence of both the injection pressure and the screw RPM, an ideal configuration of the process was obtained. A screw RPM of 450 and injection pressure of 100 bar (in combination with the previously mentioned process conditions) resulted in a minimal required amount of approximately 3 grams powder to perform a singular shot, which is exceptionally low in standard injection moulding applications. In contrast to the screw RPM, the injection pressure has proven to exhibit a non-beneficial effect on the processability of low amounts of powdered material. An increase in injection pressure resulted in an increase of required amount of material to perform a single shot. It was further demonstrated that it was possible to execute a perfectly smooth  $\mu$ IM-run with as little as 10 g of standard PP material even if it is available in a powder form.

Next, the system purging was analysed in order to decrease the amount of material wastage required to completely perform a material change. The system purging is mainly determined by the material changing profile (less to more viscous or vice-versa), the injection pressure, and the temperature profile. When a less viscous material is purged with a more viscous material, a low temperature profile is desired in combination with a low screw RPM and a low injection pressure. The least amount of purging material required with these settings amounted to approximately 12 grams virgin material. On the other hand, when is changed from a less viscous to a more viscous material, a high temperature profile in combination with a high injection pressure, and high screw RPM. The least amount of purging material required with these settings amounted to approximately 14 grams virgin material. It is important to note that for these experiments two different types of PP were used (less viscous: 515A and more viscous: PHC31). These obtained purging amounts are completely material bound; if different types of polymer or different types of PP (e.g. more functional groups  $\approx$  structural changes) are processed, complete different values are possible. However, these results provide a better insight into the system purging process. It is still recommended to attain these settings when a system purge is performed, with good understanding of the utilized materials.

In order to characterize small-scale  $\mu$ IM specimens, a miniaturized rheological test was developed. Specifically, a small-size 8mm plate-plate geometry (PP08) was used, while the conventional PP25 served as a benchmark. Direct comparison of both systems revealed insufficient data quality particularly at low frequencies when PP08 was used. Overall, the standard deviation of the data resulting from the PP25 probe amounted to 1.27 – 1.71% and 10.37 – 36.25% for the PP08 probe, which is a significant amount. When the viscosity values obtained from both probes are compared to the Carreau – Yasuda fit, the values coming from the PP08 differ between 12.33 and 18.14%, compared to 0.88 and 1.84% from the PP25 probe.

In the attempt to overcome the large deviation and difference resulting from the PP08, a time-temperature superposition was performed to analyse materials at a lower temperature and predict values at higher temperatures with determined shift factors. This was done to increase the generated torque

during analyses and thus analysis accuracy. For the PP25 the mean deviation amounted to values between 6.29 and 17.02%. It could be derived that, the higher the temperature, the higher the mean deviation; as less torque is generated during measurements. It is important to note that the mean difference between both probes was lower than expected. However, at 210 °C the highest mean difference percentage was obtained of 29.1%. On the other hand, at 200 °C, the mean difference only amounted to 2.75%, which is a significantly low value. In conclusion, it is not recommended to utilize the PP08 for rheological analyses as a primary choice; but the PP08 still allows the collection of meaningful data at lower temperatures in combination with higher frequencies.

In order to properly characterize the smaller-size samples, conventional, existing mechanical analysis techniques needed to be evaluated regarding their accuracy and reproducibility. The tensile strength analyses were performed with the Quasar 50kN tensile testing machine. The tensile analysis has proven to be a very viable method to characterize the tensile strength of smaller-size samples. The overall deviation between analyses performed on the small-size samples only amounted to 7%, with a mean difference of only 1.15% in comparison to conventional sized samples. On the other hand, the tensile analysis has proven to be unsuitable to analyse the E-moduli and Rp values for the smaller-size samples. This was the result from the second elongation mechanism occurring at the end of the sample, resulting into a second elongation peak.

The second mechanical characterization technique evaluated was the three-point loading flexibility test. This technique has proven to be a very accurate and reproducible method to characterize the E-modulus of samples. Overall, the deviation between analyses performed on the small-size samples only amounted to 9%, with a mean difference of only 2.73% in comparison to analyses on conventional sized samples.

## References

- [1] S. Bindgen, “SMaRT people.” <https://cit.kuleuven.be/smart/people> (accessed Mar. 28, 2022).
- [2] S. Bindgen, “SMaRT research.” <https://cit.kuleuven.be/smart/research/index> (accessed Mar. 28, 2022).
- [3] T. A. Adegbola, O. Agboola, and O. S. I. Fayomi, “Trends in Polymer Development: Effects and Consolidation Processes,” *IOP Conference Series: Materials Science and Engineering*, vol. 1107, no. 1, p. 012108, Apr. 2021, doi: 10.1088/1757-899x/1107/1/012108.
- [4] S. Petisco-Ferrero, R. Cardinaels, and L. C. A. van Breemen, “Miniaturized characterization of polymers: From synthesis to rheological and mechanical properties in 30 mg,” *Polymer (Guildf)*, vol. 185, p. 121918, 2019, doi: 10.1016/j.polymer.2019.121918.
- [5] U. Sancin and B. Dolsak, “Decision Support System for Designing with Polymer Materials – Current Challenges and Future Expectations,” *Efficient Decision Support Systems - Practice and Challenges From Current to Future*, no. June, 2011, doi: 10.5772/18194.
- [6] J. Giboz, T. Copponnex, and P. Mélé, “Microinjection molding of thermoplastic polymers: A review,” *Journal of Micromechanics and Microengineering*, vol. 17, no. 6, 2007, doi: 10.1088/0960-1317/17/6/R02.
- [7] R. Surace, G. Trotta, V. Bellantone, and I. Fassi, “the Micro Injection Moulding Process for Polymeric Components Manufacturing,” *New Technologies - Trends, Innovations and Research*, no. March, 2012, doi: 10.5772/35299.
- [8] G. F. Schiller, *A Practical Approach to Scientific Molding*. Munich: Hanser, 2018.
- [9] M. Packianather, C. Griffiths, and W. Kadir, “Micro injection moulding process parameter tuning,” *Procedia CIRP*, vol. 33, pp. 400–405, 2015, doi: 10.1016/j.procir.2015.06.093.
- [10] Cel Kunststoffen research group - KU Leuven, “Users Manual - Rotational Compact Disk Rheometer Anton Paar - MCR302e,” 2021.
- [11] W. J. Sichina, “DSC as Problem Solving Tool: Measurement of Percent Crystallinity of Thermoplastics,” 2000, Accessed: Apr. 10, 2022. [Online]. Available: [www.perkinelmer.com](http://www.perkinelmer.com).
- [12] R. K. Laser, *Laser Welding of Plastics Related Titles Macromolecules Principles of Laser Materials Processing Handbook of Plastic Processes*. Weinheim: Wiley-VCH, 2011.
- [13] J. Mewis and N. Wagner, *Colloidal Suspension Rheology*, vol. 1. Cambridge, United Kingdom: Cambridge University Press, New York, 2012.
- [14] C. W. Macosko, *Rheology: Principles, Measurements and Applications*, vol. 86, no. 3. New York: Wiley-VCH, 1996. doi: 10.1016/s0032-5910(96)90008-x.
- [15] D. Liepsch, “A Basic Introduction to Rheology Shear Flow,” *J Biomech*, vol. 35, no. 4, pp. 415–435, 2016, Accessed: Apr. 17, 2022. [Online]. Available: <https://cdn.technologynetworks.com/TN/Resources/PDF/WP160620BasicIntroRheology.pdf>
- [16] H. Münstedt, “Rheological measurements and structural analysis of polymeric materials,” *Polymers (Basel)*, vol. 13, no. 7, 2021, doi: 10.3390/polym13071123.

- [17] A. Eckstein *et al.*, “Determination of Plateau Moduli and Entanglement Molecular Weights of Isotactic, Syndiotactic, and Atactic Polypropylenes Synthesized with Metallocene Catalysts,” 1998. Accessed: Apr. 19, 2022. [Online]. Available: <https://pubs.acs.org/sharingguidelines>
- [18] B. H. Stuart, *POLYMER ANALYSIS*. Sydney, Australia: John Wiley & Sons, Ltd, 2002.
- [19] M. Fujiyama and S. Kimura, “Effect of molecular parameters on the shrinkage of injection-molded polypropylene,” *Journal of Applied Polymer Science*, vol. 22, no. 5, pp. 1225–1241, 1978, doi: 10.1002/app.1978.070220506.
- [20] gpambala.ac.in, “Molecular Weight and Molecular Weight Distribution (2).” <https://gpambala.ac.in/wp-content/uploads/2018/04/Digital-Contents-Plastic-Technology.pdf> (accessed Apr. 24, 2022).
- [21] R. Oboigbaotor. Ebewele, *Polymer science and technology*. Boca Raton: CRC Press, 2000.
- [22] P. D. Coates, B. R. Whiteside, M. T. Martyn, R. Spares, and T. Gough, “Micromoulding – precision processing for controlled products,” in *4M 2006 - Second International Conference on Multi-Material Micro Manufacture -*, 1st ed., vol. 1, no. 1, W. Menz, S. Dimov, and B. Fillon, Eds. Oxford: Elsevier Ltd, 2006, pp. 13–15.
- [23] J. M. Fischer, “Introduction to Injection Molding,” in *Handbook of Molded Part Shrinkage and Warp*, Elsevier, 2013, pp. 1–7. doi: 10.1016/b978-1-4557-2597-7.00001-x.
- [24] A. L. Andrady and M. A. Neal, “Applications and societal benefits of plastics,” *Philosophical Transactions of the Royal Society B: Biological Sciences*, vol. 364, no. 1526, pp. 1977–1984, 2009, doi: 10.1098/rstb.2008.0304.
- [25] Dynalon, “Polypropylene properties.” [https://www.dynalon.com/PublicStore/pages/Polypropylene\\_Properties.aspx](https://www.dynalon.com/PublicStore/pages/Polypropylene_Properties.aspx) (accessed Apr. 02, 2022).
- [26] Z. M. Ariff, A. Ariffin, N. A. A. Rahim, and S. S. Jikan, “Rheological Behaviour of Polypropylene Through Extrusion and Capillary Rheometry,” *InTech*, no. May 2014, pp. 29–48, 2012, Accessed: May 20, 2022. [Online]. Available: <https://www.intechopen.com/books/polypropylene/rheological-behaviour-of-polypropylene-through-extrusion-and-capillary-rheometry>
- [27] W.-F. Su, “Principles of Polymer Design and Synthesis.” Accessed: Apr. 20, 2022. [Online]. Available: <http://www.springer.com/series/632>
- [28] Hisham A. Maddah, “Polypropylene as a Promising Plastic: A Review,” 2016. doi: 10.5923/j.ajps.20160601.01.
- [29] J. A. Brydson, *Plastics materials*, 7th ed. Oxford, United Kingdom: Butterworth-Heinemann, 1999.
- [30] S. Edition, “Plastics Materials,” *Analysis and Deformation of Polymeric Materials*, pp. 153–171, 2005, doi: 10.1007/0-306-46908-1\_8.
- [31] Fanuc, “Injection molding: electric vs. hydraulic.” <https://www.fanuc.eu/be/nl/roboshot/injection-moulding-electric-vs-hydraulic> (accessed Apr. 05, 2022).

- [32] G. Gullo, “Hydraulic injection moulding machine vs all-electric injection moulding machine,” Oct. 01, 2018. <https://www.linkedin.com/pulse/hydraulic-injection-moulding-machine-vs-all-electric-giuseppe-gullo/> (accessed Apr. 05, 2022).
- [33] SIMTEC, “Injection Molds: Hot Runner vs. Cold Runner Molds.” <https://www.simtec-silicone.com/blogs/injection-molds-hot-runner-vs-cold-runner-molds/> (accessed Apr. 17, 2022).
- [34] G. Wang, G. Zhao, H. Li, and Y. Guan, “Research on a new variotherm injection molding technology and its application on the molding of a large LCD panel,” *Polymer - Plastics Technology and Engineering*, vol. 48, no. 7, pp. 671–681, 2009, doi: 10.1080/03602550902824549.
- [35] M. S. Despa, K. W. Kelly, and J. R. Collier, “Injection molding of polymeric LIGA HARMs,” *Microsystem Technologies*, vol. 6, no. 2, pp. 60–66, 1999, doi: 10.1007/s005420050176.
- [36] C. Yang, X. H. Yin, and G. M. Cheng, “Microinjection molding of microsystem components: New aspects in improving performance,” *Journal of Micromechanics and Microengineering*, vol. 23, no. 9, 2013, doi: 10.1088/0960-1317/23/9/093001.
- [37] P. C. Hiemenz and T. P. Lodge, *Polymer Chemistry*, 2nd ed. Boca Raton: CRC Press, 2007.
- [38] T. Osswald and G. Menges, *Materials Science of Polymers for Engineers*, 3rd ed., no. 6. Munich: Hanser, 2012. doi: 10.1109/mei.1996.546279.
- [39] C. A. Hieber and H. H. Chiang, “Some correlations involving the shear viscosity of polystyrene melts,” *Rheologica Acta*, vol. 28, no. 4, pp. 321–332, 1989, doi: 10.1007/BF01329342.
- [40] T. Chen, “Preventing Wall Slip in Rheology Experiments,” New Castle. Accessed: May 21, 2022. [Online]. Available: <https://www.tainstruments.com/pdf/literature/RH094.pdf>
- [41] G. Trotta, B. Stampone, I. Fassi, and L. Tricarico, “Study of rheological behaviour of polymer melt in micro injection moulding with a miniaturized parallel plate rheometer,” *Polymer Testing*, vol. 96, Apr. 2021, doi: 10.1016/j.polymertesting.2021.107068.
- [42] U. M. Attia, S. Marson, and J. R. Alcock, “Micro-injection moulding of polymer microfluidic devices,” 2009. doi: 10.1007/s10404-009-0421-x.
- [43] D. v. Rosato, D. v. Rosato, and M. G. Rosato, *Injection Molding Handbook*, 3rd ed. Boston, MA: Springer US, 2000. doi: 10.1007/978-1-4615-4597-2.
- [44] Y. Heijligen, A. van Bael, and J. Kerremans, “Master’s thesis: analysis of the microinjection molding parameters with the use of variotherm process conditions,” UHasselt, Diepenbeek, 2015.
- [45] A. Routsis and Milacron, “Injection Molding Reference Guide.” Accessed: Apr. 25, 2022. [Online]. Available: [www.traininteractive.com](http://www.traininteractive.com).
- [46] J. Z. Liang and J. N. Ness, “The calculation of cooling time in injection moulding,” Guangzhou, 1996. Accessed: May 27, 2022. [Online]. Available: <https://www.sciencedirect.com/science/article/abs/pii/0924013695020446>
- [47] C. Ruan, “‘Skin-core-skin’ structure of polymer crystallization investigated by multiscale simulation,” *Materials*, vol. 11, no. 4, Apr. 2018, doi: 10.3390/ma11040610.

- [48] J. W. Housmans, G. W. M. Peters, and H. E. H. Meijer, "Flow-induced crystallization of propylene/ethylene random copolymers," *Journal of Thermal Analysis and Calorimetry*, vol. 98, no. 3, pp. 693–705, Dec. 2009, doi: 10.1007/s10973-009-0532-3.
- [49] M. Gahleitner, J. Fiebig, J. Wolfschwenger, G. Dreiling, and C. Paulik, "Post-crystallization and physical aging of polypropylene: Material and processing effects," in *Journal of Macromolecular Science - Physics*, Jul. 2002, vol. 41 B, no. 4–6, pp. 833–849. doi: 10.1081/MB-120013068.
- [50] K. Shelesh-Nezhad and A. Taghizadeh, "Shrinkage behavior and mechanical performances of injection molded polypropylene/talc composites," *Polymer Engineering and Science*, vol. 47, no. 12, pp. 2124–2128, Dec. 2007, doi: 10.1002/pen.20940.
- [51] U. M. Attia, "Micro-Injection Moulding of Three-Dimensional Integrated Microfluidic Devices," *Engineering*, vol. 2009, no. 1, pp. 2–3, 2009, [Online]. Available: <http://scholar.google.com/scholar?hl=en&btnG=Search&q=intitle:Cranfield+university#5>
- [52] Z. Peng, L. Gang, T. Yangchao, and T. Xuehong, "The properties of demoulding of Ni and Ni-PTFE moulding inserts," *Sensors and Actuators, A: Physical*, vol. 118, no. 2, pp. 338–341, Feb. 2005, doi: 10.1016/j.sna.2004.01.042.
- [53] J. Ullah *et al.*, "The effect of masterbatch pigments on the crystallisation , morphology , and shrinkage behaviour of Isotactic Polypropylene," *Journal of Polymer Research*, 2022, doi: 10.1007/s10965-022-03028-z.
- [54] V. Kausalyah, E. N. M. Nik Maisara, and S. Shasthri, "Experimental analysis on the effects of pigmentation in the defects formation of the polypropylene plastic injection moulding," *IOP Conference Series: Materials Science and Engineering*, vol. 834, no. 1, 2020, doi: 10.1088/1757-899X/834/1/012038.
- [55] D. v. Rosato and D. v. Rosato, *Plastics Processing Data Handbook*. New York: Van Nostrand Reinhold, 1990. doi: 10.1007/978-94-010-9658-4.
- [56] O. Chukwubuike, "Purging Mixture for Extruder Title: Purging mixture for extruder Supervisor (Arcada): Valeria Poliakova Examiner (Arcada) Mirja Anderson TABLE OF CONTENTS".
- [57] R. Singh, F. Fraternali, I. Farina, and M. S. J. Hashmi, "Experimental Investigations for Development of Hybrid Feed Stock Filament of Fused Deposition Modeling," Elsevier Ltd., 2018. doi: 10.1016/b978-0-12-803581-8.10392-3.
- [58] J. Mohr, "LIGA - A technology for fabricating microstructures and microsystems," *Sensors and Materials*, vol. 10, no. 6, pp. 363–373, 1998.
- [59] B. Zhao, Y. Qiang, W. Wu, and B. Jiang, "Tuning power ultrasound for enhanced performance of thermoplastic micro-injection molding: Principles, methods, and performances," *Polymers (Basel)*, vol. 13, no. 17, 2021, doi: 10.3390/polym13172877.
- [60] B. J. Hunt and M. I. Jamer, *Polymer Characterisation*, 2nd ed. Dordrecht: Springer Science + Business Media, B.V., 1993. doi: 10.1007/978-94-011-2160-6.
- [61] j. F. Richardson and R. P. CHHABRA, "Non-Newtonian Flow and Applied Rheology," *Non-Newtonian Flow and Applied Rheology: Engineering Applications*, vol. 2, pp. 1–523, 1999.

- [62] A. U. Khan, N. Mahmood, and A. A. Bazmi, "Direct comparison between rotational and extrusion rheometers," *Scielo.br*, Accessed: Apr. 09, 2022. [Online]. Available: <https://www.scielo.br/j/mr/a/3TXq47rzftk6nGghpB3LXPr/?lang=en>
- [63] M. Laun *et al.*, "Guidelines for checking performance and verifying accuracy of rotational rheometers: Viscosity measurements in steady and oscillatory shear (IUPAC Technical Report)," *Pure and Applied Chemistry*, vol. 86, no. 12, pp. 1945–1968, 2014, doi: 10.1515/pac-2013-0601.
- [64] T. Chen, "Rheology – Multi-Wave Oscillation." Accessed: Apr. 11, 2022. [Online]. Available: <https://www.tainstruments.com/pdf/literature/RH096.pdf>
- [65] PerkinElmer and Inc, "Dynamic Mechanical Analysis (DMA) A Beginner's Guide."
- [66] T. A. Strivens, *An introduction to rheology*. Amsterdam: Elsevier Science Publishers B.V., 1999. doi: 10.1533/9781855737006.550.
- [67] Cel Kunststoffen, "Users manual MDSC (Modulated differential scanning calorimeter 2920 TA)," Diepenbeek, 2012.
- [68] A. P. Gray, "POLYMER CRYSTALLINITY DETERMINATIONS BY DSC".
- [69] R. Brown, "Book Review: Handbook of Polymer Testing Short-Term Mechanical Tests," *International Journal of Materials and Product Technology*, vol. 27, no. 3/4, p. 293, 2006, doi: 10.1504/ijmpt.2006.011280.
- [70] asahikawa-nct.ac.jp, "Asahikawa-nct.ac facilities and factory: practical training factory." <https://www.asahikawa-nct.ac.jp/en/facilities/factory/> (accessed Apr. 05, 2022).
- [71] Fanuc, "FANUC ROBOSHOT S-2000\*," 2008.
- [72] M. K. Fong, "Manual Tensile testing machine QUASAR 50."
- [73] Sabic, "SABIC PP PHC31-81 PP impact for Automotive injection moulding moulding," 2015. Accessed: Apr. 20, 2022. [Online]. Available: <https://www.sabic.com/en/products/documents/phc31-81-00900-automotive-standards-declaration/en>
- [74] Sabic, "Sabic PP PHC31-81 PP impact copolymer," 2022. Accessed: Apr. 21, 2022. [Online]. Available: [https://www.sabic.com/en/products/documents/sabic-pp\\_phc31-81\\_global\\_technical\\_data\\_sheet/en](https://www.sabic.com/en/products/documents/sabic-pp_phc31-81_global_technical_data_sheet/en)
- [75] Prospector, "Sabic® PP 515A," no. 1, pp. 1–2, 2019, Accessed: Apr. 21, 2022. [Online]. Available: <https://materials.ulprospector.com/en/profile/default?e=70754%0D>
- [76] T. G. Mezger, *The Rheology Handbook : 4th Edition.*, 4th ed. Hanover: Vincentz Network, 2014.
- [77] J. Giboz, T. Copponnex, and P. Mélé, "Microinjection molding of thermoplastic polymers: Morphological comparison with conventional injection molding," *Journal of Micromechanics and Microengineering*, vol. 19, no. 2, 2009, doi: 10.1088/0960-1317/19/2/025023.
- [78] Z. Tadmor and C. G. Gogos, *Principles of polymer processing*. Hoboken, New Jersey: Wiley & Sons, Inc., 2006.

- [79] Z. Lu and K. F. Zhang, “Morphology and mechanical properties of polypropylene micro-arrays by micro-injection molding,” *International Journal of Advanced Manufacturing Technology*, vol. 40, no. 5–6, pp. 490–496, 2009, doi: 10.1007/s00170-007-1364-6.
- [80] Ecomolding, “Conditions of Nylon plastic Injection Molding Process.” [https://www.ecomolding.com/nylon-injection-molding/#:~:text=Conditions of Nylon plastic Injection Molding Process&text=80 – 90 degrees Celsius \(176, greatly influences its mechanical properties. \(accessed May 22, 2022\).](https://www.ecomolding.com/nylon-injection-molding/#:~:text=Conditions of Nylon plastic Injection Molding Process&text=80 – 90 degrees Celsius (176, greatly influences its mechanical properties. (accessed May 22, 2022).)
- [81] T. Ferreira, P. E. Lopes, A. J. Pontes, and M. C. Paiva, “Microinjection molding of polyamide 6,” *Polymers for Advanced Technologies*, vol. 25, no. 8, pp. 891–895, 2014, doi: 10.1002/pat.3322.
- [82] Z. Dekel and S. Kenig, “Micro-Injection Molding of Polymer Nanocomposites Composition-Process-Properties Relationship,” *International Polymer Processing*, vol. 36, no. 3, pp. 276–286, 2021, doi: 10.1515/ipp-2020-4065.
- [83] U. M. Attia and J. R. Alcock, “A process chain for integrating microfluidic interconnection elements by micro-overmoulding of thermoplastic elastomers,” *Journal of Micromechanics and Microengineering*, vol. 20, no. 5, 2010, doi: 10.1088/0960-1317/20/5/055017.

## Appendices

Table 28: Overview of different materials for micro moulding.

Nature	Polymer	Full name	T <sub>melt</sub> (°C)	μIM T <sub>mould</sub> (°C)	IM T <sub>mould</sub> (°C)	Applications	References
Semi-crystalline	HDPE	High-density polyethylene	230	125 – 150	30 – 60	Mechanical stable polymer	[6] [7] [77]
	LCP	Liquid crystal polymer	335 – 345	80 – 120	50 – 120	Mechanical, chemical, and electrical properties: fibres, cables, bulletproof vests	[6] [7]
	PBT	Polybutylene terephthalate	224 – 236	120	80 40 – 60	Household and automotive applications	[6] [78]
	PSU	Polysulfone	360 – 365	138 – 160		Housings for microfluidic devices	[6] [7] [51]
	POM	Polyoxy-methylene	190 – 230	60 – 100	70 – 90	Micro gears and micro fillers	[6][7]
	PEEK	Polyether-etherketone	335 – 350	180	143	Micro bearings and pistons	[7] [38] [78]
	iPP	Polypropylene (isotactic)	164 – 170	90 – 163	30 – 60	Dashboards, door liners	[6] [79]
	PA	Polyamide	230 – 280	100	80 – 90	Micro gear wheels	[7] [80] [81]
Amorphous	PC	Polycarbonate	290 – 320	60-140 125 – 135 93 100	90 – 110	Optical applications: lenses and sensor discs	[6] [7] [82]
	PMMA	Polymethyl-methacrylate	260	84	50 – 80	Plexiglass, fibre connector, computer casings, lenses	[7] [83]
	PS	Polystyrene	240	163 – 175	140	Packaging, housewares, electrical components	[6] [38]

Table 29: Commercially available micro injection moulding machines and their characteristics.

Company	Model	Injection capacity (cm <sup>3</sup> )	Injection pressure (bar)	Injection speed (mm/s)	Clamp force (kN)	Plasticizer type
APM	SM-5EJ	1	2450	800	50	14 mm screw
Arburg	220s	15	2500	112	150	8 mm screw 15 mm screw
Babyplast	Babyplast 6/10P	4	2650	/	62.5	10 mm plunger
Battenfeld	Microsystem 50	1.1	2500	760	56	14 mm screw
Boy	12/AM 129-11	4.5	2450	/	129	12 mm screw
	XS	4.5	3130	/	100	12 mm screw
Desma	FormicaPlast	0.15	3000	500	10	6 mm plunger 3 mm plunger
Fanuc	Roboshot S2000-I 5A	6	2000	300	50	14 mm screw
Lawton	Sesame Nanomoulder Sm-5EJ	0.082	3500	1200	13.6	10 mm plunger

MCP	12/90 HSE	7	1728	100	90	16 mm screw
Milacron	Si-B17 A	6.2	2452	/	147	14 mm screw
Nissei	AU3E	3.1	/	/	30	8 mm plunger 14 mm screw
	EP5 Real Mini	8	1960	250	49	16 mm screw
Rondol	High Force 5	4.5	1600	/	50	20 mm screw
Sodick	TR05EH	4.5	1970	300	49	14 mm screw
	LP10EH2	2	1970	1500	100	8 mm plunger 14 mm screw
Sumimoto	SE7M	6.2	1960	300	69	14 mm screw
	SE18DUZ	6.2	2230	500	170	14 mm screw
Toshiba	EC5-A	5.6	2000	150	48	14 mm screw
	EC5-01.A	6	2000	150	50	14 mm screw
	NP7	10	2270	180	69	16 mm screw
Wittmann- Battenfeld	MicroPower 5	1.2	3000	750	50	5 mm plunger 14 mm screw

---

**FANUC**  
**ROBOSHOT**  
**S-2000i30B**

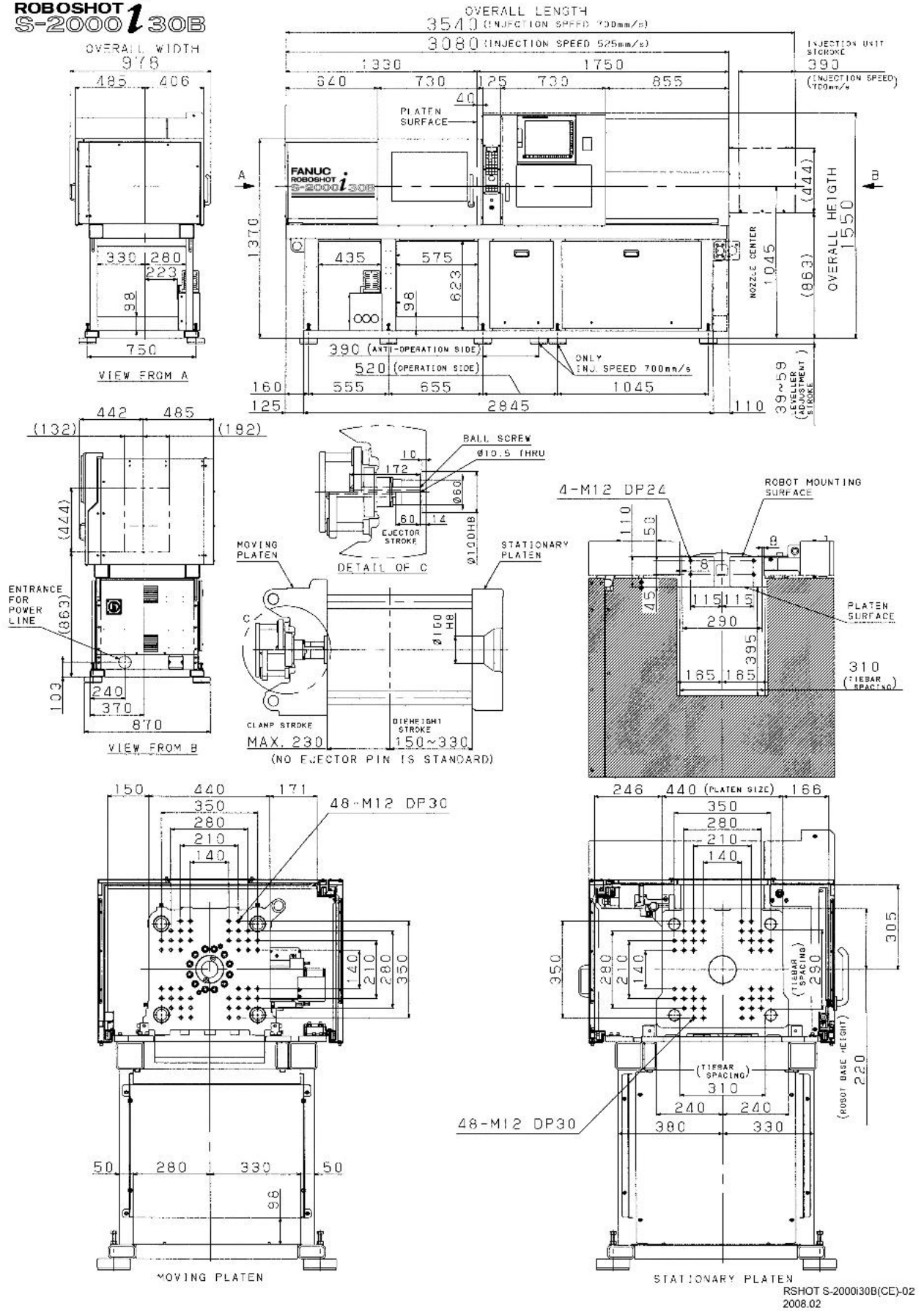


Figure 45: Dimensions of the Fanuc Roboshot S-2000i30B [71].